

# Lyman Alpha and MgII as Probes of Galaxies and their Environment

Luke A. Barnes

*Super Science Fellow, Sydney Institute for Astronomy,  
School of Physics, University of Sydney, Australia*

L.Barnes@physics.usyd.edu.au

and

Thibault Garel and Glenn G. Kacprzak

*Super Science Fellow, Center for Astrophysics & Supercomputing,  
Swinburne University of Technology, Hawthorn, VIC 3122, Australia*

## ABSTRACT

Ly $\alpha$  emission, Ly $\alpha$  absorption and MgII absorption are powerful tracers of neutral hydrogen. Hydrogen is the most abundant element in the universe and plays a central role in galaxy formation via gas accretion and outflows, as well as being the precursor to molecular clouds, the sites of star formation. Since 21cm emission from neutral hydrogen can only be directly observed in the local universe, we rely on Ly $\alpha$  emission, and Ly $\alpha$  and MgII absorption to probe the physics that drives galaxy evolution at higher redshifts. Furthermore, these tracers are sensitive to a range of hydrogen densities that cover the interstellar medium, the circumgalactic medium and the intergalactic medium, providing an invaluable means of studying gas physics in regimes where it is poorly understood. At high redshift, Ly $\alpha$  emission line searches have discovered thousands of star-forming galaxies out to  $z = 7$ . The large Ly $\alpha$  scattering cross-section makes observations of this line sensitive to even very diffuse gas outside of galaxies. Several thousand more high-redshift galaxies are known from damped Ly $\alpha$  absorption lines and absorption by the MgII doublet in quasar and GRB spectra. MgII, in particular, probes metal-enriched neutral gas inside galaxy haloes in a wide range of environments and redshifts ( $0.1 < z < 6.3$ ), including the so-called redshift desert. Here we review what observations and theoretical models of Ly $\alpha$  emission, Ly $\alpha$  and MgII absorption have told us about the interstellar, circumgalactic and intergalactic medium in the context of galaxy formation and evolution.

*Subject headings:* galaxies: evolution — galaxies: formation — galaxies: ISM

## 1. Introduction

In the modern picture of galaxy formation, primordial gas from the intergalactic medium (IGM) falling into the gravitational potential well of dark matter haloes can accrete onto galaxies to feed the interstellar medium (ISM) and fuel star formation. Feedback mechanisms powered by supernovae and active galactic nuclei are able to heat surrounding gas, and reprocess material from the galaxy into

the circumgalactic medium (CGM) in the form of galactic winds.

As the most abundant element in the Universe, hydrogen is a unique tracer of the formation and evolution of galaxies, and its neutral atomic form (HI) can probe gas at various scales (ISM, CGM and IGM). Much of what we know about neutral hydrogen in the ISM comes from 21cm observations of the Milky Way, local galaxies, and the low-redshift Universe ( $z \lesssim 0.05$ ). Future surveys with

the Square Kilometer Array (SKA) pathfinders, such as the Australian SKA Pathfinder (ASKAP Johnston et al. 2008), the Karoo Array Telescope (MeerKAT Booth et al. 2009) and APERTure Tile In Focus (APERTIF Verheijen et al. 2008), will be restricted to redshifts less than 1, which will not allow to carry out HI surveys at earlier epochs, i.e. when galaxies were forming stars at the highest rate ( $z \gtrsim 1.5 - 2$ ). Until the large field of view and high sensitivity of the SKA become available, other tracers of the hydrogen gas are then needed at high redshift.

The Lyman Alpha ( $\text{Ly}\alpha$ ) line offers an invaluable insight into the gas physics that drives galaxy formation. The  $\text{Ly}\alpha$  line results from a transition between the  $2^2P$  state and the  $1^2S$  (ground) state in hydrogen atoms ( $\lambda = 1215.67\text{\AA}$ ), that can be observed from the ground at  $z \gtrsim 2$ , both in emission or in absorption.

In star-forming galaxies, intense  $\text{Ly}\alpha$  emission lines can be produced in the ISM as the result of the photoionisation and the subsequent recombination of hydrogen by massive, short-lived stars.  $\text{Ly}\alpha$  emission features are commonly observed in high-redshift galaxies, and thousands of so-called Lyman-Alpha emitters (LAEs) have been detected at  $z = 2 - 7$  (e.g. Hu et al. 1998; Rhoads et al. 2000; Ouchi et al. 2008; Cassata et al. 2011). A major uncertainty in the interpretation of the data comes from the resonant scattering of  $\text{Ly}\alpha$  photons by HI atoms in the interstellar, circumgalactic, and intergalactic medium. Indeed, it has been observationally shown that the emergent  $\text{Ly}\alpha$  line profile and  $\text{Ly}\alpha$  spatial extent can be highly affected by the kinematics, geometry, and ionisation state of the gas in and around galaxies (e.g. Shapley et al. 2003; Ostlin et al. 2009; Steidel et al. 2010).

In absorption, the large cross-section for the  $\text{Ly}\alpha$  transition makes it the most sensitive method for detecting baryons at any redshift (e.g. Rauch 1998). Close to 7000 absorption systems with  $z > 2.15$  have been detected with HI column densities  $N_{\text{HI}} > 2 \times 10^{20} \text{ cm}^{-2}$ , suggestive of the ISM of galaxies.

In addition to  $\text{Ly}\alpha$ , metal-lines, such as the  $\text{MgII } \lambda\lambda 2796, 2803$  doublet, provide a direct tracer of neutral hydrogen column densities,  $10^{16} \lesssim N_{\text{HI}} \lesssim 10^{22} \text{ cm}^{-2}$  (Churchill et al. 2000a; Rigby, Charlton, & Churchill 2002), and can be observed in a redshift range much of which

cannot be accessed in  $\text{Ly}\alpha$  from the ground ( $0.1 < z < 6.3$ ). These metal-lines can be used to study the HI when it is not directly detected or can be used in tandem to determine the origins of the gas.

A particularly important motivation for this review is the ability of  $\text{Ly}\alpha$  and the  $\text{MgII } \lambda\lambda 2796, 2803$  doublet to shed light on the circumgalactic medium, roughly defined as the 100–300 kpc region around a galaxy, distinct from the stellar system but within the virial radius of its halo. The CGM has been the subject of intense theoretical study in recent years, as it is where accretion (cold and hot) and feedback (supernovae and AGN) meet. Bahcall & Spitzer (1969) were the first to suggest that quasar absorption lines are caused by “tenuous gas in extended haloes of normal galaxies”. Together,  $\text{Ly}\alpha$  scattering and emission, and  $\text{Ly}\alpha$  and metal-line absorption hold great potential to learn about gas in galaxies and their surroundings, and the mechanisms that govern their formation and evolution.

Here, we review observations and models of neutral hydrogen in and around galaxies in the high-redshift universe. Section 2 will examine  $\text{Ly}\alpha$  in absorption, focusing on observations and simulations of damped  $\text{Ly}\alpha$  absorption systems (DLAs). Section 3 will examine the  $\text{MgII } \lambda\lambda 2796, 2803$  doublet and how it is used to trace the processes that shape the CGM. Section 4 will consider  $\text{Ly}\alpha$  in emission: the physics of its production and scattering, observations and models of  $\text{Ly}\alpha$  emitting galaxies, and its illumination of the wider cosmological context of galaxy formation.

## 2. Lyman Alpha in Absorption

Lyman alpha photons are strongly scattered by HI. There are no other states between the  $2^2P$  state and the ground state in an HI atom; thus, when the probability of collisional de-excitation is negligible (as it almost always is in astrophysical contexts), the absorption of a  $\text{Ly}\alpha$  photon by an HI atom is almost immediately ( $A_{21}^{-1} = 1.6 \times 10^{-9}\text{s}$ ) followed by the re-emission of a  $\text{Ly}\alpha$  photon. This can be thought of as a scattering process. A  $\text{Ly}\alpha$  photon (at line centre) passing through an HI region with column density  $N_{\text{HI}}$  and temperature  $T$

encounters an optical depth of,

$$\tau_0 \approx 0.59 \left( \frac{T}{10^4 \text{ K}} \right)^{-\frac{1}{2}} \left( \frac{N_{\text{HI}}}{10^{13} \text{ cm}^{-2}} \right). \quad (1)$$

Lyman alpha in absorption is observed in the spectra of quasars and gamma ray bursts (Figure 1). Three classes of absorbers are distinguished by their neutral hydrogen column density,  $N_{\text{HI}}$ . Ly $\alpha$  forest absorbers have  $N_{\text{HI}} < 10^{17} \text{ cm}^{-2}$ , making them optically thin to ionizing radiation. Lyman limit systems (LLS) have  $10^{17} \text{ cm}^{-2} < N_{\text{HI}} < 2 \times 10^{20} \text{ cm}^{-2}$ . Damped Ly $\alpha$  absorption systems (DLAs) are the highest column density systems, with  $N_{\text{HI}} > 2 \times 10^{20} \text{ cm}^{-2}$ . Damped Ly $\alpha$  absorption profiles are characterized by their Lorentz or damping wings: at such high column densities, unit optical depth occurs in the damping wings of the profile function, beyond the inner Doppler core. The equivalent width of the line is independent of the velocity and temperature structure of the absorber. The column density  $N_{\text{HI}} = 2 \times 10^{20} \text{ cm}^{-2}$  also fortuitously separates the predominantly ionized LLS population from DLAs, in which the hydrogen is mainly neutral due to self-shielding. We will focus here on the properties of DLAs, believed to probe galaxies and their immediate surroundings.

## 2.1. Observed Properties of DLAs

Wolfe (1986) conducted the first DLA survey, using quasar spectra to detect neutral gas in absorption in the disks of high-redshift galaxies. To identify a DLA, one must distinguish a single absorption line, broadened by damping, from an absorption feature caused by the blending of Doppler-broadened, low column density systems. The Ly $\alpha$  forest also generates confusion noise, contaminating the damping wings. The Sloan Digital Sky Survey (SDSS Prochaska & Herbert-Fort 2004; Prochaska et al. 2005) overcame these problems using high-quality, good spectral resolution ( $R \sim 2000$ ) that do not require higher-resolution follow-up spectroscopy to accurately fit Voigt profiles to the data. Using such methods, around ten thousand DLAs have been observed. The largest DLA survey to date is the Baryon Oscillation Spectroscopic Survey (BOSS, Dawson et al. 2013), part of the Sloan Digital Sky Survey (SDSS) III (Eisenstein et al. 2011). The full sample, based on SDSS Data Release 9, contains over

150,000 quasar spectra over the redshift range  $2.15 < z < 3.5$  and has discovered 6,839 DLAs, which is an order of magnitude larger than SDSS II.

The statistical properties of the DLA population can be summarised by its distribution function: the number of absorbers ( $d^2\mathcal{N}$ ) along a random line of sight in the redshift range  $(z, z + dz)$  that have HI column densities in the range  $(N_{\text{HI}}, N_{\text{HI}} + dN_{\text{HI}})$  is,

$$d^2\mathcal{N} = n_{N_{\text{HI}}}(N_{\text{HI}}, z) \sigma_{\text{DLA}}(z) (1+z)^3 \frac{dl_p}{dz} dN_{\text{HI}} dz \quad (2)$$

$$\equiv f(N_{\text{HI}}, X) dN_{\text{HI}} dX, \quad (3)$$

where  $n_{N_{\text{HI}}} dN_{\text{HI}}$  is the comoving number density of DLAs within  $(N_{\text{HI}}, N_{\text{HI}} + dN_{\text{HI}})$ ,  $\sigma_{\text{DLA}}$  is the DLA absorption cross-section,  $\frac{dl_p}{dz} = \frac{c}{H(z)(1+z)}$  is the ratio of proper distance interval to redshift interval, and the so-called absorption distance  $X$  is defined by  $dX \equiv \frac{H_0}{H(z)} (1+z)^2 dz$ . Figure 2 shows the results of Noterdaeme et al. (2012b), derived from 5428 DLA systems observed as part of the BOSS survey.

$f(N_{\text{HI}}, X)$  can be approximated by a double power law. The distribution has a low- $N_{\text{HI}}$  dependence of  $f \propto N_{\text{HI}}^{-2}$ , and drops more steeply above  $N_{\text{HI}} = 10^{21.2} \text{ cm}^{-2}$ , which has been attributed to the high-mass turnover of the halo mass function, the impact of stellar feedback, and the formation of molecular hydrogen in the highest column density clouds. A similar turnover is seen in the HI column density profiles of local THINGS galaxies, which Erkal, Gnedin, & Kravtsov (2012) show is not strongly correlated with gas metallicity. This suggests that the HI- $H_2$  transition is not the primary driver of this feature of  $f(N_{\text{HI}}, X)$ .

The zeroth moment of  $f(N_{\text{HI}}, X)$  gives the number of DLAs encountered along a line of sight per unit absorption distance  $dX$ , i.e. the line density of DLAs,

$$l_{\text{DLA}}(X) dX \equiv \int_{N_{\text{DLA}}}^{\infty} f(N_{\text{HI}}, X) dN_{\text{HI}} dX, \quad (4)$$

where  $N_{\text{DLA}} = 2 \times 10^{20} \text{ cm}^{-2}$ . Alternatively, we can define this quantity in terms of  $dz$ ;  $l_{\text{DLA}}(z) \equiv d\mathcal{N}/dz$  is often referred to as the DLA covering fraction per unit redshift. Prochaska & Wolfe (2009), using SDSS Data Release 5, show that

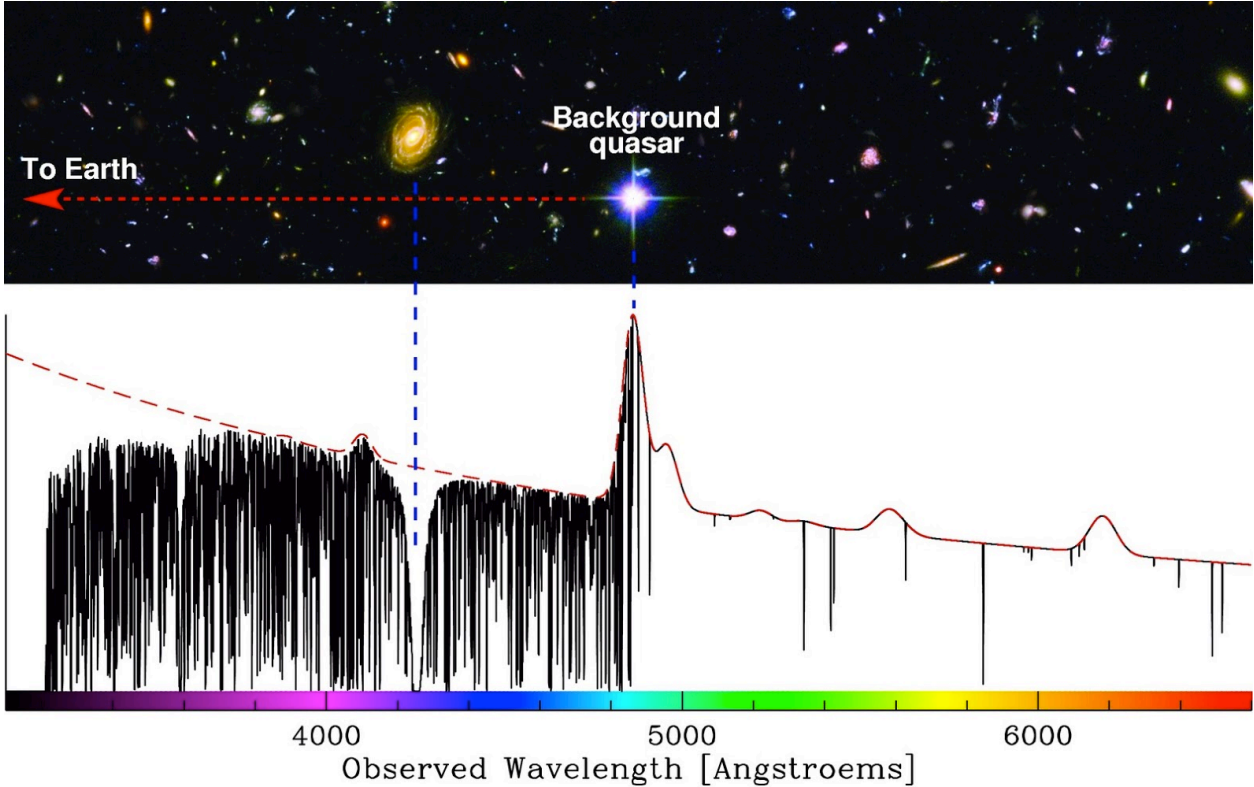


Fig. 1.— A schematic illustration of Ly $\alpha$  absorption seen in the spectra of quasars. At wavelengths shorter than the (redshifted) Ly $\alpha$  emission from the quasar, Ly $\alpha$  is seen in absorption, as intervening HI scatters the quasar continuum out of the line of sight. The large column of density HI in intervening galaxies causes a broad, damped Ly $\alpha$  absorption trough, along with associated metal absorption lines at the same redshift. Figure courtesy of Michael Murphy. An excellent movie of Ly $\alpha$  absorption can be found on Andrew Pontzen’s website: [http://www.cosmocrunch.co.uk/media/dla\\_credited.mov](http://www.cosmocrunch.co.uk/media/dla_credited.mov) .

$l_{\text{DLA}}(X)$  drops from 0.08 at  $z \sim 3 - 4$  to 0.05 at  $z \sim 2.2$ , at which point it is consistent with the present-day value estimated from 21cm observations (Ryan-Weber, Webster, & Staveley-Smith 2003; Zwaan et al. 2005, note however Braun 2012). This indicates surprisingly little evolution in galactic HI gas for the last  $\sim 10$  Gyr.

The first moment of  $f(N_{\text{HI}}, X)$  can be related to the mass density of gas associated with DLAs,

$$\Omega_g^{\text{DLA}}(X) = \frac{\mu m_{\text{H}} H_0}{c \rho_{\text{crit}}} \int_{N_{\text{DLA}}}^{\infty} N_{\text{HI}} f(N_{\text{HI}}, X) dN, \quad (5)$$

where  $\mu$  is the mean molecular mass of the gas; see Prochaska et al. (2005) for a discussion of the limits of the integral, and the contribution of LLSs to the mass density of gas associated with HI atoms.

DLAs dominate the neutral gas content of the Universe in the redshift interval  $z = 0 - 5$ . Further, DLAs between  $z \sim 3.0 - 4.5$  contain sufficient neutral hydrogen to account for a significant fraction of the gas mass in stars in present-day galaxies. DLAs plausibly contain or are related to the reservoirs of gas needed to fuel star formation for much of the history of the Universe (Wolfe et al. 2005).

## 2.2. DLA Kinematics

An important clue as to the nature of DLAs comes from the velocity profiles of associated metal lines. Because unit optical depth occurs outside the Doppler core, the observed Ly $\alpha$  absorption profiles of DLAs contain no information about the velocity structure of the gas. Observers have used high-resolution spectroscopy to study

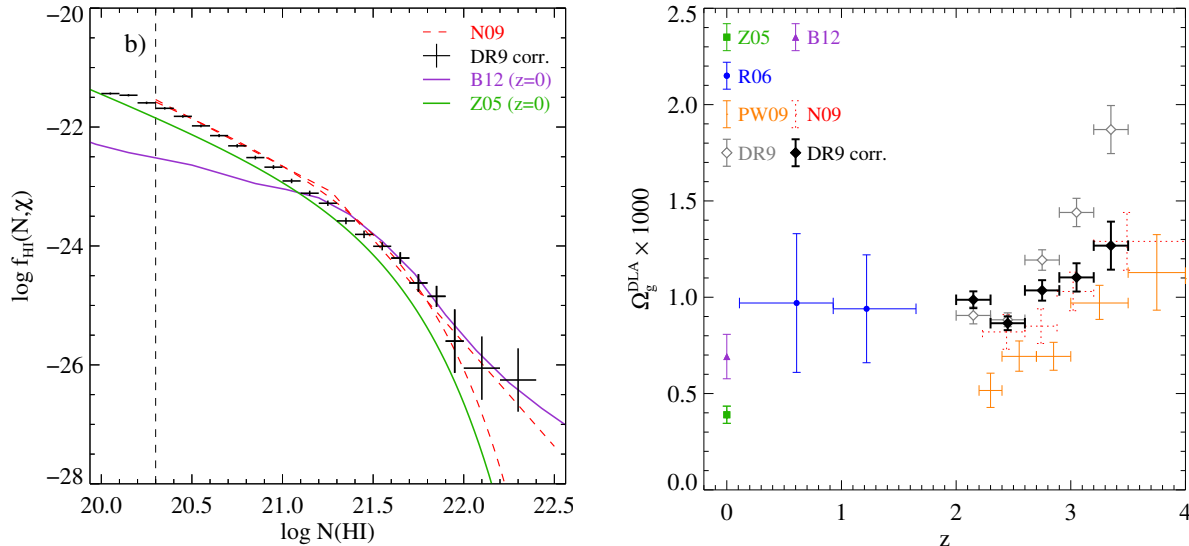


Fig. 2.— *Left*: Column density distribution function  $f(N_{\text{HI}}, X)$  at  $\langle z \rangle = 2.5$  from Noterdaeme et al. (2012b). Horizontal bars represent the bin over which  $f$  is calculated and vertical error bars represent Poissonian uncertainty. The double power-law and  $\Gamma$ -function fits to the DR7 distribution of Noterdaeme et al. (2009) at  $\langle z \rangle = 2.9$  are shown as red dashed lines.  $f(N_{\text{HI}}, X)(z = 0)$  is taken from Braun (2012, purple) and Zwaan et al. (2005, green). *Right*: Cosmological mass density of neutral gas in DLAs as a function of redshift [Z05: Zwaan et al. (2005); B12: Braun (2012); R06: Rao et al. (2006); PW09: Prochaska & Wolfe (2009); DR9: Noterdaeme et al. (2012b)]. Credit: Noterdaeme et al., A&A, 547, L1, 2012, reproduced with permission ©ESO.

so-called low-ionisation metals (or low-ions). For example, MgI (MgII) has an ionisation potential of 7.65 eV (15.04 eV) (Dopita & Sutherland 2003). Thus, in a region where neutral hydrogen is self-shielded from photons with energies above its ionisation potential (13.6 eV), the dominant ion of magnesium will be MgII. Other low-ions include SiII, FeII and NiII, while NI and OI have ionisation potentials that are greater than 13.6 eV and are thus predominantly neutral in a self-shielded HI region (Viegas 1995). Thus, absorption features from low-ionisation metals at the same redshift as the DLA give us crucial information about the kinematics of the neutral gas.

The most common statistic used to characterise the width of a low-ion metal absorption feature is  $\Delta v_{90}$ , defined by Prochaska & Wolfe (1997) in their pioneering survey as the velocity interval encompassing 90% of the total integrated optical depth. (We will often use the more compact notation  $v_w$ .) Figure 3 shows the observations of Prochaska et al. (2008). The mean redshift of the DLA sample is  $\langle z \rangle = 3$ ; Pontzen et al.

(2008) and Neeleman et al. (2013) note that there is negligible redshift evolution of the distribution. DLAs velocity widths range from  $15 \text{ km s}^{-1}$  to several hundred  $\text{km s}^{-1}$  with a median of  $\approx 80 \text{ km s}^{-1}$ . The high-velocity tail has been the subject of much theoretical attention, following the claim by Prochaska & Wolfe (1997) that it conflicts with the predictions of hierarchical structure growth within CDM cosmologies (see Section 2.6).

An important low-redshift insight into DLA kinematics comes from 21cm emission from HI in local galaxy disks. Zwaan et al. (2008) use high-quality HI 21cm data to measure the distribution of  $\Delta v_{90}$  for local galaxies with  $N_{\text{HI}} > 2 \times 10^{20} \text{ cm}^{-2}$ . The observed distribution peaks sharply at around  $30 \text{ km s}^{-1}$ , with a FWHM of  $\sim 20 \text{ km s}^{-1}$  and a shallow tail out to  $\sim 200 \text{ km s}^{-1}$ . This distribution is very different to that shown in Figure 3 for high-redshift DLAs — the median is smaller by more than a factor of two. Zwaan et al. (2008) conclude that gas kinematics at high redshifts must be increasingly influenced by gas that does not participate in ordered rota-

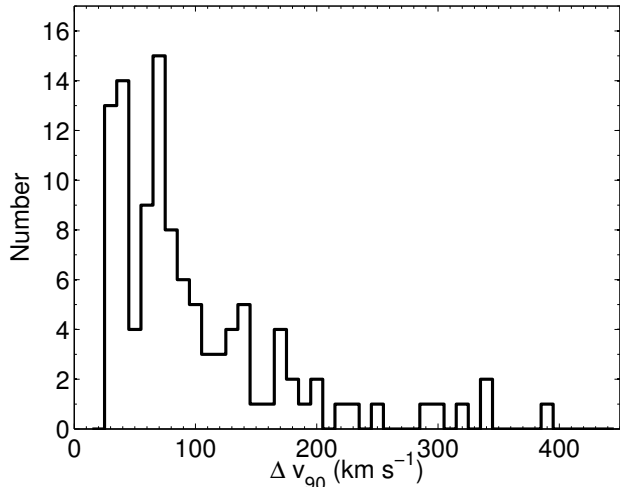


Fig. 3.— Histogram of the velocity width,  $\Delta v_{90}$ , of low-ions associated with the sample of DLAs found in Prochaska et al. (2008). The sample shows velocity widths ranging from 15 km s $^{-1}$  to several hundred km s $^{-1}$  with a median of  $\approx 80$  km s $^{-1}$ . The mean redshift of the DLAs is  $\langle z \rangle = 3$ ; Pontzen et al. (2008) and Neeleman et al. (2013) note that there is negligible redshift evolution of the distribution.

tion in cold disks.

### 2.3. DLA Metallicity

The metallicity of DLAs can shed light on their expected connection to star formation. The elemental abundances of DLAs are the most accurate measurements in the high-redshift Universe of the chemical enrichment of gas by stars. Furthermore, regardless of their exact identity, the mean metallicity of DLAs is the best measure we have of the amount of metal enrichment of neutral gas in the Universe at a given epoch. This subsection will follow the reviews of Pettini (2004, 2006); Wolfe et al. (2005).

DLAs are generally metal-poor at all redshifts. This points to DLAs as arising in gas that is in its earliest stages of star formation. However, DLAs are not primordial clouds. No DLAs have been found without significant metal absorption. Prochaska et al. (2003) report a “metallicity floor”: though their observations are sensitive to  $[M/H] < -4$ , none were found with  $[M/H] < -3$ . Rafelski et al. (2012) show that this metallicity

floor continues out to  $z \sim 5$ . Within the population of DLAs at a particular redshift, there is a wide scatter of metallicities, indicating different rates and stages of star formation within the DLA population.

DLAs can trace the cosmic evolution of metallicity. Wolfe et al. (2005), Neeleman et al. (2013) and Rafelski et al. (2013) report a statistically significant increase in the cosmic metallicity in DLAs with decreasing redshift, in contrast to the earlier conclusions of Pettini (2004). This is in keeping with the expectation that star formation will pollute the neutral gas with metals via supernovae and stellar winds. Rafelski et al. (2013) further report evidence of a rapid increase in DLA metallicity between  $z = 5$  and  $z = 4.5$ .

DLAs can also trace the large-scale distribution of metals. In particular, *Proximate* DLAs (PDLAs), defined to have a velocity offset  $< 3,000$  km s $^{-1}$  relative to their background quasar, are known to have higher metallicities than intervening DLAs, and higher metallicities as the quasar is approached (Ellison et al. 2010; Ellison, Prochaska, & Mendel 2011). This suggests PDLAs trace high-mass galaxies in the overdense regions of the universe that host quasars. Indeed, quasars with higher UV luminosities are associated with lower-metallicity PDLAs. This is evidence of the direct impact of the quasar on surrounding galaxies, possibly involving the shutting-off of star-formation.

Ledoux et al. (2006) find evidence of a velocity-metallicity correlation in DLAs,  $[X/H] = 1.55 \log(v_w) - 4.33$ , with  $X = \text{Zn}, \text{S}$  or  $\text{Si}$ . This has been confirmed by Neeleman et al. (2013) and Møller et al. (2013), though with shallower slopes: 0.74 and 1.12 respectively. This correlation can be used to constrain the DLA mass-metallicity relationship (Barnes & Haehnelt 2014), who conclude that metallicity increases with DLA host-halo mass as  $[M/H]_{\text{mean}} = 0.7 \log\left(\frac{M_v}{10^{11} M_\odot}\right) - 1.8$ . There is some evidence, too, that at a fixed halo mass, DLAs with above average velocity width (and thus presumably above average star formation rate) have above average metallicity.

An intriguing clue to the nature of DLA comes from observations of so-called *sub-DLAs*, with  $10^{19} \text{ cm}^{-2} < N_{\text{HI}} < 2 \times 10^{20} \text{ cm}^{-2}$ . Imaging searches for DLA and sub-DLA galaxies show that

DLAs probe smaller sightlines: median impact parameter is 17.4 kpc for the DLA galaxy sample and 33.3 kpc for the sub-DLA sample of Rao et al. (2011). Given the expectation that DLAs probe the densest, inner-most, star-forming regions of galaxies, we might expect the sub-DLA population to probe the more pristine, outer regions of galaxies and their surroundings. Somewhat surprisingly, then, sub-DLAs are more metal-rich than DLAs, particularly at low redshift ( $z < 1.5$ ) (Kulkarni et al. 2010). The metallicities of DLAs and sub-DLAs decrease with increasing  $N_{\text{HI}}$  (Khare et al. 2007). Given the mass-metallicity relation, this plausibly implies that sub-DLAs are associated with higher-mass systems. One must keep in mind that the properties of DLAs and sub-DLAs vary both with the properties of its host system and the properties of the sightline through said system.

Recently, Cooke et al. (2011a,b) have reported observations of extremely metal-poor DLAs as probes of near-pristine clouds of star-formation fuelling gas. The abundance patterns of these systems are consistent with predictions of Population III supernovae, suggesting that these DLAs retain the signature of the earliest episodes of star-formation. Intriguingly, some of these systems also show an enhancement of carbon relative to other metals, reminiscent of carbon-enhanced-metal-poor (CEMP) stars — a population of galactic halo stars whose abundances suggest that they were born from gas enriched by the first stars (Beers & Christlieb 2005; Lucatello et al. 2006).

#### 2.4. The Search for DLA Host Galaxies

Searches for the galaxies that are responsible for damped absorption in QSO spectra have a long history. The most common technique is to search adjacent to quasar sightlines with known absorption systems (Fynbo et al. 1999; Bunker et al. 1999; Kulkarni et al. 2000, 2001; Warren et al. 2001; Christensen et al. 2007). This is a difficult task, as the light of the extremely bright quasar must be accurately subtracted in order to study the light from the galaxy, which is very faint in comparison. Kulkarni et al. (2000) and others caution that a given emission feature could be a Point Source Function (PSF) artefact rather than a real source. For many years, this search resulted in mostly non-detections (Lowenthal et

al. 1995; Bunker et al. 1999; Kulkarni et al. 2000, 2001, 2006; Christensen et al. 2009). Warren et al. (2001) searched around 23 high-redshift, high-column density Ly $\alpha$  absorbers with NICMOS, finding 41 candidates. Christensen et al. (2007) report that, for  $z > 2$ , six DLA galaxies have been confirmed through spectroscopic observation of Ly $\alpha$  emission, with other techniques producing a few additional candidates. Christensen et al. added another six Ly $\alpha$  emission candidates to this group. A few DLA counterparts have been discovered by searching in the damped Ly $\alpha$  trough for Ly $\alpha$  emission, beginning with Hunstead, Pettini, & Fletcher (1990), although that particular system failed to be detected by Wolfe et al. (1992) and Lowenthal et al. (1995), only to reappear in Pettini, Smith, King, & Hunstead (1997). Further Ly $\alpha$  detections were reported by Fynbo et al. (1999); Møller et al. (2002, 2004).

Recent success has followed from improved methods. For example, Fumagalli et al. (2010) use higher-redshift absorbers to do the QSO subtraction for lower redshift systems, detecting one DLA in rest-frame FUV continuum emission. Fynbo et al. (2010, 2011), noting theoretical predictions and tentative observational evidence of a luminosity-metallicity relation in DLAs, target high-metallicity DLAs and detect two systems in emission. Péroux et al. (2011a,b, 2012) used SINFONI integral field spectroscopy to detect faint DLA and LLS galaxies near bright quasars. They detect 5 galaxies (3 DLAs, 2 LLSs) in H $\alpha$  emission, 4 at  $z \lesssim 1$ , and the other at  $z = 2.35$ . Noterdaeme et al. (2012a) and Krogager et al. (2013) detect Ly $\alpha$ , [OIII], and H $\alpha$  emission from DLAs at  $z \sim 2.2$ . (We will discuss these systems further in Section 4.5.) Rahmani et al. (2010) stack the spectra from 341 DLAs observed in the Sloan Digital Sky Survey at  $\langle z \rangle = 2.86$ , searching for Ly $\alpha$  emission from the DLA host. They report a non-detection of emission at line centre, which ignores the possible effects of Ly $\alpha$  radiative transfer. Rauch & Haehnelt (2011), by relaxing this assumption, report a  $2.7\sigma$  detection. DLA host searches at lower redshift have had more success: Rao et al. (2011) use photometric redshifts and colours to detect 27 DLAs (selected as MgII absorbers) in emission at  $0.1 \leq z \leq 1.0$ .

With relatively few DLA host galaxies known at  $z \gtrsim 2$ , conclusions drawn about DLAs in emis-

sion must be tentative. Krogager et al. (2012) use a sample of 10 DLAs in emission to argue for two correlations. Firstly, the DLA impact parameter (the distance between the centre of the host and the QSO line of sight) decreases with increasing HI column density. This reflects the decrease in column density with distance from the centre of the host galaxy, as predicted by simulations (Pontzen et al. 2008; Hummels et al. 2012). Second, DLA metallicity increases with impact parameter, which is interpreted as a corollary of the correlation between DLA cross section and mass, and between mass and metallicity, though selection biases make comparison with observations difficult.

Rahmati & Schaye (2014) provide a table of 13 confirmed  $z \sim 2 - 3$  DLA-galaxy pairs from the literature. Proper impact parameter varies from  $\sim 1 - 25$  kpc, with a median of 8 kpc. Noting that observations are typically only able to detect galaxies with  $\text{SFR} \gtrsim 1 - 10 M_{\odot} \text{ yr}^{-1}$ , the observed star formation rates vary from  $\sim 3 - 70 M_{\odot} \text{ yr}^{-1}$ , with a median of  $\sim 20 M_{\odot} \text{ yr}^{-1}$ . Note that the SFR's are often based on Ly $\alpha$  emission, which is difficult to correct for dust extinction. The associated Ly $\alpha$  luminosities (from Equation 8, Section 4.3) range from  $3 - 80 \times 10^{42} \text{ erg s}^{-1}$ . The two galaxies with measured stellar masses have  $M_{*} = 2 - 12.6 \times 10^9 M_{\odot}$ . The simulations of Rahmati & Schaye (2014), which incorporate the physics of radiative transfer of the UVB and recombination radiation, show good agreement with these observations, though the problem of small number statistics is exacerbated by a lack of information about non-detections and detection limits (in both luminosity and impact parameter). Such simulations are discussed further in Section 2.6.

## 2.5. DLAs in Gamma-Ray Burst Afterglows

Seeing HI in absorption at cosmological distances requires an extremely bright background source. Quasars are very useful to this end, as we have seen. DLAs can also be seen in the afterglow of Gamma-Ray Bursts (GRBs). Importantly, the absorption seen in GRB-DLAs is intrinsic rather than intervening, that is, the absorbing gas is inside the GRB host galaxy. Thus, GRB-DLAs provide detailed information on the kinematics, chemical abundances, and physical state of the gaseous

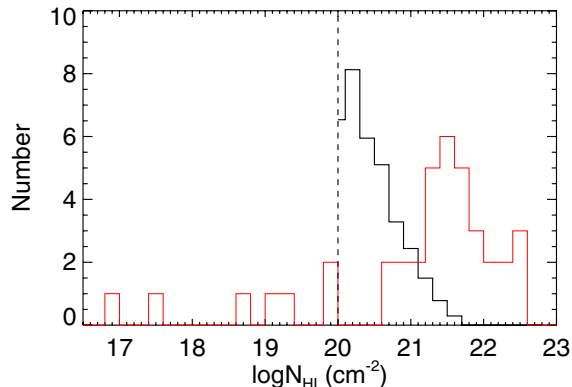


Fig. 4.— A comparison of the HI column density distributions of QSO-DLAs (black) and GRB-DLAs (red). The numbers of QSO-DLAs have been renormalized to the same number of objects as the GRB absorbers. Figure from Fynbo et al. (2009); reproduced by permission of the AAS.

component of their host galaxy (Fiore 2001; Fynbo et al. 2001; Savaglio, Fall, & Fiore 2003; Vreeswijk et al. 2004; Prochaska et al. 2004; Jakobsson et al. 2004, 2006; Fynbo et al. 2006; Prochaska, Chen, & Bloom 2006; Watson et al. 2006). Here, we will briefly review the properties of GRB-DLAs, highlighting clues as to their relationship to QSO-DLAs and other high-redshift galaxies.

- GRB-DLAs have a dramatically different column density distribution to QSO-DLAs, as shown in Figure 4, from Fynbo et al. (2009). While QSO-DLA column density distribution is a monotonically decreasing function of  $N_{\text{HI}}$ , the GRB-DLA distribution displays a prominent peak at  $N_{\text{HI}} = 10^{21.5} \text{ cm}^{-2}$ . Only 1% of QSO-DLAs display such high columns (Pontzen et al. 2010).
- At  $z > 2$ , GRB-DLAs display a range of metallicities, from 1/100 solar (Rau et al. 2010) to super-solar (Savaglio et al. 2012). Unlike QSO-DLAs, there is no clear trend of mean metallicity with redshift. Savaglio et al. (2012) has shown that the mean GRB-DLA metallicity for  $z = 2 - 4.5$  is somewhat higher ( $\log(Z/Z_{\odot}) = -0.83 \pm 0.76$ ) compared to QSO-DLAs ( $\log(Z/Z_{\odot}) = -1.39 \pm 0.61$ ) (see also Savaglio 2006; Fynbo et al. 2006, 2008; Prochaska et al. 2007).

Metal absorption features in GRB-DLAs tend to be, on average, 2.5 times stronger and slightly more ionized than those of QSO-DLAs (de Ugarte Postigo et al. 2012).

- The velocity width ( $v_w$ ) distribution of GRB-DLAs is consistent with that of QSO-DLAs, with a median of  $\approx 80 \text{ km s}^{-1}$  and a high-velocity tail out to  $200 - 300 \text{ km s}^{-1}$  (Prochaska et al. 2008), though there are only 9 GRBs in the GRB-DLA  $v_w$  sample. This suggests that the two populations inhabit parent haloes of comparable mass.
- There is some evidence that GRB-DLAs are not significantly statistically distinct from the high-column density tail of QSO-DLAs. GRB-DLAs seem to smoothly extend the dust properties and metallicity of QSO-DLAs to larger column densities (Fynbo et al. 2009; Guimarães et al. 2012; De Cia et al. 2013).

Given that GRB-DLAs are plausibly selected by their intense star formation, as opposed to the HI cross-section selection of QSO-DLAs (Fynbo et al. 2008), Pontzen et al. (2010) modelled GRB sight-lines in a cosmological simulation by associating them with young star particles. The result was a successful prediction of the GRB-DLA column density distribution, and broad agreement with the range of metallicities. In the simulations, GRB-DLAs occupy dark matter host haloes that are an order of magnitude larger than their QSO counterparts, and probe regions typically four times closer to the centre of their host haloes. This is in agreement with the schematic picture of GRB-DLAs as resulting from sight lines that probe the denser, central regions of their host galaxies, as opposed to intervening absorbers where most of the cross-sectional area is in the outskirts of the galaxy (Prochaska et al. 2007). This picture also explains why GRB-DLA metallicities are systematically higher than the QSO-DLA metallicities (Fynbo et al. 2008). By simultaneously probing star-formation and ISM gas physics of galaxies, GRB-DLAs provide a much-needed test of galaxy formation simulations.

## 2.6. Theoretical models of DLAs

### 2.6.1. Early Models of DLAs: From Galaxy Disks to $\Lambda$ CDM

In the local Universe, most HI atoms are found in the disks of  $L_*$ -type galaxies. Thus, DLAs have traditionally been considered to be high-redshift galactic disks. This motivated Wolfe (1986) to search for the disks of such galaxies at high redshift by looking for high column density HI in absorption in the spectra of quasars. A variety of models have been proposed, as discussed in this section.

Arons (1972) was the first to suggest that absorption lines in high-redshift QSO spectra could be Ly $\alpha$  absorption from HI in protogalaxies, though in those models the gas is highly ionized and thus not directly relevant to DLAs. York et al. (1986) suggested that some DLAs could be associated with gas-rich dwarf galaxies, which would explain the complexity of the metal line profiles. Schiano et al. (1990) used hydrodynamic simulations of the collapse of a gaseous corona into a “Ly $\alpha$  disk” via radiative cooling to test the idea that DLAs originate in large, massive disks of gas that are the progenitors of present-day galaxies. They conclude that such a scenario is plausible, provided there is sufficient metallicity to allow for rapid cooling. Lu et al. (1996), by considering elemental abundances, found that DLAs are much less metal-enriched than the Galactic disk in its past. They concluded that DLAs are not high-redshift spiral disks in the traditional sense, postulating thick disks or spheroidal components of (dwarf) galaxies as more likely scenarios.

Within the CDM model of cosmic structure formation, Mo & Miralda-Escude (1994) modelled DLAs as gaseous disks within dark matter haloes. Such models were refined and extended by Kauffmann (1996), who based a disk-formation model on the paradigm of White & Rees (1978): galaxies form by the continuous cooling and accretion of gas within a merging hierarchy of dark matter haloes. The model also incorporates star formation, with the gas supply regulated by infall from the surrounding halo. Chemical enrichment occurs through the ejection of metals back into the hot IGM by supernovae; this gas then cools back onto the disk. This model predicts, with reasonable success, the redshift dependence of  $\Omega_{\text{HI}}$  as well as  $f(N_{\text{HI}}, X)$ . DLAs are predicted to be

smaller, more compact, and less luminous than today’s galaxies.

Mo et al. (1998) placed rotationally-supported disks within haloes with an NFW density profile (Navarro et al. 1996), allowing the spin parameter  $\lambda$  to vary over a lognormal distribution. These models successfully reproduce  $dN/dz$  at  $z = 2.5$  by including the contribution of disks with rotation velocities down to  $50\text{--}100 \text{ km s}^{-1}$ . An important unknown in this and later models is the smallest halo that can host a DLA. Higher resolution simulations of smaller cosmological volumes by Quinn et al. (1996) indicated that haloes as small as  $35 \text{ km s}^{-1}$  can host DLAs.

Gardner et al. (1997a) were among the first to study DLAs using numerical simulations of cosmological structure formation. While extending the simulations of Katz et al. (1996a,b), their simulations could not resolve dark matter haloes below  $100 \text{ km s}^{-1}$ . They used the Press-Schechter formalism to extrapolate the results of their simulation to smaller circular velocities. The results for  $dN/dz$  are in good agreement with observations for  $z = 2 - 4$  in an  $\Omega_m = 1$  universe. Gardner et al. (1997b), however, applied this method to other cosmological models, showing that in a  $\Lambda$ CDM universe (with  $\sigma_8 = 0.79$ ), absorbers are underproduced at  $2 \lesssim z \lesssim 3$  by a factor of 3. Further simulations (Gardner et al. 2001) produced a more adequate fit to the data, though precise predictions were affected by the uncertainty in determining the smallest halo capable of hosting a DLA.

Prochaska & Wolfe (1997) showed that kinematical data present a considerable challenge to theoretical models of DLAs. They traced sightlines through disk galaxies, their favoured model being a single thick, cold disk ( $h = 0.4R_d$ ,  $\sigma_{cc} = 10 \text{ km s}^{-1} \ll v_{\text{rot}}$ ,  $v_{\text{rot}} = 250 \text{ km s}^{-1}$ , where  $\sigma_{cc}$  is the isotropic velocity dispersion of absorbing clouds within the disk). A CDM-inspired model fared much worse. In this model,  $v_{\text{rot}}$  for the thick disk is chosen from the distribution  $P(v_{\text{rot}})$  calculated by Kauffmann (1996) for a CDM cosmology. This model fails to reproduce the velocity width distribution because of the predominance of small haloes with slowly rotating disks. The simulated profiles are also significantly more symmetric than is observed.

Haehnelt et al. (1998) challenged the assump-

tion that the velocity widths of high-redshift galaxies are due solely to rotational motion in disks. In hierarchical structure formation, galaxies are built up from the merging of protogalactic clumps, often moving along filaments. Haehnelt et al. (1998) thus considered absorption arising in more realistic, irregular protogalactic clumps, whose velocity field is a mixture of rotation, infall, merging, and random motion (Similarly complex velocity fields are seen in recent IFS observations of DLA galaxies, e.g. Bouché et al. 2013; Péroux et al. 2013; Jorgenson & Wolfe 2014). Their simulations, which resolved the substructure of the clumps, produced a population of DLAs that was able to reproduce the kinematic data of Prochaska & Wolfe (1997).

### 2.6.2. The CGM in Cosmological Simulations

In light of the realisation that DLAs cannot be explained within a  $\Lambda$ CDM cosmology as isolated systems, the next generation of cosmological simulations sought to place DLAs within their full cosmological context, and in particular within the immediate surroundings of galaxies: the circumgalactic medium. The CGM is roughly defined as the  $100\text{--}300 \text{ kpc}$  region around a galaxy, distinct from the stellar system but within the virial radius of its halo. Before we discuss the particular place of DLAs in cosmological simulations, we will here give a brief overview of the CGM in cosmological simulations. This is particularly important as recent theoretical studies have markedly changed our picture of how galaxies get their gas.

The cooling of gas in dark matter haloes has long been recognised as a crucial ingredient in galaxy formation (Binney 1977; Silk 1977; White & Rees 1978). In the classic picture of White and Rees, gas that falls into a dark matter halo is shock-heated at the virial radius to the virial temperature ( $\sim 10^6 \text{ K}$ ). The gas then accretes quasi-spherically when cooling (primarily via bremsstrahlung) removes the pressure-support of the gas against gravity. This process is inefficient above a halo mass of  $5 \times 10^{12} M_\odot$  (Kereš et al. 2009), because of low densities and long associated cooling times. This mode of accretion is known as “hot mode” accretion, to contrast it with another mode of accretion identified by Birnboim & Dekel (2003) and Kereš et al. (2005). In “cold mode” accretion, gas that has never been

shock heated ( $T \ll T_{\text{vir}}$ ) radiates its potential energy and falls onto the central galaxy along thin filaments. This mode of accretion dominates in low-mass haloes ( $M_{\text{halo}} \lesssim 2 - 3 \times 10^{11} M_{\odot}$ ), and is therefore the main accretion mechanism at high redshift. Both modes can coexist in massive haloes at high redshift, where cold, dense filaments are able to penetrate hot virialized haloes (Dekel & Birnboim 2006; Ocvirk et al. 2008; Dekel et al. 2009; Fumagalli et al. 2013)<sup>1</sup>.

The gas in cold streams penetrates deep inside the virial radius (Dekel et al. 2009). The interaction of cold streams with hot halo gas as it settles into a rotating disks has been used to model a population of large, clumpy, rapidly star-forming disk galaxies at high redshift (Dekel, Sari, & Ceverino 2009; Agertz et al. 2009). The newly-accreted gas will fragment to form large ( $10^7 - 10^9 M_{\odot}$ ) star-forming clumps in an extended  $\sim 10$  kpc disc. While the inner parts of the disc have on average solar metallicity, the clump-forming region is only  $0.1 Z_{\odot}$ . Brooks et al. (2009) note that star formation in stellar disks of galaxies up to Milky Way mass is primarily fuelled at all times by gas that has accreted cold; such gas can dominate the supply of the stellar disk even in high mass haloes where most of the gas flowing through the virial radius is hot. The dominant gas supply at all masses is from smoothly accreted gas that has never belonged to another galaxy halo.

Inflowing gas is only half the story, however. Galactic winds, powered by some combination of stellar winds, supernovae, cosmic ray heating and AGN, are ubiquitous in both the local and distant universe (see Veilleux et al. 2005, for a compre-

hensive review). As Steidel et al. (2010) notes, virtually every  $z > 2$  galaxy bright enough to be observed spectroscopically is driving out material at velocities of at least several hundred  $\text{km s}^{-1}$ . Such winds are the primary mechanism by which star-formation feeds back upon itself and energy and metals are circulated within galaxies and their environment. This feedback is widely believed to explain why stellar mass fails to follow halo mass in a  $\Lambda$ CDM cosmology, especially at low masses ( $M_{\text{halo}} \lesssim 10^{11} M_{\odot}$ ; see Silk & Mamon 2012). Hydrodynamical simulations that fail to model feedback inevitably form galaxies with too many baryons.

Simulations of galactic winds, particularly those in a cosmological context, must rely on unresolved subgrid physics to approximate the combined effect of stellar and SN feedback. A range of prescriptions are available (e.g. Springel & Hernquist 2003; Oppenheimer & Davé 2006, 2008; Governato et al. 2007; Hopkins et al. 2011, 2012; Barai et al. 2012); all are poorly constrained by observations and ‘first principles’ simulations. The simulations of Shen et al. (2012) show inflowing and outflowing gas coexisting in the CGM: about one third of all the gas within the virial radius is outflowing. This outflowing gas is enriched with the products of star-formation, so that at the virial radius inflowing gas has metallicity  $0.05 Z_{\odot}$ , while the mean metallicity of outflowing gas is  $0.56 Z_{\odot}$ . Outflows tend to be bipolar, taking the path of least resistance perpendicular to the plane of the disk, in agreement with observations at both low (Lynds & Sandage 1963; Bland & Tully 1988; Ohya et al. 2002, e.g. M82) and high (Bordoloi et al. 2011, 2012; Bouché et al. 2012) redshift. The launching of a large-scale galactic wind is not guaranteed, as the energy input may only pressurise the ISM (Kereš et al. 2009). Oppenheimer et al. (2010) find that the mean recycling time decreases with halo mass, meaning that recycled wind material is an important mode of accretion (distinct from cold and hot modes) in high mass haloes. In particular, in their favoured momentum-driven wind model, gas accreted via the fountain mode fuels over 50 per cent of the global star formation density at  $z \lesssim 1.7$ .

<sup>1</sup>While the conclusions of Kereš et al. (2005) have been reproduced in higher resolution SPH simulations (Brooks et al. 2009; Kereš et al. 2009) and AMR simulations (Ocvirk et al. 2008; Agertz et al. 2009; Dekel et al. 2009), they have recently been challenged by the moving mesh simulations of the AREPO code (Nelson et al. 2013). While there is still a low vs. high mass dichotomy for cold vs. hot accretion, AREPO concludes that more massive haloes ( $M_{\text{halo}} \gtrsim 10^{10.5} M_{\odot}$ ) have a much smaller cold fraction than is seen in SPH simulations. This is due to both an order of magnitude higher hot accretion rate, and a factor-of-two lower cold accretion rate. For cold streams, the AREPO flows are disrupted in massive haloes at  $0.25 - 0.5 r_{\text{vir}}$ . Nelson et al. (2013) attribute the difference to numerical blobs of cold gas in SPH simulations. The situation, and the implications for the observable properties of gas accretion, remains unclear.

### 2.6.3. DLAs in Cosmological Simulations

Returning to DLAs within cosmological simulations, Nagamine et al. (2004) used Smoothed-Particle Hydrodynamics (SPH) simulations in the context of the  $\Lambda$ CDM model. Their simulations included the effects of radiative cooling, the Ultra Violet Background (UVB), star formation, supernovae feedback, and in particular considered the effect of galactic winds using a simple phenomenological model that involves giving gas particles a “kick” in a random direction to drive them out of dense star-forming regions. They used the Press-Schechter formalism to extend their results below the resolution limit of their simulations. The result was a reasonable agreement with  $\Omega_{\text{HI}}(z)$  so long as “strong” winds were invoked; otherwise, there was too much gas left in the DLAs. Their prediction for  $dN/dz(z)$  was also reasonably successful. Finally,  $f(N_{\text{HI}}, X)$  is slightly underpredicted, with strong winds necessary to prevent overprediction at high- $N$ . Nagamine et al. (2007) refined the previous models with a more careful consideration of winds, concluding that DLAs are hosted by small ( $M_{\text{halo}} < 10^{12} h^{-1} M_{\odot}$ ), faint galaxies.

Further cosmological simulations have been able to model the DLA population without using analytic extensions based on the Press-Schechter formalism. The first to accomplish this was Razoumov et al. (2006), who used AMR cosmological simulations to address both the neutral gas cross-section and the gas kinematics. Their results show that  $f(N_{\text{HI}}, X)$  is overpredicted for  $N_{\text{HI}} > 10^{21} \text{ cm}^{-2}$ , which may be due to the effects of grid resolution or the absence of a model for the formation of  $\text{H}_2$ , which will affect the highest density systems. The velocity width distribution is dramatically underpredicted at high- $v_w$ , even when star-formation is taken into account (Razoumov et al. 2008). Another surprising conclusion of these simulations was the abundance of DLAs that are not associated with any halo — intergalactic DLAs were found in tidal tails and quasi-filamentary structures.

Pontzen et al. (2008) analysed DLAs in the galaxy formation simulations of Governato et al. (2007, 2008) and Brooks et al. (2007). These simulations produce impressively realistic disk galaxies at  $z = 0$ . It is thus a major success that the sim-

ulations, with no further tweaking of free parameters, are able also to match  $f(N_{\text{HI}}, X)$  at  $z = 3$ , apart from a slight overprediction at high- $N_{\text{HI}}$ . Good agreement is also found with the distribution of metallicities in DLAs, something previous simulations were unable to do. However, as before, DLA velocity width data is not reproduced, with too few high- $v_w$  systems. Tescari et al. (2009) followed a familiar pattern — success with  $f(N_{\text{HI}}, X)$  but too few large  $v_w$  systems, possibly due to inadequate mixing of wind-phase metals.

Hong et al. (2010) mimicked metal diffusion by tying metals directly to HI, and had somewhat more success in producing large  $v_w$  systems. Cen (2012) used an adaptive mesh-refinement code to study DLAs in two small cosmological volumes (for resolution reasons), one centred on a  $1.8\sigma$  overdensity and one on a  $1\sigma$  underdensity. These simulations bracket the observed column density and velocity width distributions. The Over-Whelmingly Large Simulations (OWLS) project has been used to study QSO absorption systems, often in conjunction with post-processing to account for  $\text{H}_2$  formation and ionizing radiation. The simulations have studied the observed  $z = 3$  abundance of Ly $\alpha$  forest, Lyman limit, and DLA absorption systems probed by quasar sight lines over 10 orders of magnitude in column density (Altay et al. 2011), the lack of evolution in  $f(N_{\text{HI}}, X)$  below  $z = 3$  (Yajima, Choi, & Nagamine 2012), and the effect of subgrid feedback prescriptions (Altay et al. 2013) and ionizing radiation from the UV background and local stellar sources (Rahmati et al. 2013) on the DLA population. There is some tension between Rahmati et al. (2013), who conclude that their predictions are highly sensitive to assumptions about the ISM, especially for  $N_{\text{HI}} > 10^{21} \text{ cm}^{-2}$ , and Yajima, Choi, & Nagamine (2012), who conclude that ionizing radiation from stars makes little difference to DLAs as it is absorbed in very dense, compact clouds that contribute little to the DLA cross section.

Berry et al. (2013) studied DLAs using semi-analytical models of galaxy formation. They found that they needed to “extend” their gas disks by giving them more than their share of the halo angular momentum in order to reproduce the observed properties of DLAs at  $z < 3$ , while all models failed at  $z > 3$ .

An important constraint on models of DLAs

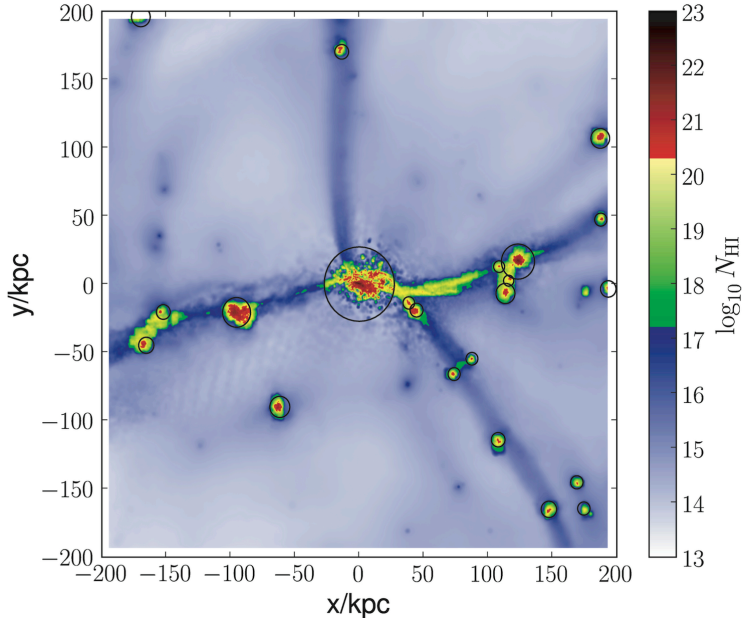


Fig. 5.— The  $z = 3$  neutral column density of HI in a 400kpc cube centred on the major progenitor to a  $z = 0$  Milky Way type galaxy in the simulations of Pontzen et al. (2008). The colours are such that DLAs ( $N_{\text{HI}} > 10^{20.3} \text{ cm}^{-2}$ ) appear in dark red and Lyman limit systems ( $10^{20.3} \text{ cm}^{-2} > N_{\text{HI}} > 10^{17.2} \text{ cm}^{-2}$ ) appear in green and yellow. The circles indicate the projected positions and virial radii of all dark-matter haloes with  $M_{\text{halo}} > 5 \times 10^8 M_{\odot}$ . All units are physical. In these and later simulations, almost all DLAs arise inside dark matter haloes, probing the ISM and CGM on typical scales of  $\sim 10\%$  of the virial radius (Rahmati & Schaye 2013b). Figure from Pontzen et al. (2008, Figure 2); used with permission.

comes from the use of cross-correlation to study host halo masses. For example, Gawiser et al. (2001); Adelberger et al. (2003); Bouché & Lowenthal (2004); Cooke et al. (2006) measured the cross-correlation of DLAs with Lyman Break Galaxies. These observations, together with the modelling of Lee et al. (2011), suggest that DLAs inhabit smaller haloes than LBGs, with average halo masses of DLAs of  $10^{11} M_{\odot}$  compared to  $10^{11.5-12} M_{\odot}$  for LBGs.

More recently, however, Font-Ribera et al. (2012) calculated the cross-correlation of DLAs in the BOSS survey with the Ly $\alpha$  forest, concluding that the derived DLA bias indicated a significantly larger typical halo mass of  $\sim 10^{12} M_{\odot}$ . This conclusion was supported by Barnes & Haehnelt (2014). They used a simple analytical model of DLAs, which reproduces the column density and velocity width distribution of DLAs, to argue that the observed DLA bias presents a significant challenge to existing DLA models and galaxy formation simulations more generally, plausibly indicating that photoionisation and stellar feedback are more efficient in ionizing and/or ejecting HI from 50 - 90  $\text{km s}^{-1}$  haloes than is accounted for in current subgrid models.

The physical picture of DLAs that emerges from these simulations can be summarised as fol-

lows.

- DLAs arise in the ISM and CGM of low-mass, gas-rich galaxies. Most absorbers with  $N_{\text{HI}} > 10^{17} \text{ cm}^{-2}$  at  $z = 3$  reside inside galaxy haloes, and either have been ejected from the ISM or will become part of the ISM by  $z = 2$  (van de Voort et al. 2012). For DLAs, ISM absorption is most likely for systems with  $N_{\text{HI}} > 10^{21} \text{ cm}^{-2}$ , with a significant fraction of DLAs not arising from the gaseous disks of spiral galaxies but rather from filaments, streams and clumps (Fumagalli et al. 2011). An example is shown in Figure 5. DLAs typically probe galaxies on  $\sim \text{kpc}$  scales, or the inner  $\sim 10\%$  of the virial radius (Rahmati & Schaye 2013b).
- DLAs arise in dark matter haloes in the mass range  $10^{10} - 10^{12} M_{\odot}$ , which have very low stellar masses  $< 10^8 M_{\odot}$  (Rahmati & Schaye 2013b). DLAs host haloes are generally smaller than the host haloes of LBGs. In this mass range, gas accretion is predicted to be via cold streams (Birnboim & Dekel 2003; Kereš et al. 2005), that is, gas which enters dark matter haloes without being shock heated above  $\sim 10^6 \text{ K}$ . Van de Voort et al. (2012) show that most of the gas in LLSs and DLAs has never been shock-heated, though

the smooth component of cold streams is highly ionized (Fumagalli et al. 2011). LLSs and DLAs at high redshift thus plausibly include the elusive cold streams of cosmological simulations.

- DLA kinematics, derived from associated metal line absorbers, remain a significant hurdle for simulations. To reproduce the high- $v_w$  systems, significant “non-gravitational” sources of motion are required, that is, velocity components beyond that of a purely virialised halo of gas. Plausible sources include the motion of satellite haloes inside a larger parent halo, and supernovae-driven galactic winds.
- The relatively low metallicity and low internal star-formation rates of DLA gas are explained by the fact that, at high redshift, they arise in gas which is on the outskirts of or outside of the ISM of small galaxies.

The typical limitations of cosmological hydrodynamical simulations — resolution, box size, sub-grid physics — all apply here. In particular, the importance of stellar and supernovae feedback to the properties of the ISM and CGM, and hence DLAs, makes theoretical predictions dependent on the details of processes that no simulation can yet resolve. The ability of Lyman alpha absorption to probe ISM and CGM gas at high redshift makes it one of the most important tests of galaxy formation simulations.

### 3. MgII Absorption Tracing HI

The MgII  $\lambda\lambda 2796, 2803$  doublet probes a large range of neutral hydrogen column densities,  $10^{16} \lesssim N(\text{HI}) \lesssim 10^{22} \text{ cm}^{-2}$  (Churchill et al. 2000a; Rigby, Charlton, & Churchill 2002), having typical temperatures of 30,000 – 40,000 K and average total hydrogen densities of  $\sim 0.1 \text{ atoms cm}^{-3}$  (Churchill, Vogt, & Charlton 2001; Ding, Charlton, & Churchill 2005). Such conditions yield a large range of MgII rest-frame equivalent widths,  $0.02 \lesssim W_r(2796) \lesssim 10 \text{ \AA}$ , that are detectable in the spectra of background quasars and galaxies probing intervening foreground objects. It has been convincingly demonstrated that MgII absorption is produced within gaseous haloes surrounding galaxies and is not produced within

the diffuse intergalactic medium (see review by Churchill, Kacprzak, & Steidel 2005).

A significant quantity of HI is probed by MgII absorption, comparable to roughly 15% of the gas residing in DLAs and 5% of the total hydrogen in stars (Kacprzak & Churchill 2011; Ménard & Fukugita 2012). Roughly 20% [50%] of all MgII absorption systems with  $0.6 \leq W_r(2796) \leq 1.7 \text{ \AA}$  [ $W_r(2796) > 1.7 \text{ \AA}$ ] are associated with DLAs. Furthermore, Ménard & Chelouche (2009) demonstrated a direct relation between the MgII rest equivalent width and the HI column density such that the geometric mean column density is  $N(\text{HI}) = AW_r(2796)^\beta$ , where  $A = (3.06 \pm 0.55) \times 10^{19} \text{ cm}^{-2} \text{ \AA}^{-\beta}$  and  $\beta = 1.73 \pm 0.26$  and is valid for  $0.5 \leq W_r(2796) \leq 3 \text{ \AA}$  and  $0.5 \leq z \leq 1.4$ .

### 3.1. MgII Absorption Statistics

Current surveys place the number of known MgII absorbers at around  $\sim 41,000$  systems spanning a redshift range of  $0.1 < z < 2.3$  (e.g., Sargent, Boksenberg & Steidel 1988; Steidel & Sargent 1992; Churchill et al. 1999; Narayanan et al. 2007; Barton & Cooke 2009; Chen et al. 2010a; Quider et al. 2011; Werk et al. 2012; Zhu & Ménard 2013; Seyffert et al. 2013) and  $\sim 100$  MgII systems spanning a redshift range of  $1.9 < z < 6.3$  (Matejek & Simcoe 2012a). The distribution of MgII rest-frame equivalent widths consists of two distinct populations: Strong systems,  $W_r(2796) > 0.3 \text{ \AA}$ , are well described by an exponential distribution (Nestor et al. 2005; Zhu & Ménard 2013; Seyffert et al. 2013), while weaker systems follow a power-law distribution (Churchill et al. 1999; Narayanan et al. 2007). These two distinct populations can be simultaneously described with a Schechter function (Kacprzak et al. 2011b).

The incidence rate  $dN/dz$  of absorption systems (number per unit redshift and rest equivalent width) provides detailed information on their cross-section and number density as a function of redshift. Seyffert et al. (2013) found that the physical cross-section of MgII absorbers increases by a factor of three between  $0.4 < z < 2.3$  for  $W_r(2796) \geq 0.8 \text{ \AA}$ . Over the redshift range  $0.4 < z < 5.5$ , the rate of incidence of weaker absorbers ( $0.6 < W_r(2796) < 1.0 \text{ \AA}$ ) is roughly constant, which suggests that these absorbers are established early and are being constantly replenished as a function of time (Zhu & Ménard 2013;

Matejek & Simcoe 2012a). Meanwhile, the incidence rate for stronger absorbers ( $W_r(2796) > 1.0 \text{ \AA}$ ) increases towards  $z \sim 2$  and then decreases towards  $z \sim 5$ , similarly to the cosmic star formation history (e.g., Bouwens et al. 2011). The strikingly similar shapes of these two quantities points to a direct connection between strong absorbers and star formation (Zhu & Ménard 2013; Matejek & Simcoe 2012a).

### 3.2. Association with Galaxies

The pioneering work of Bergeron (1988) and Bergeron & Boissé (1991) identified the first galaxies in close proximity to a quasar sight-line and at the same redshift as absorbing gas traced by MgII absorption. Of the  $\sim 41,000$  known MgII absorbers, there are  $\sim 300$  galaxies that are spectroscopically confirmed to reside at same redshift as the absorber (e.g., Nielsen et al. 2012; Werk et al. 2012). These galaxies span a redshift range of  $z = 0.1$  (Barton & Cooke 2009; Kacprzak et al. 2011a) to  $z = 2$  (Bouché et al. 2012; Lundgren et al. 2012). The small galaxy sample sizes reflect only the difficulty of obtaining large amounts of telescope time required to complete these spectroscopic surveys around quasars. In addition, stacking techniques have been used to probe 1000's of galaxy haloes (Zibetti et al. 2007; Bordoloi et al. 2011; Ménard et al. 2009).

Absorption by MgII around galaxies extends to projected galactocentric distances ( $D$ ) of  $\sim 200$  kpc. Host halo size scales with galaxy luminosity and halo mass with some dependence on galaxy colour (Steidel 1995; Zibetti et al. 2007; Kacprzak et al. 2008; Chen et al. 2010a; Nielsen et al. 2012; Churchill et al. 2013b). Using clever stacking and cross-correlation techniques between MgII absorption systems and massive red galaxies, Zhu et al. (2014) and Pérez-Ràfols et al. (2014) detect absorption out to 20 Mpc around galaxies with  $< M_h \geq 10^{13.5} M_\odot$ . These extended MgII profiles appear to change slope on scales of  $\sim 1$  Mpc, which is the expected transition from being dominated by the dark matter halo to where it is dominated by halo-halo correlations (Zhu et al. 2014).

Within these MgII haloes, the average gas covering fraction is estimated to be  $\sim 50 - 90\%$  for galaxies at  $z \sim 0.6$  (Tripp & Bowen 2005; Chen & Tinker 2008; Kacprzak et al. 2008; Chen et al.

2010a; Nielsen et al. 2012; Churchill et al. 2013a), possibly decreasing to 25% at  $z \sim 0.1$  (Barton & Cooke 2009). The gas covering fraction has a radial and azimuthal dependence that increases towards the host galaxy center and also along its major and minor axes (Nielsen et al. 2012; Kacprzak et al. 2012a). Furthermore, from halo abundance matching (see Trujillo-Gomez et al. 2011), we know that the covering fraction within a given  $D$  is constant with halo mass,  $M_h$ , over the range  $10.4 \leq \log M_h \leq 13.3$  (Churchill et al. 2013a).

It has been firmly established that rest-frame equivalent width is anti-correlated with  $D$  at the  $8\sigma$  level (Lanzetta & Bowen 1990; Steidel 1995; Churchill et al. 2000b; Kacprzak et al. 2008; Chen et al. 2010a; Rao et al. 2011; Nielsen et al. 2012; Kacprzak et al. 2013). The anti-correlation can be represented by a single log-linear relation  $\log[W_r(2796)] = (-0.015 \pm 0.002) \times D + (0.27 \pm 0.11)$  that is found to be valid for MgII absorption around galaxies within  $0 < D < 200$  kpc (Nielsen et al. 2012; Kacprzak et al. 2013). This anti-correlation could be interpreted as a radially decreasing gas density profile surrounding galaxies, although the complex velocity structure of the absorption systems, which is independent of  $D$ , suggests that the absorption arises from a variety of ongoing dynamical events within the galaxy and halo (Churchill, Steidel, & Vogt 1996). Recent work has shown that host galaxy virial mass determines the extent and strength of the MgII absorption: the mean equivalent width increases with virial mass at fixed  $D$ , and decreases with  $D$  for fixed virial mass with the majority of the absorption produced within 0.3 virial radii (Churchill et al. 2013b). On average, it appears that the MgII equivalent width is not dependent on, or is weakly correlated with, galaxy halo mass (Bouché et al. 2006; Gauthier et al. 2009; Lundgren et al. 2009; Churchill et al. 2013b; Gauthier et al. 2014).

### 3.3. Theory

Semi-analytical models and isolated galaxy simulations (e.g., Mo & Miralda-Escude 1996; Burkert & Lin 2000; Lin & Murray 2000; Maller & Bullock 2004; Chen & Tinker 2008; Kaufmann et al. 2008; Tinker & Chen 2008) have been invoked to study isolated galaxy haloes. In these models, MgII absorption typically arises from condensed, infalling,

pressure confined gas clouds within the cooling radius of the hot halo. These models reproduce the general statistical properties of the absorber population. However, they lack the dynamic influences of cosmic structures and local environments.

Currently, one of the limitations of cosmological simulations is that local sources of ionizing radiation are not properly accounted for, although some attempts have been made (Gorodt et al. 2012). Ionizing radiation can have a significant effect on high column density absorbers with  $N(\text{HI}) > 10^{17} \text{ cm}^{-2}$  where MgII absorption is typically found (Rahmati et al. 2013). None-the-less, there have been some attempts to study MgII absorption in simulations. Using simulated quasar absorption-line sightlines through cosmological simulations, Kacprzak et al. (2010a) demonstrated that MgII absorption arises in filaments and tidal streams with the gas infalling with velocities in the range of the rotation velocity of the simulated galaxy. This is consistent with simulations of Stewart et al. (2011) who showed that these cold-flows produce a circumgalactic co-rotating gaseous disk that is infalling towards the galaxy. In absorption these structures are expected to produce  $\sim 100 \text{ km s}^{-1}$  velocity offsets relative to the host galaxy in the same direction of galaxy rotation, which is consistent with observations (Steidel et al. 2002; Kacprzak et al. 2010a). The accreting gas spends only 1–2 dynamical times in this disk before accreting onto the host galaxy (Stewart et al. 2013).

Simulations have yet to consistently reproduce the observed MgII covering fractions (Ford et al. 2013, though some recent simulations are very close), which are typically underestimated by a factor of two or more. However, Stewart et al. (2011) showed that the MgII covering fraction drops dramatically for galaxies with a halo mass above  $M_h > 10^{12} M_\odot$  where cold mode accretion is predicted to be quenched when the halo is massive enough to support a stable shock near the virial radius (e.g., Dekel & Birnboim 2006; Dekel et al. 2009; Kereš et al. 2009; van de Voort et al. 2011). This phenomena may have been directly observed for one galaxy (Churchill et al. 2012b), however, Churchill et al. (2013a) has shown statistically that the covering fraction does not precipitously drop for  $M_h > 10^{12} M_\odot$ , which is in direct conflict with theoretical expectations of a mass de-

pendant truncation of cold-mode accretion.

### 3.4. Sources of MgII Absorption

The goal of absorption-line studies is to determine the exact source of the absorption so we can study specific phenomena/physics in detail. However, we have yet to determine an efficient method of conclusively determining the origin of individual systems. In general, there are five likely sources of MgII absorption: 1) ISM, 2) HVCs, 3) tidal debris, 4) galactic outflows, and 5) filamentary accretion.

#### *ISM*

A significant fraction of cool gas is located within the ISM of galaxies. MgII absorption is always detected along quasar sight-lines that probe the ISM of our Milky Way (e.g., Savage et al. 2000; Bowen et al. 1995). The majority of absorption seen in galaxy spectra arises from the ISM; only a small fraction of the absorbing gas appears to be outflowing/infalling (see Martin et al. 2012, and references therein). It is increasingly difficult to find extremely low impact parameter systems as the quasar either outshines faint foreground galaxies or becomes more obscured by large low redshift foreground galaxies. However, several studies report MgII absorption systems detected within  $\sim 5 \text{ kpc}$  of local (Bowen et al. 1996) and low-redshift galaxies (Kacprzak et al. 2013) that have a similar  $W_r(2796)$  distribution to that of the Milky Way.

#### *HVCs*

HVCs are expected to contribute to the covering fraction of MgII absorbers because they are sources of MgII absorption around local galaxies (e.g., Savage et al. 2000; Herenz et al. 2013). This contribution is difficult to compute, because we can only currently measure it for the local galaxy population. It has been estimated that roughly 30–50% of known strong MgII absorbers arise from HVCs (Richter 2012; Herenz et al. 2013). This suggests that the majority of absorbers have an alternative origin.

#### *Tidal Debris*

Low-redshift HI surveys show that galaxies having undergone a minor merger/interaction typically exhibit a perturbed/warped HI disk that is

more extended than those of isolated galaxies (e.g., Fraternali et al. 2002; Chynoweth et al. 2008; Sancisi et al. 2008). It is common to detect MgII absorption near galaxy groups. In most cases, the absorbing gas tends to have lower metallicity than the nearby host galaxies, and the absorption-line kinematics tend to be more complex. In addition, stellar tidal features are commonly seen for galaxy group members. All of the above suggests that the gas has a tidal origin within the intragroup medium (York et al. 1986; Kacprzak et al. 2007, 2010b; Rubin et al. 2010; Meiring et al. 2011; Battisti et al. 2012; Gauthier 2013). Chen et al. (2010a) demonstrates that group galaxies do not follow the well known anti-correlation between  $W_r(2796)$  and  $D$  but exhibit a more random distribution of  $W_r(2796)$  as a function of  $D$  (also see Yoon & Putman 2013). These results suggest that galaxy environment plays a role in the metal distribution within galaxy haloes.

The extreme role of environment is further evident in galaxy clusters where HI disks are truncated (e.g., Chung et al. 2009) and the CGM covering fraction is significantly reduced (Yoon & Putman 2013). In addition, MgII haloes in galaxy clusters are only  $\sim 10$  kpc in size (Lopez et al. 2008; Padilla et al. 2009).

### *Galactic Outflows*

High equivalent width MgII absorption has been observed to directly trace 100–1000 km s<sup>-1</sup> galactic-scale outflows originating from their host galaxies (Tremonti et al. 2007; Weiner et al. 2009; Martin & Bouché 2009; Rubin et al. 2010; Chelouche & Bowen 2010; Coil et al. 2011; Lundgren et al. 2012; Martin et al. 2012; Rubin et al. 2013; Bordoloi et al. 2013). These outflows can extend out to  $\sim 50$  kpc and are orientated along the galaxy minor axis (Bordoloi et al. 2011; Bouché et al. 2012; Gauthier & Chen 2012; Kacprzak et al. 2012a; Bordoloi et al. 2012; Kacprzak et al. 2014), having opening angles of  $\sim 100$  degrees (Kacprzak et al. 2012a; Bordoloi et al. 2012; Martin et al. 2012). The outflows observed in disk galaxies produce MgII equivalent widths and velocities that are higher for the face-on systems compared to the edge-on ones, which is consistent with a primarily bipolar outflow geometry (Bordoloi et al. 2013). Furthermore, the outflowing absorbing gas velocities originating from the host

galaxies appear to correlate with the host galaxy star formation rates (SFRs) and B-band magnitude/mass (Weiner et al. 2009; Rubin et al. 2010; Martin et al. 2012; Kornei et al. 2012; Bordoloi et al. 2013). Similarly, correlations between host galaxy colours and SFRs with MgII equivalent widths detected along quasar sight-lines probing their haloes also indirectly suggest that absorption is produced in outflows (Zibetti et al. 2007; Noterdaeme et al. 2010; Nestor et al. 2011).

Additional evidence of outflows is provided by a handful of absorption systems with measured metallicities near solar that exist near galaxies (Noterdaeme et al. 2012a; Krogager et al. 2013; Péroux et al. 2013; Crighton et al. 2014; Kacprzak et al. 2014). It is expected that these high metallicity systems are outflowing from their host galaxies. This is supported by the fact that some of these quasar sight-lines tend to probe galaxies along their projected minor axis, which is where outflows are expected to exist (Péroux et al. 2013; Kacprzak et al. 2014). Further evidence supporting outflows comes from combined kinematic, geometric and metallicity arguments showing that the velocities of gas outflowing directly from a galaxy at  $z = 0.2$  can reproduce the observed transverse absorption velocities found at 58 kpc along the galaxy’s projected minor axis (Kacprzak et al. 2014).

### *Filamentary Accretion*

MgII absorption has been observed infalling (Martin et al. 2012) onto highly inclined galaxies with velocities of  $\sim 200$  km s<sup>-1</sup> (Rubin et al. 2012). This is consistent with Kacprzak et al. (2011b) who showed that  $W_r(2796)$  is correlated with galaxy inclination, implying a significant fraction of absorption systems are coplanar and likely accreting toward the galaxy. The bimodal azimuthal angle distribution of quasar sight-lines with detected MgII absorption around host galaxies, shown in Figure 6, also suggests that infall occurs along the projected galaxy major axis (Bouché et al. 2012; Kacprzak et al. 2012a).

The co-rotating and infalling accretion seen in the simulations of Stewart et al. (2011) is consistent with observations of Steidel et al. (2002) and Kacprzak et al. (2010a) that show MgII absorption residing fully to one side of the galaxy systemic velocity and aligned with expected galaxy rotation

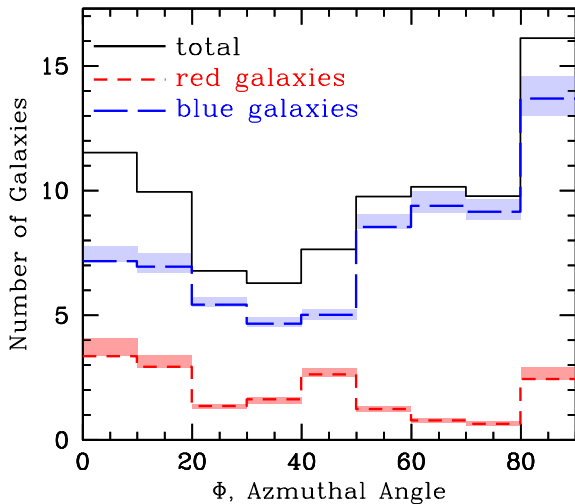


Fig. 6.— Binned azimuthal angle mean probability distribution function for all absorbing galaxies (solid line) and for blue (dash line) and red (dotted line) absorbing galaxies from Kacprzak et al. (2012a). The areas of the histograms are normalized to the total number of galaxies in each subsample. The shaded regions are  $1\sigma$  confidence intervals. The bimodal distribution suggests a preference for MgII absorbing gas toward the galaxy projected major axis ( $\Phi = 0^\circ$ ) and along the projected minor axis ( $\Phi = 90^\circ$ ). Blue galaxies dominate the bimodal distribution while red galaxies tend to have a flatter distribution.

direction — mimicking the rotation curve out into the halo.

Additional key evidence is provided by a handful of systems with measured absorption-line metallicities ranging between  $[M/H] < -1.8$  to  $-1$  that exist near galaxies that have nearly solar metallicities (Zonak et al. 2004; Chen et al. 2005; Tripp et al. 2005; Cooksey et al. 2008; Kacprzak et al. 2010b; Ribaldo et al. 2011; Thom et al. 2011; Bouché et al. 2013; Crighton et al. 2013). It is expected that these low metallicity systems are accreting onto their host galaxies and possibly trace cold mode accretion.

### 3.5. Future Progress

A large body of evidence suggests that the majority of MgII absorption traces both outflows from star-forming galaxies and accretion onto host

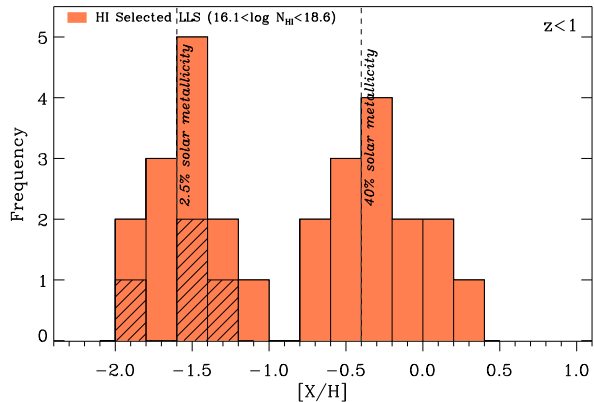


Fig. 7.— Metallicity distribution function of absorption systems with column densities of  $16.2 \leq N(\text{HI}) \leq 19$  at  $z \leq 1$  from Lehner et al. (2013). The hashed histograms highlight values that are upper limits. The metallicity distribution is bimodal where the peak values are indicated. These results are suggestive of two dominant sources giving rise to the majority of absorption-line systems: The metal-rich population tracing winds, recycled outflows, and tidally stripped gas and the metal-poor population tracing cold accretion.

galaxies. While it is clear both processes are occurring, it remains difficult to disentangle which absorption systems may be uniquely associated with either process.

Two measurements may aid in identifying which absorption systems are associated with either outflows or accretion: galaxy orientation with respect to the quasar sight-line and the absorption-line metallicity. The MgII spatial distribution relative to the host galaxy provides a promising test since outflows are expected to extend along the host galaxy minor axis (e.g., Strickland et al. 2004), while accretion should progress along filaments towards the galaxy major axis (e.g., Stewart et al. 2011). In Figure 6, Kacprzak et al. (2012a) shows that MgII absorption is primarily concentrated around the projected major and minor axis of host galaxies. Galaxies with no measurable absorption have a random distribution of quasar line-of-sight position angles. Furthermore, star-forming galaxies drive the bimodal distribution while red galaxies show some signs of gas accretion along the projected major axis

(Kacprzak et al. 2012a). This is consistent with previous works and recent models (Bordoloi et al. 2011; Bouché et al. 2012; Bordoloi et al. 2012).

In addition, since outflows are expected to be metal-enriched and accreting material metal-poor, comparing the absorption-line and host galaxy metallicity provides another suitable test for discriminating outflows from accretion (e.g., Bouché et al. 2013; Crighton et al. 2014, and references therein). Recent work by Lehner et al. (2013) shows that the metallicity distribution of Lyman limit systems,  $16.2 \leq N(\text{HI}) \leq 19$ , is bimodal with metal-poor and metal-rich populations which peak at 2.5% and 40% of solar metallicity (Figure 7). Thus, similarly to the galaxy orientation bimodality, it is suggestive of two dominant sources of the majority of absorption-line systems: the metal-rich population likely traces winds, recycled outflows, and tidally stripped gas while the metal-poor population is consistent with cold accretion.

Measuring the metallicity and relative orientations, combined with relative kinematics, yields the most promising selection criteria in isolating individual sources producing MgII absorption (see Kacprzak et al. 2014). Future HI surveys, such as WALLABY (targeting 600,000 galaxies at  $z = 0 - 0.25$ ) and DINGO (targeting 100,000 galaxies at  $z = 0 - 0.40$ ), using the Australian Square Kilometer Array Pathfinder (ASKAP) will provide complementary data that will aid in our understanding of galaxy evolution and feedback processes.

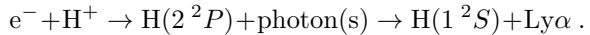
## 4. Lyman Alpha in Emission

### 4.1. Physics of Lyman Alpha Emission

Partridge & Peebles (1967) predicted that Ly $\alpha$  emission would be an excellent tracer of young galaxies. Unlike absorption lines studies, which give one-dimensional information, Ly $\alpha$  emission can trace gas in three dimensions (two spatial and one wavelength). While it was three decades before observational searches for Ly $\alpha$  emitters were successful, the detection of Ly $\alpha$  emission is now an important window into the high-redshift Universe.

The physics of Lyman alpha emission is neatly summarised by the mechanisms by which a hydrogen atom is excited into the  $2^2P$  state.

**Recombination:** when an electron and a proton combine to make neutral hydrogen, the electron may pass through the  $2^2P$  state on its way to the ground state:



For atoms at  $T = 10^4$  K, with only a weak dependence on temperature,  $\sim 42\%$  of recombinations will pass through the  $2^2P$  state on their way to the ground state and produce a Ly $\alpha$  photon,  $\sim 38\%$  will go directly to the ground state and produce an ionizing photon, and  $\sim 20\%$  go to the  $2^2S$  state, producing 2 continuum photons in a forbidden transition to the ground state (Gould & Weinberg 1996). If the surrounding medium is optically thick to ionizing radiation, then ionizing photons will be reprocessed, while Ly $\alpha$  photons are simply scattered. In this case, known as *Case B*, Ly $\alpha$  photons are emitted at  $\sim 68\%$  of the rate at which ionizing radiation is absorbed<sup>2</sup>.

Thus, the photoionisation of neutral hydrogen will produce Lyman alpha radiation. The HI could surround the photoionising source, producing *nebular* emission. In star-forming galaxies, for example, massive O and B stars (and PopIII stars) produce copious ionizing radiation (Bromm et al. 2001; Schaerer 2003; Raiter, Schaerer, & Fosbury 2010), which immediately encounters HI in the surrounding ISM from which the stars formed. Upon recombination, Ly $\alpha$  photons are emitted. Because the Ly $\alpha$  line is narrow and strong, it should (in theory) provide a signature of primeval, high-redshift galaxies.

For the same reason, ionizing radiation from quasars should light up the surrounding gas in Ly $\alpha$ . Haiman & Rees (2001) studied the effect of a quasar turning on within an assembling protogalaxy, and found that it would boost Ly $\alpha$  emission in a spatially extended region dubbed “Ly $\alpha$  fuzz”. While, observations show that the fraction of LAEs associated with AGN is a few percent (Gawiser et al. 2006; Ouchi et al. 2008), the brightest, most spatially extended emitters (“blobs”) could be driven by an obscured quasar (Overzier et al. 2013).

<sup>2</sup>Resonant absorption of a higher Lyman-series photon (Ly $\beta$ +) will also result in a cascade back to the ground state, possibly resulting in Lyman alpha emission. The Ly $\beta$ + photon itself will result from recombination or excitation, and so can be included in the respective case.

An HI cloud can also be illuminated by an external source of ionizing photons, such as the UV background or a nearby quasar. Observations of these Fluorescent Ly $\alpha$  Emitters (FLEs) hold great potential — they illuminate gas *outside* of galaxies, where most of the baryons are at high redshift. Further, for clouds that are optically thick to ionizing radiation, the surface brightness of the fluorescent emission is set by the strength of the ionizing background (Gould & Weinberg 1996; Cantalupo et al. 2007).

**Excitation:** A HI atom can be placed in the  $2^2P$  state via collisional excitation. Most collisions at the relevant temperatures place the HI atom in an  $n = 2$  state:  $\sim 25\%$  go to the  $2^2S$  and  $\sim 75\%$  go to the  $2^2P$ . Approximately 10% of the energy is lost to bremsstrahlung, meaning that  $\sim 68\%$  of the thermal energy that is radiated away by collisional excitation is in the form of Ly $\alpha$  photons (Gould & Weinberg 1996). However, the Ly $\alpha$  collisional emissivity is a strong function of temperature. For example, for gas in collisional ionisation equilibrium (e.g. self-shielded), the emissivity drops by  $\gtrsim 3 \times 10^3$  between its peak at  $1.8 \times 10^4$  K and  $1 \times 10^4$  K (Thoul & Weinberg 1995).

There is thus an important connection between Ly $\alpha$  emission and cooling radiation, long recognised as a crucial ingredient in galaxy formation (Binney 1977; Silk 1977; White & Rees 1978). Birnboim & Dekel (2003) and Kereš et al. (2005) found that gas accretes onto galaxies in two modes: a hot mode, where particles are heated to  $T_{\text{vir}} \sim 10^6$  K before cooling via bremsstrahlung and accreting onto the galaxy quasi-spherically; and a cold mode, where particles that have never been heated above  $\sim 10^5$  K are accreted along filaments, and cool primarily by Ly $\alpha$  line emission. Thus, gas that is cooling within dark matter haloes is expected to radiate a substantial fraction of its gravitational energy via collisionally excited Ly $\alpha$  emission (Haiman et al. 2000; Fardal et al. 2001).

We will examine these mechanisms and emitters in more detail in later sections. Next, we will survey the history and current status of observations of Ly $\alpha$  emission from the high-redshift universe.

## 4.2. Physics of Lyman Alpha Scattering

Lyman alpha photons are strongly scattered by HI, and so an understanding of radiative transfer effects is crucial to interpreting Ly $\alpha$  observations. With quasar absorption spectra frequently revealing HI regions with column densities  $N_{\text{HI}}$  of order  $10^{16} - 10^{22} \text{ cm}^{-2}$  (Section 2, extremely large optical depths of  $\tau_0 = 10^3 - 10^9$  are likely to be encountered by emitted Ly $\alpha$  photons (see Equation 1). This is particularly true when ionizing radiation is the source of Ly $\alpha$  photons. At temperatures of  $\sim 10^4$  K, the optical depth of HI in Ly $\alpha$  is about  $10^4$  times larger than the optical depth at the Lyman limit (Osterbrock 1989, pg. 77). A Lyman limit photon that enters an HI region will be absorbed at a depth of  $\tau_{LL} \sim 1$ . When recombination produces a Ly $\alpha$  photon, this photon will find itself at an optical depth of  $\tau_{\text{Ly}\alpha} \simeq 10^4$ .

Radiative transfer calculations are necessary for any theoretical prediction of the spectra and spatial distribution of Ly $\alpha$  emission. Ly $\alpha$  photons will typically undergo many scatterings before escaping an HI region. The properties of the emergent radiation depend sensitively on the spatial distribution, kinematics, temperature and dust content of the gas.

We will begin by examining a simple scenario for which an analytic solution is available. Harrington (1973) and Neufeld (1990) derived an analytic expression for the spectrum  $J(x, \tau_0)$  of radiation emerging from an optically thick ( $\sqrt{\pi}\tau_0 \gtrsim 10^3/a$ ), uniform, static slab of neutral hydrogen, where line-centre photons are injected at the centre of the slab, atomic recoil is neglected,  $\tau_0$  is the centre-to-edge optical depth at line-centre,  $x$  is the frequency of Ly $\alpha$  radiation relative to line centre and in units of the thermal Doppler frequency width, and  $a$  is the ratio of the Lorentz to (twice) the Doppler width. The analogue of this solution for a uniform sphere is shown in Figure 8.

The key to understanding this spectrum is that the photon executes a random walk in *both frequency and physical space*. When a photon is in the Doppler core, its mean free path is very short, so there is very little spatial diffusion. Most scatterings are with atoms that have the same velocity along its direction of motion as the atom that emitted the photon. Occasionally, however,

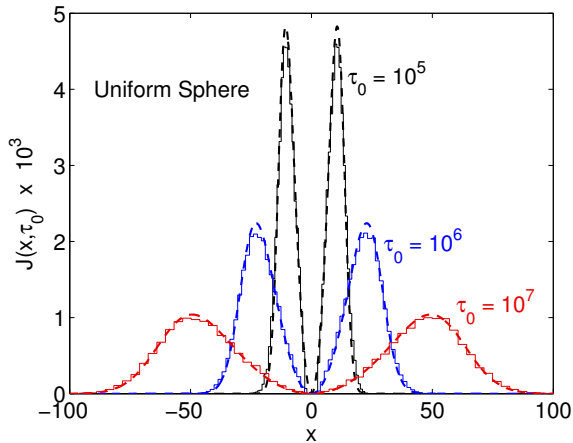


Fig. 8.— The emergent spectrum for an optically thick ( $\sqrt{\pi}\tau_0 \gtrsim 10^3/a$ ), uniform, static sphere of neutral hydrogen, where line-centre photons are injected at the centre of the slab. The  $x$ -axis shows the frequency of the emergent radiation, relative to line centre, in units of the thermal Doppler frequency width. We set the temperature of the gas to  $T = 10$  K, and  $\tau_0$  is the line-centre, centre-to-edge optical depth as labelled on the plot. The dotted line shows the analytic solution of Dijkstra et al. (2006). This solution is used as a test for Ly $\alpha$  Monte Carlo radiative transfer codes; the solid histogram shows the result of the code of Barnes & Haehnelt (2010).

the photon will collide with a very fast moving atom from the tail of the Maxwell-Boltzmann distribution, with large velocities perpendicular to the photon’s direction. When this photon is re-emitted, it will be far from line-centre. The photon is now travelling through a slab that is comparatively optically thin. What happens next depends on the optical depth of the slab ( $\tau_0$ ).

In the case of moderate optical depth ( $a\tau_0 \lesssim 10^3$ ), a single “catastrophic” scattering into the wings is enough to render the slab optically thin to the photon. A rough estimate of the frequency of the escaping photons ( $x_e$ ) is given by,

$$\tau \approx \tau_0 e^{-x_e^2} \approx 1 \quad \Rightarrow \quad x_e \approx \pm \sqrt{\ln \tau_0}. \quad (6)$$

This case is discussed in Osterbrock (1962). Adams (1972) introduced the term *single longest flight* to describe this scenario.

For extremely optically thick media ( $a\tau_0 \gtrsim 10^3$ ),

however, the optical depth in the damping wings is enough to prevent the photon from escaping from the medium in a single long flight. Instead, the photon will execute a random walk in physical space with a relatively long mean free path. Osterbrock (1962) showed that during this ‘walk in the wings’, there will also be a random walk in frequency space: the rms Doppler shift of each scatter is  $x \sim 1$ , with a mean shift per scatter of  $1/|x|$ , biased to return the photon to line-centre. Thus, after a large number of scatterings, the photon will return to the Doppler core and once again experience very little spatial diffusion. The cycle of an initial scatter to the wings followed by the random walk back to the core (in frequency space) is termed an *excursion* (Adams 1972).

It is at this point that Adams (1972) points out a mistake in Osterbrock (1962), the resolution of which is quite illuminating. Osterbrock (1962) assumes that, in extremely optically thick media, the distance travelled in any particular excursion will be small compared to the size of the region. Thus, each excursion can be considered to be a single step in an ordinary random walk. However, Adams (1972) points out that we can test this assumption by asking which is more likely to happen first: the photon uses a large number of small excursions to random-walk out of the medium, or the photon uses one large excursion to escape? Adams (1972) showed that it is the second option — photons will escape the medium on their *single longest excursion*.

We can again give a rough estimate of the escape frequency of the photons. If a photon is scattered to frequency  $x$  in the wings, and each scattering sends the frequency on average  $1/|x|$  back to the core, then each excursion will contain  $\mathcal{N} \sim x^2$  scatterings. Between each scattering, the photon will travel a physical distance  $\Delta s$  defined by  $\sigma_x n_{\text{HI}} \Delta s \sim 1$ . If this distance were travelled at line-centre, it would correspond to an optical depth of  $\Delta\tau_0 = \sigma_0 n_{\text{HI}} \Delta s = \sigma_0/\sigma_x$ . Now,  $\sigma_0/\sigma_x \approx 1/H(a, x) \sim x^2/a$ , where we have (reasonably) assumed that we are in the damping wings of the Voigt function  $H$ . Thus, between each scattering, the photon will travel a line-centre optical depth of  $\Delta\tau_0 \sim x^2/a$ . Further, after  $\mathcal{N}$  scatterings, the photon will have travelled an rms line-centre optical depth of  $\tau_0^{\text{rms}} \sim \sqrt{\mathcal{N}} \Delta\tau_0 = |x|^3/a$  (see, e.g. Rybicki & Lightman 1979, pg. 35).

The photon will escape when, in the course of an excursion, it can diffuse a distance comparable with the size of the medium, i.e.  $\tau_0^{\text{rms}} \sim \tau_0$ . Putting the above equations together, we find that the critical escape frequency is  $x_e \sim \pm(a\tau_0)^{1/3}$ . This agrees very well with the analytic solution of Harrington (1973) and Neufeld (1990) for a static slab, which has its peak at  $x_p = \pm 1.06(a\tau_0)^{1/3}$ . The static sphere solution of Dijkstra et al. (2006) has its peak at  $x_p = \pm 0.92(a\tau_0)^{1/3}$ . This means that if we modelled a DLA as a static sphere of HI at temperature  $T$  with maximum edge-to-edge column density  $N_{\text{HI}}$ , a Ly $\alpha$  photon emitted at the centre of the system will emerge with a characteristic frequency (expressed as a velocity) of:

$$v_p = 165.7 \text{ km s}^{-1} \left( \frac{T}{10^4 \text{ K}} \right)^{\frac{1}{6}} \left( \frac{N_{\text{HI}}}{2 \times 10^{20} \text{ cm}^{-2}} \right)^{\frac{1}{3}}, \quad (7)$$

even though the gas itself is static.

Given the complexity expected of the distribution and kinematics of HI in the real universe, Monte Carlo simulations are the method of choice for Ly $\alpha$  radiative transfer models. In full generality, a radiative transfer problem is specified by the number density of HI ( $n_{\text{HI}}$ ), the Ly $\alpha$  emissivity ( $\epsilon$ , in photons/s/cm<sup>3</sup>), the bulk velocity  $\mathbf{v}_b$ , the temperature ( $T$ ), and the dust number density ( $n_d$ ) and scattering/absorption properties, all as a function of position. The Monte Carlo algorithm involves creating a photon and propagating it in a random direction for a certain distance (that depends on the optical depth), at which point the photon will interact with an atom. After the interaction, the photon will have a new frequency and a new direction chosen from an appropriate distribution. We repeat until the photon escapes the system. Mock observations of the system are built up from the escaping photons. The algorithm is discussed in detail in Barnes (2009)<sup>3</sup>. A plethora of Ly $\alpha$  radiation transfer codes, based on the Monte-Carlo technique, have been published (Ahn, Lee, & Lee 2001; Zheng & Miralda-Escudé 2002; Cantalupo et al. 2005; Verhamme et al. 2006; Dijkstra et al. 2006; Hansen & Oh 2006; Tasitsiomi 2006; Laursen & Sommer-Larsen 2007; Barnes et al. 2011; Yajima et al. 2012a). Different geometrical and kinematic configurations can be tested

with these models. We will consider specific applications of such simulations in the following sections.

### 4.3. Lyman Alpha Emitters (LAEs)

**The search for Ly $\alpha$  Emitters:** For many years, attempts to detect the population of high-redshift Ly $\alpha$  Emitters (LAE) proved mostly unsuccessful (e.g. Koo & Kron 1980; Meier & Terlevich 1981; Djorgovski & Thompson 1992; de Propriis et al. 1993; Pritchett 1994; Thompson et al. 1995), with the discovery of only a handful of candidates (Wolfe et al. 1992; Møller & Warren 1993; Macchetto et al. 1993). This was in strong disagreement with the predictions of Partridge & Peebles (1967), who predicted emission lines as intense as a few  $10^{45}$  erg s<sup>-1</sup> (corresponding to fluxes of a few  $10^{-14}$  erg s<sup>-1</sup> cm<sup>-2</sup> at  $z = 3$ ), that should have been seen by the aforementioned surveys. For example, Thompson et al. (1995) conducted both shallow/wide survey ( $F_{\text{Ly}\alpha} \gtrsim 10^{-16}$  erg s<sup>-1</sup> cm<sup>-2</sup> over  $\approx 10^5$  Mpc<sup>3</sup>) and a deeper/smaller one ( $F_{\text{Ly}\alpha} \gtrsim 10^{-17}$  erg s<sup>-1</sup> cm<sup>-2</sup> over  $\approx 10^3$  Mpc<sup>3</sup>) using narrow-band (NB) imaging at  $\sim 3 - 5$  that led to no detections.

Telescopes remained blind to the long-sought distant Ly $\alpha$  galaxy population until the late 90's, and the advent of high-sensitivity and larger collecting-area instruments. Hu et al. (1998) detected 10 LAE candidates with the 10m Keck II telescope in a deeper survey at  $z = 3.4$  spanning only 46 arcmin<sup>2</sup> over  $\delta z = 0.07$ . Their sensitivity ( $L_{\text{Ly}\alpha} \gtrsim 10^{42}$  erg s<sup>-1</sup>) enabled them to find a more common, faint, LAE population. Rhoads et al. (2000) found  $\sim 150$  bright LAEs ( $L_{\text{Ly}\alpha} \gtrsim 5.10^{42}$  erg s<sup>-1</sup>) at  $z = 4.5$  as part of the Large Area Lyman Alpha survey (Rhoads et al. 2000; Malhotra & Rhoads 2002). Their observations took advantage of the 8192<sup>2</sup> pixel CCD Mosaic camera at the 4 m Mayall telescope of Kitt Peak National Observatory to cover 0.72 deg<sup>2</sup> in the redshift range  $4.37 \leq z \leq 4.57$ , corresponding to a volume of almost  $10^6$  Mpc<sup>3</sup>. The large surveyed volume allowed them to probe rarer, brighter LAEs.

Many ideas have been suggested to explain the previous failures to uncover high-redshift LAEs, e.g. short Ly $\alpha$  emission duty cycle (Charlot & Fall 1993), stellar absorption (Valls-Gabaud 1993), or line suppression due to metals and dust (Meier & Terlevich 1981; Hartmann et al. 1988; Charlot &

<sup>3</sup>Available at [www.dspace.cam.ac.uk/handle/1810/224480](http://www.dspace.cam.ac.uk/handle/1810/224480).

Fall 1993). In addition, the models of Partridge & Peebles (1967) were based on the monolithic collapse paradigm of galaxy formation, which overpredicts the Ly $\alpha$  luminosities of galaxies in the early Universe.

Haiman & Spaans (1999), using a hierarchical galaxy formation formalism and a simple model of dust extinction, showed that the properties of the population observed by Hu et al. (1998) could be roughly recovered. Moreover, the escape of Ly $\alpha$  photons from galaxies is very sensitive to resonant scattering in HI gas (e.g. Hummer 1962; Auer 1968; Harrington 1973; Ahn, Lee, & Lee 2001). Indeed, even for low dust content the observed fluxes can be considerably reduced because of dust grain absorption along the increased path of resonantly scattered Ly $\alpha$  photons (Hummer & Kunasz 1980; Neufeld 1990; Charlot & Fall 1991). An extreme example of the impact of Ly $\alpha$  resonant scattering is the strong Ly $\alpha$  absorption profile observed in metal/dust-poor low-redshift galaxies (Kunth et al. 1994; Ostlin et al. 2009). Similar processes are thought to alter Ly $\alpha$  spectra of high-redshift galaxies, and therefore the visibility of LAEs (see Section 4.2).

Ly $\alpha$  radiative transfer is strongly affected by interstellar gas kinematics, geometry and ionisation state (Kunth et al. 1998; Tenorio-Tagle et al. 1999; Shapley et al. 2003; Mas-Hesse et al. 2003; Verhamme et al. 2006; Laursen et al. 2009; Yajima et al. 2012a), dust distribution (Neufeld 1991; Hansen & Oh 2006), intergalactic attenuation (Madau 1995; Dijkstra et al. 2007a), making the interpretation of Ly $\alpha$  observations difficult. We will next discuss such observations of LAEs, returning to theory in Section 4.4.

**Observational Methods:** Ly $\alpha$  photons emitted at high redshift ( $2 \lesssim z \lesssim 7$ ) can be detected from the ground in the optical and near infrared. However, only certain spectral ranges are free from confusion due to night sky line emission. This translates into a series of redshift windows at which LAEs can be observed from earth.

At low redshift ( $z \lesssim 2$ ), the Ly $\alpha$  line is seen in the ultra-violet and one needs to utilise space instrumentation. Observations in the local universe are even more restricted due to (i) the strong geocoronal emission which blinds nearby

Ly $\alpha$  emission lines, and (ii) the damped HI absorption produced by the Galactic centre, which suppresses many lines of sight. Nevertheless, low-redshift LAEs have been studied by space-based telescopes, e.g. with the HST (*Hubble Space Telescope*, Kunth et al. 1998; Ostlin et al. 2009), IUE (*International Ultraviolet Observatory*, Meier & Terlevich 1981; Terlevich et al. 1993) and GALEX (*Galaxy Evolution Explorer*, Deharveng et al. 2008; Cowie et al. 2010). Observations of nearby LAEs probe galaxies on small scales, providing detailed Ly $\alpha$  and multi-wavelength mapping of the interstellar and circumgalactic media (e.g. Hayes et al. 2013a). Although samples are still rather small, the analysis of well-resolved objects can serve as a useful benchmark for interpreting high-redshift data (Mas-Hesse et al. 2009).

At high redshift, thousands of galaxies have been found via the Ly $\alpha$  emission line; Table 1 presents a compilation of Ly $\alpha$  surveys. The most popular imaging technique to detect LAEs requires a set of broad- and narrow-band (NB) filters to detect the emission line at the redshifted Ly $\alpha$  wavelength (e.g. Ouchi et al. 2008, and references in Table 1). Figure 9 shows examples of the various filters used with the Subaru/SuprimeCam to detect LAEs at  $z = 3.1, 3.7, 4.5, 4.9, 5.7$  and  $6.6$ . Colour-magnitude selections are usually applied to the NB detections to ensure the reliability of the LAE candidates and remove contaminants from the sample, such as lower redshift H $\alpha$ , OII or OIII emitters. These criteria can introduce a bias if they preferentially select LAEs with large equivalent widths, or if they eliminate objects without a signature of IGM attenuation shortward 1216 Å, hence missing galaxies located on *clean lines of sight*. Although the number of clear sightlines is reduced at high redshift as IGM opacity increases (Laursen, Sommer-Larsen, & Razoumov 2011), ionizing emission from the galaxy itself is expected to photoionise the surrounding HI gas.

Alternatively, Ly $\alpha$  emission lines can be identified spectroscopically in blind surveys, or as part of a follow-up of NB candidates. Spectroscopic observations have been carried out by several teams in the last years, e.g. Rauch et al. (2008) with VLT/FORS2, Kashikawa et al. (2011) with Subaru/FOCAS and Keck II/DEIMOS, and Cassata et al. (2011) with VLT/VIMOS. Parameters such as Ly $\alpha$  equivalent width are usually

Table 1: (Non-exhaustive) Compilation of surveys of LAEs.

Reference	Redshift	$N_{\text{obj}}$	$\text{EW}_{\text{Ly}\alpha}^{\text{lim}}$	$L_{\text{Ly}\alpha,42}^{\text{lim}}$	Ident. technique	Instrument	Area
	(1)	(2)	(3)	(4)	(5)	(6)	(7)
Barger, Cowie, & Wold (2012)	0.67 – 1.16	28	20	3	grism	GALEX	2286
Blanc et al. (2011)	1.9 – 3.8	98	20	4 ( $z \approx 3$ )	IFS	VIRUS	169
Guaita et al. (2010)	$2.07^{\pm 0.02}$	250	20	0.64	NB	MOSAIC	998
Cassata et al. (2011) (Deep)	2 – 6.62	42	–	$\approx 0.4$ ( $z \approx 3$ )	MOS	VIMOS	2230
Cassata et al. (2011) (Ultra-Deep)	2 – 4	188	–	$\approx 0.1$ ( $z \approx 3$ )	MOS	VIMOS	576
Hayes et al. (2010)	$2.2^{\pm 0.05}$	38	20	0.3	NB	FORS1	56
Nilsson et al. (2009)	$2.26^{\pm 0.05}$	170	20	2.3	NB	WFI	1190
van Breukelen et al. (2005)	2.3 – 4.6	14	–	1.1 ( $z \approx 3$ )	IFS	VIMOS	1.4
Rauch et al. (2008)	2.67 – 3.75	27	–	$\approx 0.1$ ( $z \approx 3$ )	S-S	FORS2	0.252
Grove et al. (2009)	2.8 – 3.2	83(59)	25	$\approx 0.4$	NB-MOS	FORS1-2	133
Yamada et al. (2005)	3 – 5	198	20	5 ( $z \approx 4$ )	IB	S-Cam	944
Hayashino et al. (2004)	$3.09^{\pm 0.03}$	283	37	4.1	NB	S-Cam	770
Ciardullo et al. (2012)	$3.1^{\pm 0.04}$	141	20	2.1	NB	MOSAIC II	$\approx 1000$
Gronwall et al. (2007)	$3.11^{\pm 0.02}$	162	20	1.2	NB	MOSAIC II	993
Kudritzki et al. (2000)	$3.13^{\pm 0.01}$	9	–	1.8	S-S	FORS	50
Ouchi et al. (2008)	$3.13^{\pm 0.03}$	356(41)	64	1	NB	S-Cam (FOCAS-VIMOS)	3538
Cowie & Hu (1998)	$3.44^{\pm 0.03}$	10	17	2	NB	LRIS	46
Ouchi et al. (2008)	$3.69^{\pm 0.03}$	101(26)	44	4	NB	S-Cam (FOCAS-VIMOS)	3474
Fujita et al. (2003)	$3.71^{\pm 0.12}$	6	53	5	IB	S-Cam	132
Malhotra & Rhoads (2002)	$4.47^{\pm 0.10}$	194(110)	14	5	NB	MOSAIC	1116
Ouchi et al. (2003)	$4.86^{\pm 0.03}$	87	14	0.8	NB	S-Cam	543
Shioya et al. (2009)	$4.86^{\pm 0.03}$	79	11	3	NB	S-Cam	6588
Hu et al. (2004)	$5.68^{\pm 0.05}$	24(19)	17	7.5	NB	S-Cam (DEIMOS)	918
Murayama et al. (2007)	$5.7^{\pm 0.05}$	119	18	6.3	NB	S-Cam	6696
Ajiki et al. (2003)	$5.7^{\pm 0.05}$	20(2)	25	7	NB	S-Cam (FOCAS-ESI)	720
Ajiki et al. (2006)	$5.7^{\pm 0.05}$	14	17	4.8	NB	S-Cam	320
Hu et al. (2010)	$5.7^{\pm 0.05}$	87	–	5.6	NB	S-Cam (DEIMOS)	4168
Ouchi et al. (2008)	$5.7^{\pm 0.05}$	401(17)	27	3	NB	S-Cam (FOCAS-VIMOS)	3722
Shimasaku et al. (2006)	$5.7^{\pm 0.05}$	89(28)	17	2.2	NB	S-Cam (FOCAS-DEIMOS)	725
Rhoads & Malhotra (2001)	$5.73^{\pm 0.06}$	18	14	5	NB	MOSAIC	1116
Dressler et al. (2011)	$5.75^{\pm 0.05}$	122	–	1	MNS	IMACS	110
Hu et al. (2010)	$6.54^{\pm 0.08}$	27	–	6.7	NB	S-Cam (DEIMOS)	4168
Kashikawa et al. (2006)	$6.56^{\pm 0.05}$	75(17)	17	2	NB	S-Cam (FOCAS-DEIMOS)	876
Ouchi et al. (2010)	$6.56^{\pm 0.05}$	207(24)	14	2.5	NB	S-Cam (DEIMOS)	3238
Hibon et al. (2012)	$7^{\pm 0.04}$	7	–	9	NB	S-Cam	2340
Shibuya et al. (2012)	$7.26^{\pm 0.08}$	4(1)	0	10	NB	S-Cam (FOCAS-DEIMOS)	1718
Hibon et al. (2010)	$7.7^{\pm 0.01}$	7	–	6	NB	WIRCAM	390
Tilvi et al. (2010)	$7.7^{\pm 0.005}$	4	–	5	NB	NEWFIRM	784
Krug et al. (2012)	$7.7^{\pm 0.01}$	4	–	5	NB	NEWFIRM	760

**Columns:** Col. (1): Redshift. Col. (2): Number of LAE detections (Number of candidates confirmed with spectroscopy). Col. (3): Ly $\alpha$  rest-frame Equivalent Width threshold (Å). Col. (4): Ly $\alpha$  luminosity threshold in units of  $10^{42}$  erg s $^{-1}$  (we assume  $h = 0.7$ ,  $\Omega_m = 0.3$  and  $\Omega_\Lambda = 0.7$ ). Col. (5): Observational technique to identify Ly $\alpha$  sources. Col. (6): Instrument used for detection (Instrument used for follow-up observation). Col. (7): Field size (arcmin $^2$ ).

**Acronyms:** NB: *Narrow-band imaging*. IB: *Intermediate-band imaging*. S-S: *Slit-Spectroscopy*. IFS: *Integral Field Spectroscopy*. MOS: *Multi-Object Spectroscopy*. S-Cam: *Suprime-Cam*. MNS: *Multi-slit Narrow-band Spectroscopy*.

Some flux/EW limits and survey areas/depths given in this table are only approximate values; the reader should refer to the original articles for full details on the surveys. Similarly, the number of LAEs that we quote,  $N_{\text{obj},i}$  can either correspond to the total number of detections, or to the number of objects used to compute the luminosity functions.

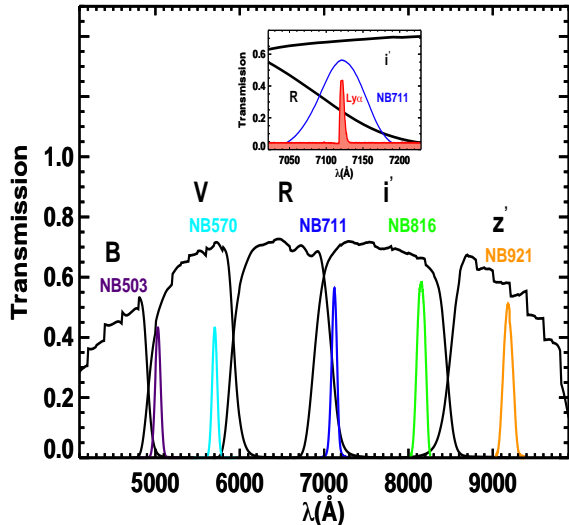


Fig. 9.— *Main panel*: Set of broad-band (black curves: B, V, R,  $i'$  and  $z'$ ) and narrow-band filters (coloured curves: NB503, 570, 711, 816, 921) used in Ouchi et al. (2003, 2008, 2010) with Subaru/SuprimeCam to detect LAEs at  $z = 3.1, 3.7, 4.5, 4.9, 5.7$  and  $6.6$ . *Inner panel*: Illustration of a  $\text{Ly}\alpha$  emission line (red curve) interpreted as a  $z = 5.7$  LAE.

measured more accurately with spectroscopy than with narrow-band imaging, but slit losses and sky noise can still introduce significant errors in the measurement of the flux.

Another efficient way to search for line emitters is Integral-Field Spectroscopy (IFS): the spectra of many sources are acquired simultaneously in a large field-of-view. At fixed sensitivity, this method considerably reduces the integration time required to observe a given number of galaxies. The first attempt to find LAEs with IFS was by van Breukelen et al. (2005) with the VLT/VIMOS integral field unit. More recently, Blanc et al. (2011) used the Visible Integral-field Replicable Unit Spectrograph (VIRUS; Hill et al. 2010) in the HETDEX Pilot survey to observe about a hundred LAEs at  $1.9 < z < 3.8$ . The Multi Unit Spectroscopic Explorer (MUSE; Bacon et al. 2006), recently installed at the VLT,

will probe LAEs at redshifts between 2.8 and 6.7, reaching  $\text{Ly}\alpha$  surface brightness limits of  $2 \times 10^{-19} \text{ erg s}^{-1} \text{ cm}^{-2} \text{ arcsec}^{-2}$  in  $\sim 80$  hour integrations. The Keck Cosmic Web Imager (KCWI; Martin et al. 2010) aims to detect faint  $\text{Ly}\alpha$  emission from the CGM at  $2 < z < 6$  to similar limiting surface brightness limits.

Another method is Multi-slit Narrow-band Spectroscopy (MNS), in which a narrow or intermediate bandpass is used to select an air-glow free spectral region to find LAE candidates. The MNS technique, pioneered by Crampton & Lilly (1999) and Martin & Sawicki (2004), was used by Martin et al. (2008) and Dressler et al. (2011) with the Inamori-Magellan Areal Camera & Spectrograph (IMACS; Dressler et al. 2006) to detect LAEs.

All methods to identify LAEs must face the problem of false positives, interlopers that can be confused with  $\text{Ly}\alpha$  emitting galaxies. In addition to low-redshift emission line objects (galaxies or AGN), AGN located at the same redshift as the targeted galaxies can contaminate LAE samples at the level of a few percent (Ouchi et al. 2008).

In addition to  $\text{Ly}\alpha$ -selected surveys,  $\text{Ly}\alpha$  emission is also often seen in Lyman Break Galaxies (hereafter, LBG; Steidel & Hamilton 1993; Steidel et al. 1999), which are selected via their a) intense UV magnitude, and b) the discontinuity caused by photoelectric absorption ( $\lambda < 912 \text{ \AA}$ ) in the interstellar medium and line blanketing by the intervening  $\text{Ly}\alpha$  forest ( $912 > \lambda > 1216 \text{ \AA}$ ). The Lyman break technique (or dropout technique) efficiently selects high-redshift, star-forming, galaxies using a set of broad-band UV and optical filters (Steidel et al. 2003; Gabasch et al. 2004; Bouwens et al. 2007; McLure et al. 2009; Bouwens et al. 2011, and references therein).

#### Statistical properties of $\text{Ly}\alpha$ Emitters:

LAEs observed in current surveys span a range of  $\text{Ly}\alpha$  luminosities from  $\sim 10^{42} \text{ erg s}^{-1}$  to a few times  $10^{43} \text{ erg s}^{-1}$  (e.g. Shimasaku et al. 2006; Gronwall et al. 2007; Ouchi et al. 2008). The typical  $\text{Ly}\alpha$  luminosity reached by wide-field surveys probes star-formation rates (SFR) greater than  $\sim 1 M_{\odot} \text{ yr}^{-1}$ , according to,

$$L_{\text{Ly}\alpha} = 1.1 \times 10^{42} \left( \frac{\text{SFR}}{M_{\odot} \text{ yr}^{-1}} \right) \text{ ergs}^{-1}. \quad (8)$$

This equation is derived from the SFR- $H\alpha$  relation for constant star formation rate (Kennicutt 1983, 1998) and the  $Ly\alpha$ - $H\alpha$  emissivity ratio under Case B recombination (Brocklehurst 1971; Osterbrock & Ferland 2006). The following assumptions are made to compute the coefficient in Eq. (8): (i) Salpeter IMF, (ii) solar metallicity, (iii) and ionisation bound nebula (no ionizing photon can escape the medium). The conversion factor can vary significantly if we modify these assumptions, especially for very low metallicities or extreme IMF cut-off (Schaerer 2003; Raiter, Schaerer, & Fosbury 2010).

The  $Ly\alpha$  Luminosity Function (LF) at various redshifts has been used to characterise the evolution of LAEs as a population. It does not seem to evolve significantly from  $z = 6$  to 3 as the characteristic number density ( $\Phi^* \sim 10^{-3} \text{ Mpc}^{-3}$ ) and luminosity of LAEs ( $L^* \sim \text{a few } 10^{42} \text{ erg s}^{-1}$ ) appear to remain almost unchanged over this redshift range (Hu et al. 1998; Ouchi et al. 2008; Cassata et al. 2011)<sup>4</sup>. It is worth noticing that, unlike the  $Ly\alpha$  LF, the UV LF of LBGs evolves significantly (as expected in a hierarchical growth scenario), its characteristic luminosity being about ten times larger at  $z = 3$  than at  $z = 6$  (Gabasch et al. 2004; Bouwens et al. 2007; McLure et al. 2009; Bouwens et al. 2011).

The non-evolution of the  $Ly\alpha$  LF is a subject of debate. Hu et al. (2010) find a significantly lower abundance of LAEs at  $z = 5.7$  than Ouchi et al. (2008) and Shimasaku et al. (2006). The former argue that the photometric sample of Ouchi et al. (2008) at the same redshift might contain a large fraction of contaminants, leading them to strongly overestimate the  $z = 5.7$  LF. However, the recent spectroscopic follow-up of the Shimasaku et al. (2006) sample at the same redshift by Kashikawa et al. (2011) seems to favour a low

<sup>4</sup>Although the  $Ly\alpha$  LFs reported by Ouchi et al. (2008), Gronwall et al. (2007) and Cassata et al. (2011) at  $z \sim 3$  are in good agreement, these surveys have applied very different LAE selection criteria. Ouchi et al. (2008) select only strong line emitters ( $EW > 64 \text{ \AA}$ ), whereas Gronwall et al. (2007) use  $EW > 20 \text{ \AA}$ . The spectroscopic survey of Cassata et al. (2011) does not apply any EW selection. A large fraction of the LAEs reported by Gronwall et al. (2007) and Cassata et al. (2011) have  $EW < 64 \text{ \AA}$ , which might have been missed by Ouchi et al. (2008). The apparent agreement between  $z = 3$  LFs may be affected by observational uncertainties and cosmic variance.

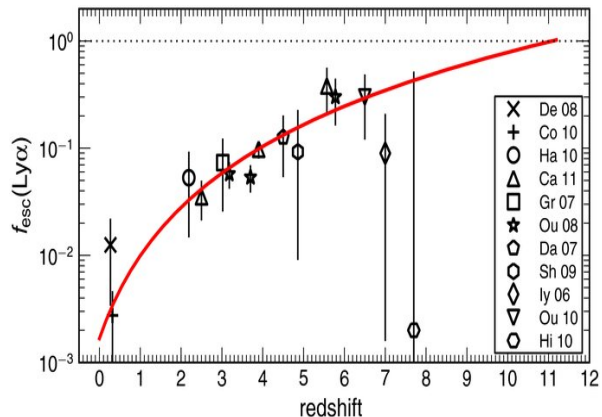


Fig. 10.— Redshift evolution of the *sampled-average volumetric*  $Ly\alpha$  escape fraction reported by Hayes et al. (2011). Symbols correspond to values derived from observations ( $Ly\alpha$ ,  $H\alpha$  and UV), and the red solid line is the best-fitting power-law to the data points ( $\propto (1+z)^{2.6}$ ). The dotted line denotes the 100% escape fraction limit, which is reached at  $z = 11$  according to the fitting relation. (Reproduced by permission of the AAS.)

contamination rate and a value of  $\Phi^*$  consistent with Ouchi et al. (2008), though slightly smaller. Additional and more homogeneous datasets with spectroscopic confirmations will refine constraints on the  $Ly\alpha$  LFs.

A differing evolution of the  $Ly\alpha$  and UV LFs would imply a variation with redshift of the mechanisms that power the  $Ly\alpha$  emission, or more probably the ability of  $Ly\alpha$  photons to escape galaxies. Hayes et al. (2011) have quantified this evolution in terms of the *sampled-average volumetric*  $Ly\alpha$  escape fraction, defined as the ratio of observed to intrinsic  $Ly\alpha$  luminosity density. Figure 10 (from Hayes et al. (2011)) illustrates the rise of this volumetric escape fraction from  $z \approx 0 - 6$ . They find an evolution of the escape fraction that scales like  $(1+z)^{2.6}$  over this redshift range (red curve). Although it is not shown on this figure, we note that the  $f_{esc}(Ly\alpha)$  value derived by Wold, Barger, & Cowie (2014) at  $z = 1$  is fully consistent with this relation.

Dijkstra & Jeesson-Daniel (2013) derive an effective  $Ly\alpha$  escape fraction from SFR and  $Ly\alpha$  luminosity functions, instead of luminosity densities (see also Blanc et al. 2011). Their results

are in good agreement with those of Hayes et al. (2011), except at  $z = 0.35$ . Indeed, the value quoted by Hayes et al. (2011) at this redshift may be underestimated, because  $f_{\text{esc}}(\text{Ly}\alpha)$  is computed by comparing the Ly $\alpha$  luminosity density (as observed above a given detection threshold) to the total SFR density.

Regarding the faint-end slope of the Ly $\alpha$  LF, and its evolution with redshift, low luminosity sources have been found in very deep surveys down to a few  $10^{-18}$  erg s $^{-1}$  cm $^{-2}$  (Rauch et al. 2008; Cassata et al. 2011; Dressler et al. 2011). The data seem to favour steeper slopes (and especially a steepening towards higher redshift). However, the number of detections at such low fluxes is limited; larger samples are required to draw robust conclusions.

A valuable observable to tackle questions of Ly $\alpha$  emission and radiative transfer is the Ly $\alpha$  equivalent width (EW), which measures the intensity of the line with respect to the adjacent continuum. Most LAEs have (*rest-frame*) Ly $\alpha$  EW between 0 and 100 Å; the tail of the distribution extends to 250 Å (Shimasaku et al. 2006; Gronwall et al. 2007; Ouchi et al. 2008; Cassata et al. 2011). Higher EW values have been claimed (e.g. Malhotra & Rhoads 2002; Dawson et al. 2007; Adams et al. 2011), and recently Kashikawa et al. (2012) reported a  $z=6.5$  LAE with  $\text{EW} = 436_{149}^{+422}$  Å. Such large EW are surprising because they exceed the standard limit of 240 Å set by theoretical models of stellar-powered Ly $\alpha$  emission (Charlot & Fall 1993). Assuming that these extreme EW are real Ly $\alpha$  sources, they might hint at a top-heavy IMF, very-low metallicity stars (Schaerer 2003) or radiative transfer effects in neutral hydrogen (see Section 4.4; and also Neufeld 1991). They could also imply that Ly $\alpha$  emission is not powered by star formation alone. Indeed, such measurements are often lower limits with no obvious continuum detection, so other processes like cooling radiation or fluorescence may contribute significantly to the Ly $\alpha$  emission.

In recent years, several groups have studied the link between LAEs and LBGs. Shapley et al. (2003) find that half of  $z = 3$  LBGs have detectable Ly $\alpha$  emission, and only 25% display a Ly $\alpha$  equivalent width larger than 20 Å. As part of a spectroscopic survey of faint LBGs, Stark et al. (2011) have characterized the fraction of

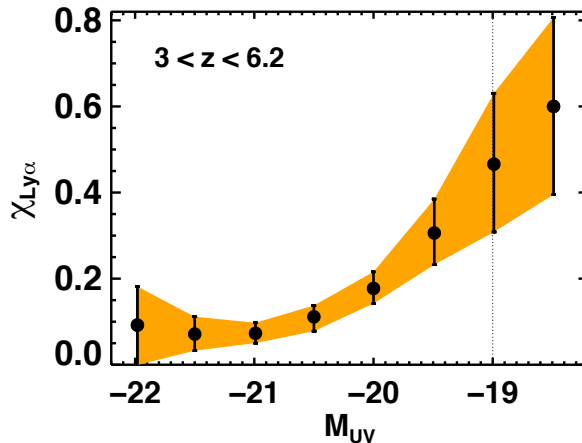


Fig. 11.— Evolution of the fraction  $\chi_{\text{Ly}\alpha}$  of strong Ly $\alpha$  emitters ( $\text{EW} > 50\text{\AA}$ ) as a function of rest-frame absolute UV magnitude for Lyman-Break galaxies between  $z = 3$  and 6.2 observed by Stark et al. (2010). Black circles correspond to the fraction  $\chi_{\text{Ly}\alpha}$  per magnitude bin, and the orange region encloses the error bars. We see that  $\chi_{\text{Ly}\alpha}$  increases gently from 10 to 50 % between  $M_{\text{UV}}^* = -22$  to  $-19$ . The dotted vertical line gives the 90% completeness limit of the dropout galaxies sample.

Ly $\alpha$  emitting galaxies within UV continuum-selected dropout galaxies between  $z = 3$  and 7. They find that the fraction of strong emitters ( $\text{EW} > 50\text{\AA}$ ) increases towards fainter UV luminosities. As shown in Figure 11 (black points and error bars), the LAE fraction increases from  $\approx 10\%$  at  $M_{\text{UV}} = -21$  to about 50% for galaxies as faint as  $M_{\text{UV}} = -19$  at  $3 < z < 6.2$ . This result echoes the observed trend between UV magnitude and Ly $\alpha$  EW: UV bright galaxies have lower Ly $\alpha$  EW, while fainter ones seem to be stronger Ly $\alpha$  emitters on average (Ando et al. 2006; Ouchi et al. 2008). Further, the fraction of Ly $\alpha$  emitting galaxies at fixed UV luminosity is found to increase from  $z \approx 3$  to 6 (Stark et al. 2010, 2011; Curtis-Lake et al. 2012). The rise is even more significant when considering weaker Ly $\alpha$  line emitters ( $\text{EW} > 25\text{\AA}$ ; Ono et al. 2012).

Untangling the relationship between the LAE and LBG populations is complicated by their re-

spective selection criteria. Gawiser et al. (2006) points out that up to 80% of narrow-band selected LAEs have the right colours to be detected by typical LBG surveys at  $z = 3$ , but only 10% are bright enough in the UV continuum (assuming a detection limit of  $R_{AB} \leq 25.5$ ). Indeed, narrow-band surveys of LAEs preferentially pick up low-continuum galaxies. Nevertheless, the fraction of LAEs among samples of dropout galaxies increases as fainter LBG surveys are carried out (e.g. Stark et al. 2010). Ly $\alpha$  emission from high-redshift sources, and its variation with respect to the physical properties of galaxies, remains to be fully understood.

**Physical properties of Ly $\alpha$  Emitters:** The HI gas distribution of LAEs can be constrained by comparing the spatial extent of Ly $\alpha$  and UV emission. Bond et al. (2011) and Gronwall et al. (2011) conducted HST imaging on a subsample of  $z = 3$  LAEs previously Ly $\alpha$ -selected by Gronwall et al. (2007). They find that the Ly $\alpha$  emission of these objects is typically compact ( $< 1.5$  kpc), and almost coincides with the far-UV ( $< 1$  kpc) that traces the young stars. This contrasts with similar observations at lower redshift, which suggest that Ly $\alpha$  is more extended than the UV continuum and H $\alpha$  emission by factors of 2-3 (Hayes et al. 2013a). This could indicate an evolution of the morphology of LAEs with redshift, or at least a change in the neutral gas distribution surrounding those galaxies (Ostlin et al. 2009; Nilsson et al. 2009; Bond et al. 2012). Deeper observations by Steidel et al. (2011) show a diffuse halo of Ly $\alpha$  emission extending well beyond the galaxy; these observations will be discussed further in Section 4.5.

Physical properties of LAEs have been studied with multiband photometry and stacking. These analyses reveal that these objects have moderate star formation rates ( $1 - 10 M_{\odot} \text{ yr}^{-1}$ ) and low stellar masses ( $10^7 - 10^9 M_{\odot}$ ) (Gawiser et al. 2006; Finkelstein et al. 2007; Ono et al. 2010b; Vargas et al. 2013), such that LAEs are thought to be the building blocks of local L\* galaxies (Gawiser et al. 2007). LAEs are also believed to host young stellar populations on average ( $\lesssim 100$  Myr) and have low dust content, as suggested by their blue colours (Ouchi et al. 2008; Ono et al. 2010b). These characteristics are also typical of local galaxies with

Ly $\alpha$  in emission (Hayes et al. 2013b). Note that higher stellar masses, older ages, and significant dust extinction have also been reported by Finkelstein et al. (2009), Pentericci et al. (2009) and Ono et al. (2010a), which may highlight an inherent spread in the population of LAEs. Further uncertainties arise from SED fitting techniques and their assorted assumptions: star formation history, IMF, dust model, nebular emission, etc (Finkelstein et al. 2009; Schaerer & de Barros 2009).

Compared to LAEs, LBGs are on average larger (a few kpc), more massive ( $10^{10} - 10^{11} M_{\odot}$ ), highly star-forming ( $10 - 1000 M_{\odot} \text{ yr}^{-1}$ ), old ( $\approx 1$  Gyr), and dusty ( $E(B-V) \approx 0.3$ ) (Adelberger & Steidel 2000; Papovich et al. 2001; Shapley et al. 2001; Giavalisco 2002). The rest frame UV sizes of LAEs and LBGs are similar at  $z \sim 5$ , and thereafter LBGs grow as  $H(z)^{-1}$  while LAEs remain remarkably constant (Malhotra et al. 2012). Shapley et al. (2001) divided their sample of  $z = 3$  LBGs in two categories, according to the age of the stellar populations. They find that the old sample ( $\approx 1$  Gyr) contains stronger Ly $\alpha$  emitters than the young galaxy sample ( $< 35$  Myr). While the two samples show rather similar stellar masses, older galaxies are more dusty and less star-forming. Shapley et al. (2001) propose an evolutionary sequence for LBGs: young, starbursting galaxies quickly produce dust, extinguishing their Ly $\alpha$  emission; later, when dust content has decreased (possibly ejected by Type II supernovae), Ly $\alpha$  is seen in emission. While supported by the work of Kornei et al. (2010) and GALEX observations of Oteo et al. (2012) at  $z \sim 0.3$ , this picture contrasts with other observations reporting that Ly $\alpha$  emission is preferentially found in younger galaxies (Gawiser et al. 2006; Pentericci et al. 2007; Finkelstein et al. 2007; Pirzkal et al. 2007; Cowie, Barger, & Hu 2011), and with the older idea that Ly $\alpha$  emission is related to an early phase of galaxy formation (Hu & McMahon 1996; Dijkstra & Wyithe 2007).

As an added complication, it has been shown that the relation between Ly $\alpha$  emission and colour excess  $E(B-V)$  is scattered. While Ly $\alpha$  emission is often found to anti-correlate with dust extinction (Shapley et al. 2003), young and dusty objects can also appear as Ly $\alpha$  emitters (Finkelstein et al.

2009; Pentericci et al. 2009; Yuma et al. 2010).

While Ly $\alpha$  emission is an excellent tool for detecting high-redshift galaxies, questions remain about the nature of LAEs and their link with LBGs. The observed scatter in the relations between Ly $\alpha$  emission and the physical properties of galaxies calls for a better understanding of the processes governing the production and the radiative transfer of Ly $\alpha$  photons. Theoretical models are therefore crucial to decyphering the Ly $\alpha$  signature of high-redshift galaxies.

#### 4.4. Ly $\alpha$ Emission in Theory - Models of LAE galaxies

The scattering of Ly $\alpha$  photons through neutral hydrogen in galaxies implies that models must take into account, and thus can potentially constrain, the kinematics, structure and composition of the ISM of high-redshift galaxies.

**Importance of ISM kinematics:** A striking feature of Ly $\alpha$  emitting galaxies is the shape of their line profiles (see Figure 12). Most show a broad, asymmetric red line; other spectral shapes are observed (P-Cygni, double-peaked, damped, etc.; Shapley et al. 2003; Mas-Hesse et al. 2003; Tapken et al. 2004; Dawson et al. 2004; Tapken et al. 2007). Though IGM absorption might be partly responsible for the attenuation of the blue side of the Ly $\alpha$  line, similar line shapes are observed in the local Universe (e.g. Kunth et al. 1998; Heckman et al. 2011). The diversity of Ly $\alpha$  profiles is largely due to radiative transfer effects in the ISM of galaxies.

Ahn, Lee, & Lee (2000, 2001, 2002)<sup>5</sup> and Zheng & Miralda-Escudé (2002) were amongst the first to use Monte Carlo radiative transfer codes to predict Ly $\alpha$  spectra from simple models of protogalaxies. Dijkstra et al. (2006) studied Ly $\alpha$  transfer through collapsing clouds, representing the gas accretion experienced by primeval galaxies (see also Zheng & Miralda-Escudé 2002). They find a boost of the blue peak and a suppression of the red part of the Ly $\alpha$  profile, at odds with what is usually observed.

Signatures of neutral gas outflows are detected ubiquitously at all redshifts in galaxies, with veloc-

ities ranging from a few tens to hundreds of km s<sup>-1</sup> (e.g. Pettini et al. 2001; Martin 2005; Weiner et al. 2009). Shapley et al. (2003) used more than 800 spectra of LBGs to construct a high-signal-to-noise composite spectrum. They find kinematic offsets between Ly $\alpha$  emission and low-ionisation interstellar (LIS) absorption lines. The absorption lines associated with outflowing gas are blueshifted compared with the systemic redshift of the galaxies, such that  $\Delta v_{\text{LIS}} \approx -150$  km s<sup>-1</sup>. In contrast, Ly $\alpha$  emission appears to be redshifted, with a typical offset of  $\Delta v_{\text{Ly}\alpha} \approx +360$  km s<sup>-1</sup>. Comparable results have been reported in both LBGs and LAEs (Steidel et al. 2010; McLinden et al. 2011; Finkelstein et al. 2011a; Kulas et al. 2012; Berry et al. 2012).

Doppler shifts induced by winds ease the escape of Ly $\alpha$ , since the photons are scattered away from the Ly $\alpha$  line centre (Kunth et al. 1998; Tenorio-Tagle et al. 1999; Mas-Hesse et al. 2003). However, an anti-correlation between Ly $\alpha$  EW and kinematic offset ( $\Delta v_{\text{Ly}\alpha} - \Delta v_{\text{LIS}}$ ) is reported (Shapley et al. 2003; Hashimoto et al. 2013): stronger Ly $\alpha$  emission is found in cases where the velocity shift is smaller. Although these results are still debated (Verhamme et al. 2008; Berry et al. 2012), it may indicate that the enhancement of dust extinction due to resonant scattering in HI remains the main driver of Ly $\alpha$  escape from galaxies. Alternatively, Ferrara & Ricotti (2006) interpret this trend as the time evolution of a galactic wind: after the starburst, the outflow slows down and the covering factor is reduced, which favours the escape of Ly $\alpha$  photons.

Radiative transfer through an expanding shell is also invoked to explain the line profiles of Ly $\alpha$  emitting galaxies (Ahn, Lee, & Lee 2003; Verhamme et al. 2006, 2008). In this model (Figure 13), an isotropic Ly $\alpha$  source is located at the center of a thin, homogeneous, and spherical shell of HI gas mixed with dust. The expanding shell mimics the gas outflow generated by strong stellar winds and supernovae during starburst events, associated with photoionisation and subsequent Ly $\alpha$  emission (Weaver et al. 1977; Chevalier & Clegg 1985; Ferrara & Ricotti 2006; Nath & Silk 2009). Using different values of the shell parameters (expansion velocity  $V_{\text{exp}}$ , HI column density, dust opacity and thermal/turbulent velocity of the gas within the shell), Verhamme et al. (2008) are able

<sup>5</sup>See also Ahn & Lee (2002); Ahn, Lee, & Lee (2003); Ahn (2003, 2004).

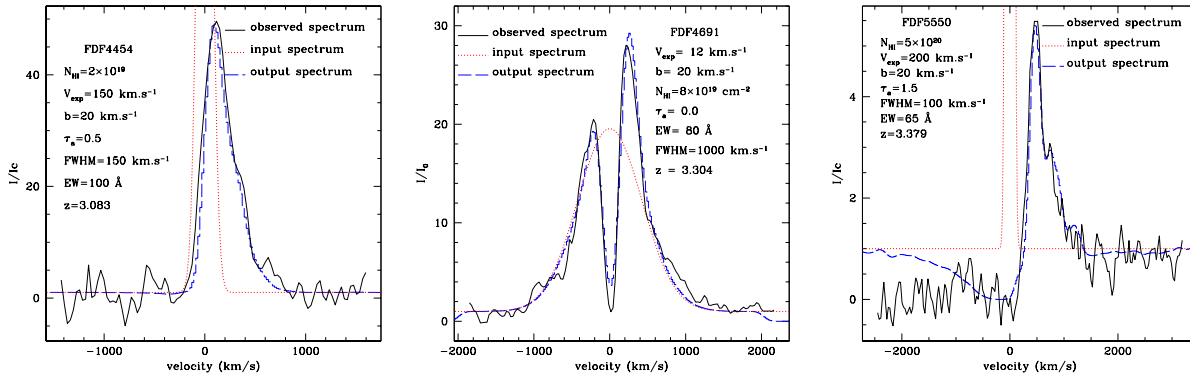


Fig. 12.— Illustration of the variety of Ly $\alpha$  line profiles observed at high redshift (black curves): asymmetric (left), double bump (middle) and P-Cygni (right). These medium-resolution ( $R = 2000$ ) spectra belong to the FORS Deep Field (FDF) sample presented by Tapken et al. (2007). The figure appears in Verhamme et al. (2008), who show that these various profiles can be reproduced with numerical models (dashed blue line). The models compute the radiative transfer of an intrinsic Ly $\alpha$  line (dotted red line) through an expanding shell. Six parameters are adjusted to fit the observed spectra: the width (FWHM) and equivalent width (EW) of the intrinsic line, the expansion velocity  $V_{\text{exp}}$ , the HI column density  $N_{\text{HI}}$ , the dust opacity  $\tau$ , and the thermal/turbulent velocity of the gas in the shell  $b$ . The values of the parameters are specified in each panel. Credit: Verhamme et al. (2008), reproduced with permission ©ESO.

to reproduce the wide variety of observed Ly $\alpha$  profiles (see also Schaerer & Verhamme 2008; Lidman et al. 2012). As an example, we show in Figure 12 three Ly $\alpha$  profiles of LBGs at  $z = 3$  from Tapken et al. (2007) that are successfully fitted by the shell model of Verhamme et al. (2008). Typical red asymmetric profiles arise from photons *backscattered* from the receding side of the shell (red arrow on Figure 13), while photons directly emitted towards the observer will be preferentially destroyed by dust due to a smaller Doppler shift (blue arrow on Figure 13).

Shell models provide a simple and physically motivated interpretation of Ly $\alpha$  spectra, but they remain very idealised. In particular, the emitted spectra does not depend on the spatial extent of the HI entrained in the wind. The observations of Steidel et al. (2010, 2011) indicate clumpy outflows and the presence of scattering gas well outside the ISM of LAEs. More realistic models of the impact of a galactic wind on the circumgalactic medium of high-redshift galaxies are required, and are discussed in Section 4.5.

**Importance of ISM structure and composition:** Hansen & Oh (2006) simulated the trans-

fer of Ly $\alpha$  photons through clumpy media. Since the analytic model of Neufeld (1991), it has been argued that a multi-phase ISM could explain the abnormally high observed Ly $\alpha$  EW, as previously discussed in Section 4.3. Of particular importance is the distribution of dust, as interactions with dust can destroy Ly $\alpha$  photons<sup>6</sup>. Neufeld (1991) models an ISM in which dust is locked in dense HI clouds that are embedded in a diffuse, dust-free, inter-cloud medium (ICM). Ly $\alpha$  and UV continuum photons are generated at the center of a plane-parallel slab in the diffuse phase. While (non-resonant) continuum radiation passes through the clouds and is attenuated by dust, Ly $\alpha$  photons are scattered off the surface of the clouds as a result of their high probability of interaction with hydrogen. The resulting Ly $\alpha$  boost is called the *Neufeld effect*, which Finkelstein et al. (2011b) quantify with the parameter  $q$ :

$$q = \tau_{\text{Ly}\alpha} / \tau_{\text{cont}} , \quad (9)$$

where  $\tau_{\text{Ly}\alpha}$  is the dust opacity of Ly $\alpha$  photons, and

<sup>6</sup>It should be remembered that while HI scattering does not destroy Ly $\alpha$  photons, it can scatter them below the surface brightness limit of observations, so that Ly $\alpha$  photons disappear in the noise, so to speak.

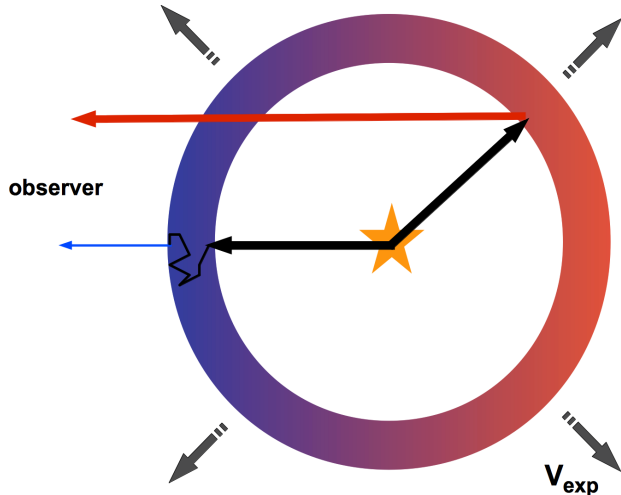


Fig. 13.— Illustration of an expanding shell model, as an ideal representation of a supernova-driven gas outflow around a source of Ly $\alpha$  emission (i.e. a star forming region: yellow star). Ly $\alpha$  photons are emitted isotropically at the centre of the shell (solid black arrows), which is expanding at speed  $V_{\text{exp}}$ . Photons emitted directly towards the observer (left) may experience strong extinction due to resonant scattering in the gaseous dusty shell. Photons emitted towards the receding shell (right) can *backscatter* towards the observer. These photons are redshifted relative to the front of the shell (and the observer), hence they have greater probability of escaping.

$\tau_{\text{cont}}$  is the dust opacity of UV-continuum photons. In the simplest case, one expects  $q \ll 1$  for a clumpy ISM, and  $q \gg 1$  for a homogeneous ISM. Note, however, the simulations of Laursen, Duval, Ostlin (2012), discussed below.

Finkelstein et al. (2011b) measured  $q$  using the ratio of emission line fluxes for a sample of 12 GALEX LAEs at  $z \sim 0.3$ . They find that most of the sample lies at  $q \sim 1 - 3$ , indicating that the ISM neither enhances nor seriously attenuates Ly $\alpha$ . Even for those LAEs with  $q < 1$  they note an important *caveat*, first discussed by Scarlata et al. (2009): if the dust is clumpy, then the observed line ratios do not follow the simple  $\exp\{-\tau_{\text{cont}}\}$  law. Further, Blanc et al. (2011) showed from the HETDEX pilot survey that the Ly $\alpha$  escape fraction, estimated from Ly $\alpha$  and (dust-corrected) UV luminosities, anti-correlates with dust extinction,

as shown in Figure 14 (see also Atek et al. 2013). The black circles correspond to the  $z = 2 - 4$  sources observed by Blanc et al. (2011). The dearth of  $q \ll 1$  objects indicates that the Neufeld effect is not a common process in LAEs. In spite of some dispersion, the cloud of points is well fitted by a  $q = 1$  model (black solid line in Figure 14) which suggests that Ly $\alpha$  and continuum photons suffer a very similar dust extinction. The green triangles indicate the objects found by Atek et al. (2009) at  $z = 0.3$ , and agree fairly well with the data of Blanc et al. (2011). The red solid line is the relation reported by Kornei et al. (2010) for LBGs at  $z = 3$ . It lies slightly below the  $q = 1$  relation measured for LAEs at the same redshift, and is consistent with the idea that LAEs are a high  $f_{\text{esc}}$  subset of the LBG population.

The simulations of Hansen & Oh (2006) suggest that the Neufeld effect will be strong if most of dust grains reside in optically thick HI clouds. Recently, Laursen, Duval, Ostlin (2012) and Duval et al. (2013) revisited this issue, finding that a significant boost requires a relatively rare confluence of conditions: high metallicity, little outflow, very high cloud density, very low density of HI in the ICM, and Ly $\alpha$  and UV photons that originate from regions deprived of neutral gas. They conclude that an EW boost is unlikely to occur in real galaxies, with  $q \ll 1$  no guarantee of a homogeneous ISM. The preferential escape of Ly $\alpha$  compared with UV continuum is also not seen in the Ly $\alpha$  RT hydrodynamic simulations of Yajima et al. (2012a) and Verhamme et al. (2012).

Although many numerical Ly $\alpha$  RT experiments have been published, only a few have focused on transfer through interstellar media in state-of-the-art hydrodynamic simulations. As they include a range of relevant physics, like gas cooling, star formation, feedback, metal enrichment or dust formation, such studies are essential to gaining insight into the complex mechanisms altering the Ly $\alpha$  line. We emphasise that the *Ly $\alpha$  escape fraction*, as calculated by simulators, usually refers to the ratio of emitted to escaping Ly $\alpha$  photons. Photons are lost only to absorption by dust. Observed escape fractions can also lose photons to scattering by the CGM/IGM, and beneath surface brightness detection limits. The observed quantity is termed “effective escape fraction” by Dijkstra & Jeason-Daniel (2013).

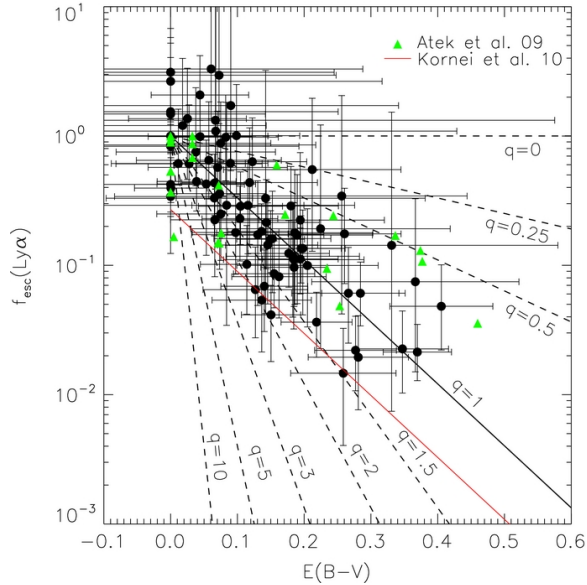


Fig. 14.— Observed relation between the Ly $\alpha$  escape fraction and the colour excess  $E(B-V)$  (Blanc et al. 2011). The black circles and the green triangles are the measurements of Blanc et al. (2011) and Atek et al. (2009) for Lyman-alpha emitters (LAE) at  $z = 2 - 4$  and 0.3 respectively. The escape of Ly $\alpha$  photons is anti-correlated with dust extinction, despite a strong dispersion. The black lines show the expected correlation for different clumpiness parameters  $q$ . The  $q = 1$  model, for which Ly $\alpha$  and continuum photons suffer a similar dust extinction, describes well the median distribution of the data. It suggests that the impact of Ly $\alpha$  resonant scattering is partly suppressed, certainly due to geometry or kinematics effects. At given  $E(B-V)$ , Lyman Break galaxies display lower  $f_{\text{esc}}$  than LAEs on average (red solid line; Kornei et al. 2010). Reproduced by permission of the AAS.

Laursen et al. (2009) analysed the transfer of Ly $\alpha$  photons in  $z \approx 3$  galaxies extracted from a cosmological N-body/hydrodynamical simulation. Although their sample contains only nine galaxies, there is a clear trend between Ly $\alpha$  escape fraction and the mass of the host halo.  $f_{\text{esc}}$  is of order unity for galaxies in  $10^9 - 10^{10} M_{\odot}$  haloes, but only a few percent for  $10^{11} - 10^{12} M_{\odot}$ . There are two complementary reasons for this trend. First, galaxies in smaller haloes form fewer stars, hence limiting the production of metals/dust. Second, the shallower gravitational potential wells of low-mass galaxies makes supernovae feedback more efficient at disturbing the ISM, which could help Ly $\alpha$  photons to escape from galaxies in smaller haloes.

Unlike most of the other models who assume density/temperature cuts to determine the state of the gas (ionized vs neutral), the simulations of Yajima et al. (2012) include the transfer of ionizing radiation. It allows them to compute (i) the recombination of hydrogen that powers the Ly $\alpha$  emission, and (ii) the ionisation state of the ISM. However, the resolution of the zoom-in region investigated by these authors ( $250h^{-1}$  comoving pc) is not sufficient to accurately model the ISM on small scales. They find that the median  $f_{\text{esc}}$  is almost constant ( $\approx 25\%$ ) between  $z = 0$  and 3, and increases towards higher redshifts to reach a value of about 90% at  $z = 10$ , mainly due to

galaxies being increasingly metal and dust poor at high redshift. They interpret the trend at low redshift as a mutual cancellation of the effects of increased metallicity and dust, and decrease ISM gas fraction. At all redshifts, the values of  $f_{\text{esc}}$  are nonetheless very scattered around the median. Yajima et al. (2012) find only weak correlations between Ly $\alpha$  escape fraction and the galaxy properties.  $f_{\text{esc}}$  anti-correlates with host halo mass, galaxy mass, dust mass, but the dispersion in these relations is again quite significant. A clearer trend is that metal-enriched galaxies have lower  $f_{\text{esc}}$ , in good agreement with the observations of Atek et al. (2009), Kornei et al. (2010), and Blanc et al. (2011), discussed above.

Verhamme et al. (2012) showed that the small-scale structure of the ISM has a strong effect on the escape of Ly $\alpha$  photons. They performed Ly $\alpha$  radiative transfer within two simulations of idealized dwarf galaxies at different resolution ( $\sim 20$  and 150 pc respectively), run with the adaptive-mesh refinement code RAMSES (Teyssier 2002). Gas density maps of the two simulations are shown in Figure 15. In the higher-resolution galaxy, the ISM can cool down to 100K via metal cooling and fragment into smaller clumps in the disk. The Ly $\alpha$  escape fraction  $f_{\text{esc}}$  is as low as 5% in this case, whereas it goes up to 50% for the lower-resolution (with smoother gas distribution) galaxy. Ver-

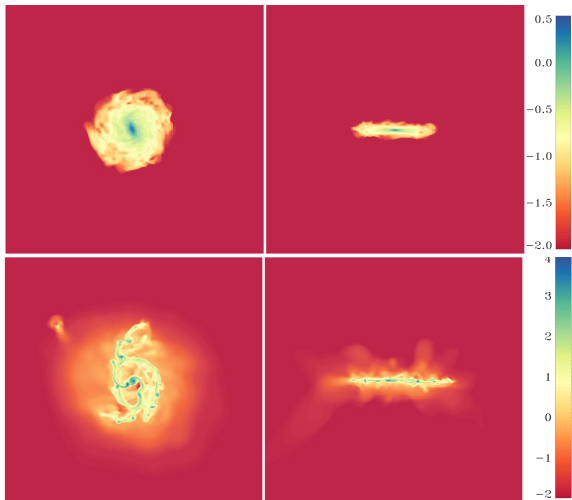


Fig. 15.— Density maps of gas distribution for the two isolated galaxies, viewed face-on (left) and edge-on (right), used by Verhamme et al. (2012) to study Ly $\alpha$  transfer in the interstellar medium (ISM). The colour scales with gas density (arbitrary log units). *Top*: Gas is allowed to cool down to  $10^4$  K in the ISM, leading to a rather smooth matter distribution. *Bottom*: Extra energy loss due to metal cooling enables the gas temperature to drop down to 100K. In this more realistic case, smaller scale structures appear. Verhamme et al. (2012) post-process the simulations with a Ly $\alpha$  transfer algorithm and find that the Ly $\alpha$  escape fraction is ten times lower in the inhomogeneous galaxy than in the smoother one. Credit: Verhamme et al. (2012), reproduced with permission ©ESO.

hamme et al. (2012) also report that the Ly $\alpha$  line profile, escape fraction, and equivalent width vary with respect to the angle at which the galaxy is viewed; especially the latter is higher in the face-on direction. As pointed out by previous studies (Charlot & Fall 1993; Laursen et al. 2009; Zheng et al. 2010; Barnes et al. 2011), orientation effects may introduce a bias in LAE observations where a Ly $\alpha$  EW detection threshold is set, which could be partly responsible for the scatter in properties of LAEs and LBGs.

While our knowledge of the ISM of high-redshift galaxies and its effect on the Ly $\alpha$  line transfer is still incomplete, the understanding of the mechanisms at play is improving. The detailed analy-

sis of observational data and the comparison with realistic theoretical models has resulted in better constraints on the emission and escape from the ISM of Ly $\alpha$  photons. The gas/dust structure and kinematics appear to be key drivers to shape the Ly $\alpha$  emission line, and more detailed descriptions of neutral outflows (Dalla Vecchia & Schaye 2012), of the ionisation state of the ISM (Yajima & Li 2012), and of its molecular hydrogen content (Vallini et al. 2012) will help refining the models.

#### 4.5. Ly $\alpha$ Emission and the CGM

The extremely large cross-section for Ly $\alpha$  scattering off HI makes Ly $\alpha$  spectra sensitive to gas *outside* of galaxies. In a hierarchical cosmology, the environment of a galaxy plays a crucial role in its formation. The CGM, introduced in Section 2.6.2, potentially includes inflowing cold streams, hot and shocked infalling gas, satellite galaxies, feedback from AGN, and outflowing galactic winds and recycling galactic fountains of hot wind fluid and entrained cool star-formation enriched gas.

What light does Ly $\alpha$  emission throw on the CGM? Ly $\alpha$  emission is an ideal tracer of the CGM, being copiously produced by star-forming galaxies and strongly scattered by HI. Further, Ly $\alpha$  is the strongest emission line from cooling gas in the universe. Fardal et al. (2001) estimate that Ly $\alpha$  emission accounts for 57% of cooling radiation, with just 2% coming from bremsstrahlung. Note, however, that they assume primordial composition gas. More recent calculations by Bertone et al. (2013), which take into account  $\sim 2000$  emission lines from 11 elements, show that while Ly $\alpha$  carries about 50% of the energy in H and He lines, it carries 13% of the total energy emitted by diffuse gas ( $n_H < 0.1 \text{ cm}^{-3}$ ) at  $z = 2$ . Most of the diffuse emission comes from dense ( $n_H \sim 10^{-3} - 10^{-1} \text{ cm}^{-3}$ ), cool ( $\sim 10^4 - 10^{4.5}$  K), metal rich (0.1-1 solar) gas, 80% in emission lines and 20% in the continuum (see Figure 14 of Bertone et al. 2013).

Spatially-resolved Ly $\alpha$  spectra are sensitive to the distribution, kinematics and dust content of CGM gas. As discussed in Section 4.4, the vast majority of Ly $\alpha$  emitting galaxies at high redshift have spectral lines shifted to the red by hundreds of  $\text{km s}^{-1}$ , in agreement with models of Ly $\alpha$  radiative transfer through an expanding galactic wind (Verhamme et al. 2006). Spectra alone, however, cannot constrain the spatial extent of the gas and

so cannot say whether the gas simply puffs up the ISM or is blasted right out of the halo. We require ultra-deep, spatially-resolved observations.

Rauch et al. (2008) performed an ultra-deep spectroscopic search for low surface brightness Ly $\alpha$  emitters at redshift  $z \sim 3$ . A 92-hour long exposure with the ESO VLT FORS2 instrument yielded a sample of 27 faint line emitters with fluxes of a few times  $10^{-18}$  erg s $^{-1}$ cm $^{-2}$ . Based on their large number density, the sample is likely dominated by Ly $\alpha$  emitters, rather than low-redshift interlopers. A number of lines of evidence lead Rauch et al. (2008) to claim that these emitters are the host galaxies of DLAs:

- Both must host extended, optically thick neutral hydrogen.
- The incidence rate ( $dN/dz$ ) for the emitters and for DLAs is consistent. The combination of the large sizes and high space density of the emitters mean that they can account for the high incidence rate of DLAs.
- Both populations have a low star formation rate, which would explain the low success rate for direct searches for the counterparts of DLAs, and the low observed metallicity of DLAs.
- Both populations have low dust content, assuming that a high dust content would extinguish the line.
- If the large sizes of the emitters are due to radiative transfer effects (which seems likely in light of the strict upper limits on *extended* star formation in DLAs derived by Wolfe & Chen 2006), then the emitters must contain significant amounts of neutral hydrogen. The majority of HI at these redshifts resides in DLAs.

Barnes & Haehnelt (2009, 2010) used an analytic model of neutral hydrogen in dark matter haloes and radiative transfer simulations to simultaneously reproduce the observed properties of DLAs and the faint Ly $\alpha$  emitters of Rauch et al. (2008). These emitters are hosted by  $10^{9.5} - 10^{12} M_{\odot}$  haloes, with little contribution from haloes with virial velocities  $\lesssim 50 - 70$  km s $^{-1}$ . Their observed sizes are due to centrally concentrated star-formation at a few tenths  $M_{\odot}$  yr $^{-1}$  producing Ly $\alpha$  photons that scatter through the

surrounding HI and are observable (at the flux limit of Rauch et al. 2008) to  $\sim 30 - 50$  kpc.

Steidel et al. (2011) used a sample of 92 continuum-selected galaxies at  $\langle z \rangle = 2.65$  to study very faint Ly $\alpha$  emission surrounding LBGs. The CGM of LBGs had previously been studied in absorption: Steidel et al. (2010) studied the CGM at  $z > 2$  within  $\sim 125$  kpc of Lyman Break galaxies using a sample of 512 close galaxy pairs. These galaxies predominantly show Ly $\alpha$  emission (when present) that is strongly redshifted ( $\Delta v_{\text{Ly}\alpha} \approx +445$  km s $^{-1}$ ), while the strong interstellar absorption lines are strongly blueshifted ( $\Delta v_{\text{IS}} \approx -160$  km s $^{-1}$ ), consistent with the presence of a galactic wind (Section 4.4). Absorption from HI and metals is observed in the CGM, with absorber equivalent width declining with impact parameter. A very rapid decline in equivalent width is observed at large distances, beginning at 70-90 kpc for all transitions except Ly $\alpha$ , which remains strong out to 250 kpc. Similarly, Rudie et al. (2012) observe that HI absorbers within  $\sim 100$  kpc of galaxies at  $z \sim 2.5$  have  $10^3$  times higher median  $N_{\text{HI}}$  than random IGM absorbers; even at 1000 kpc, HI absorbers have a median  $N_{\text{HI}}$  twice as high as the IGM.

In emission, Steidel et al. (2011) stacked UV continuum and Ly $\alpha$  line images to reach a surface brightness threshold of  $\sim 10^{-19}$  erg s $^{-1}$ cm $^{-2}$ arcsec $^{-2}$ . While the UV continuum drops with an exponential scale length of 3-4 kpc (proper) and is undetectable beyond 24 kpc, Lyman alpha emission is  $\sim 5 - 10$  times more extended, with a scale length of 20 - 30 kpc. Ly $\alpha$  remains detectable out to  $\sim 80$  kpc, comparable to the virial radius of the galaxies. Such signal is missed by NB observations and slit spectroscopy of individual objects, so that the Ly $\alpha$  flux of LAEs are underestimated. They argue that this emission arises from resonantly scattered Ly $\alpha$  photons in the CGM.

Other groups have also attempted to study the CGM through Ly $\alpha$  stacking. Matsuda et al. (2012) stacked 2128 Ly $\alpha$  emitters and 24 proto-cluster LBGs at  $z = 3.1$ , observed with a narrow-band filter on Subaru Suprime-Cam. They too found extended Ly $\alpha$  haloes down to surface brightness limits of  $\sim 10^{-18}$  erg s $^{-1}$ cm $^{-2}$ arcsec $^{-2}$ , with a trend for larger scale lengths for LAEs in higher density (Mpc) environments. Feldmeier et al. (2013), however, sound a warning: *surface pho-*

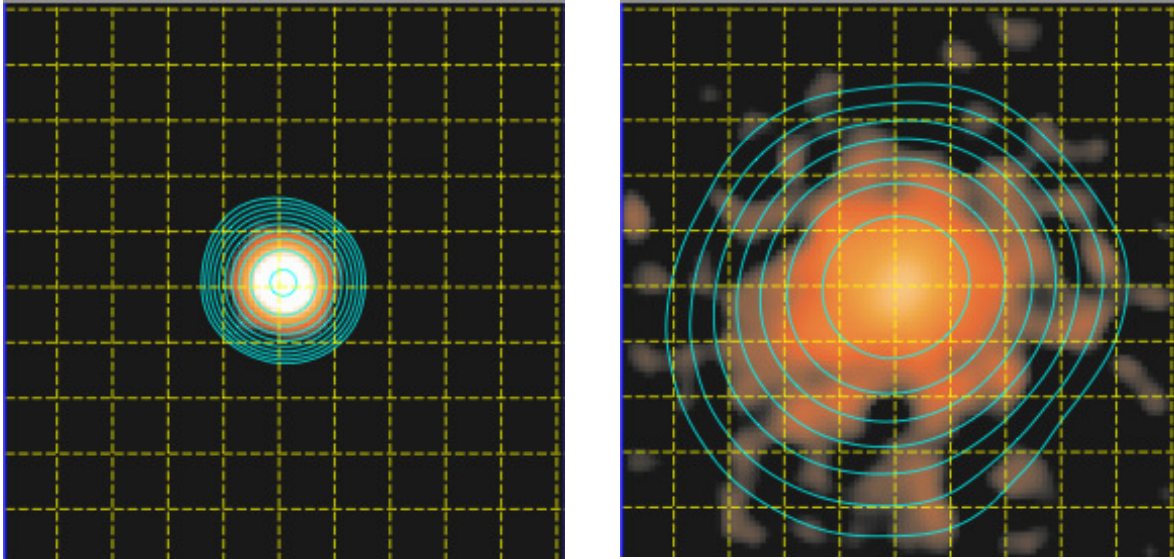


Fig. 16.— Stacked images from 92 continuum-selected LBGs from Steidel et al. (2011). The regions shown are  $20''$  ( $\approx 160$  physical kpc at  $z = 2.65$ ) on a side, with a grid spacing of  $2''$ . *Left*: scaled far-UV continuum image, drawn from three independent fields. *Right*: the continuum-subtracted, stacked Ly $\alpha$  image for the same sample of galaxies. In both panels, the contours are logarithmically spaced in surface brightness with the lowest contour shown at  $\approx 2.5 \times 10^{-19}$  erg s $^{-1}$ cm $^{-2}$ arcsec $^{-2}$ . The Ly $\alpha$  emission is seen to extend to  $\sim 80$  physical kpc, significantly beyond the continuum emission. Figures from Steidel et al. (2011); reproduced by permission of the AAS.

*tometry at very low flux levels is treacherous*, sensitive to large-scale flat-fielding and point-spread-function issues which may not have been taken into account in previous works. They observe smaller ( $5 - 8$  kpc) scale Ly $\alpha$  haloes at  $z = 3.1$  and no evidence for haloes at  $z = 2.1$ , down to  $6 - 10 \times 10^{-19}$  erg s $^{-1}$ cm $^{-2}$ arcsec $^{-2}$ . Jiang et al. (2013) find no conclusive evidence of Ly $\alpha$  haloes around  $z = 5.7$  or  $6.5$  in a stack of 40 LAEs, reaching  $1.2 \times 10^{-19}$  erg s $^{-1}$ cm $^{-2}$ arcsec $^{-2}$ . Thus, LAEs seem to have significantly fainter Ly $\alpha$  haloes than Steidel’s LBGs. This is consistent with the order of magnitude smaller star formation rates and lower mass host haloes of LAEs, implying a lower density environment (*a la* Matsuda).

The scattering of Ly $\alpha$  photons in the CGM was investigated by Barnes et al. (2011), who modelled the scattering of Ly $\alpha$  photons emitted by a central source through the ISM and CGM of galaxies drawn from an SPH cosmological simulation. The simulations reveal a Ly $\alpha$  halo extending to scales comparable to the virial radius, with an extent that depends on the wind prescription used in

the simulation. The more efficient feedback implementations result in reduced column densities at the centre and therefore reduced diffusion in frequency space and narrower spectral profiles. The simulated spectra display a more prominent blue peak than most observed LAEs, which may be due to the chosen galaxies being smaller and having lower star-formation rates than typical LBGs. This conclusion is consistent with the observations of multiply-peaked Ly $\alpha$  emission by Kulas et al. (2012), who note that such systems have systematically slower outflows (as measured by absorption lines). The Ly $\alpha$  emitting halo around star-forming galaxies is predicted to extend well beyond the CGM, though at very low surface brightness (Zheng et al. 2011; Jeesson-Daniel et al. 2012).

Because a first principle calculation of the distribution and kinematics of cold gas in galactic outflows are currently not feasible, Dijkstra & Kramer (2012) studied a phenomenological model of a galactic wind, wherein large numbers ( $\sim 10^5 - 10^6$ ) of cold, dense dusty spherical clumps of H I are outflowing isotropically in pressure equi-

librium with a hot component. Following the simple model of Steidel et al. (2011), they consider a wind which accelerates ( $a \propto r^{-\alpha}$ ,  $\alpha > 1$ ) to  $\sim 800$  km s $^{-1}$  at large distances ( $\sim 100$  kpc). The full parameter space of the model is explored using a Monte Carlo Markov Chain (MCMC) simulation, constraining the parameters using absorption line data. A suite of constrained models is used in a radiative transfer calculation to predict the Ly $\alpha$  emission. The emitters are too faint and too centrally concentrated to match observations because the clumps at large distances are too few and too fast to significantly scatter escaping Ly $\alpha$  photons. Models in which gravity decelerates the clumps beyond  $\sim 10$  kpc and in which the outflow is bipolar are more successful in reproducing both the absorption and emission line data.

Noterdaeme et al. (2012a) observed Ly $\alpha$ , [OII] and H $\alpha$  emission from a DLA, inferring a large SFR ( $\sim 25M_{\odot}$  yr $^{-1}$ ) from a low mass galaxy ( $M_{\text{halo}} \sim 10^{10}M_{\odot}$ ). The Ly $\alpha$  emission is double-peaked and spatially extended, which would suggest the static Neufeld solution (see Section 4.2 and Figure 8), except that the blue and red peaks arise from spatially distinct regions, separated by a few kpc and on opposite sides of the star-forming region. They successfully reproduce the observed properties of the system with a model in which two ionized jets expel gas through a spherical distribution of cold, neutral infalling clouds. Similarly, Christensen et al. (2012) and Krogager et al. (2013) are able to reproduce observed Ly $\alpha$  emission spectrum using a model of a dusty, clumpy outflow at  $\sim 100$  km s $^{-1}$ . These models use the MoCaLaTA code of Laursen et al. (2009), and show the need for data other than the Ly $\alpha$  spectrum to constrain the RT calculation.

In light of the faintness of the CGM, Cantalupo et al. (2005) investigated the illumination of extragalactic HI by a nearby quasar. This provides a method of observing otherwise undetectable gas in the CGM and in small, dark galaxies. The observations of Cantalupo, Lilly, & Haehnelt (2012), using VLT-FORS to perform deep narrow-band survey for Ly emission within  $\sim$ Mpc of a hyperluminous QSO at  $z = 2.4$ , reveal a population of emitters whose equivalent width distribution, luminosity function and the average luminosity versus projected distance are consistent with detailed radiative-transfer simulations of quasar fluo-

rescence. Their large EW ( $> 800 \text{ \AA}$ ) rule out internal star formation as the source of Ly $\alpha$ . Some of the emitters resemble extended filaments, compatible with the expectations for circumgalactic cold flows, though this interpretation is not unique. Very recently, Cantalupo et al. (2014) reported observations of a filamentary, 460 kpc Ly $\alpha$  emission region that includes a radio-quiet quasar but extends well beyond the virial radius. This object is plausibly the cosmic web, lit up in Ly $\alpha$  by the quasar, a conclusion supported by cosmological hydrodynamical simulations combined with Ly $\alpha$  and ionisation radiative transfer.

Hennawi & Prochaska (2013) simultaneously analyzed absorption and emission from HI in the CGM of quasars using close projected quasar pairs. While extended Ly $\alpha$  fuzz is detected on 50kpc scales in  $\sim 30\%$  of the sample (possibly up to 50 – 70% when the effects of the single slit are accounted for), it is significantly less emission than would be naively expected given the covering fraction of optically thick HI absorbers and the ionizing flux from the quasar. This is argued to be evidence of anisotropic quasar emission.

**Ly $\alpha$  Blobs (LABs):** There is another class of Lyman alpha emitter at high redshift, which are extended ( $\sim 10 - 150$  kpc), extremely luminous ( $L_{\text{Ly}\alpha} \sim 10^{43} - 10^{44}$  erg s $^{-1}$ ) and rare, with a number density of  $\sim 10^{-3.8}$  comov.Mpc $^{-3}$  (Dijkstra & Loeb 2009), as compared to  $\sim 10^{-2.7}$  comov.Mpc $^{-3}$  for the population of Ly $\alpha$  emitters in van Breukelen et al. (2005). These are the imaginatively-named Lyman Alpha Blobs (LABs) (Fynbo et al. 1999; Keel, Cohen, Windhorst, & Waddington 1999; Steidel et al. 2000; Francis et al. 2001; Palunas et al. 2004; Matsuda et al. 2004; Chapman et al. 2004; Bower et al. 2004; Villar-Martín, Tadhunter, Morganti, & Holt 2005; Dey et al. 2005; Matsuda et al. 2006; Nilsson et al. 2006; Prescott, Dey, & Jannuzi 2009, 2013; Francis et al. 2013). Their physical nature remains mysterious, and it is not clear where they stand in relation to the astrophysical sources of Ly $\alpha$  outlined above. Intriguingly, Keel, White, Chapman, & Windhorst (2009) find a dearth of LABs at low redshift ( $z = 0.8$ ). Three mechanisms are suggested as the energy source for LABs. They are not mutually exclusive.

- (a) Internal photoionizing sources: LABs are the Ly $\alpha$  fuzz predicted by Haiman & Rees (2001), or the Ly $\alpha$  coronae predicted by Furlanetto et al. (2005). LABs contain internal sources of ionizing radiation in the form of an AGN or star-forming galaxy, possibly obscured. The cosmological simulations of Cen & Zheng (2012) suggest that star-bursts are responsible for the majority of Ly $\alpha$  from LABs. This is the scenario suggested, for example, by the multiwavelength studies of Chapman et al. (2004), Geach et al. (2007, 2009), and Overzier et al. (2013). The polarisation of Ly $\alpha$  emission from LAB1 is evidence of scattering, suggesting a central source of Ly $\alpha$  photons (Hayes, Scarlata, & Siana 2011). However, the 1.1-mm imaging survey of Tamura et al. (2013) places strict a upper limit on ultra-luminous obscured star-formation, indicating that most LABs are not powered by intense, dusty star-formation. The population of dusty Ly $\alpha$  emitters discovered by Bridge et al. (2012), 50% of which are extended ( $\gtrsim 25$  kpc), show warm far-IR colours consistent with being in a short-lived AGN feedback phase. LABs have also been discovered around high-redshift quasars (Smith et al. 2009; North et al. 2012).
- (b) Cooling radiation: LABs consist of gas that is radiating away its gravitational potential energy as it cools into massive galaxies. Dijkstra et al. (2006), Dijkstra, Haiman, & Spaans (2006), and Dijkstra & Loeb (2009) considered simple analytic models of this scenario, showing that the Ly $\alpha$  linewidths and number densities of LABs can be reproduced by cold accretion if  $\sim 20\%$  of the gravitational potential energy of the gas is converted to radiation. More detailed hydrodynamical simulations of the connection between LABs and cold flows have been performed by Faucher-Giguère et al. (2010), Goerdt et al. (2010) and Rosdahl & Blaizot (2012). These simulations do not agree on whether cooling radiation alone can power LABs — the sensitivity of collisional ionisation and the cooling rate to the temperature, density, and metallicity of the gas make such calculations worryingly dependent on resolution, subgrid physics, self-shielding and ionising radiative transfer, heating-cooling balance, and other bugbears of numerical simulation. The simulations of Goerdt et al. (2010) support the analytic findings of Dijkstra & Loeb (2009), that haloes of mass  $\sim 10^{12} - 10^{13} M_{\odot}$  at  $z \sim 3$  can reproduce the extent, luminosity and irregular morphologies of LABs, with most of the Ly $\alpha$  emission coming from 50-100 kpc cold streams. This scenario is argued for observationally by Nilsson et al. (2006); Smith & Jarvis (2007); Smith et al. (2008), usually on the basis of a non-detection of associated AGN or star-formation. (But if the accretion rate is so high, why doesn't it fuel an AGN and/or form stars?)
- (c) Galactic superwinds: a starburst powers a barrage of supernovae, which sweep cooling, dense, radiating shells of HI into the IGM (Taniguchi & Shioya 2000; Mori, Umemura, & Ferrara 2004). This scenario is favoured observationally by Ohyama et al. (2003) and Saito et al. (2008) on the basis of broad wing emission components on the red side, and a sharp cutoff on the blue side of the Ly $\alpha$  line as predicted by wind models (Section 4.4). Observations of associated, spatially-extended narrow Ly $\alpha$  absorption lines in the spectra of active galaxies (e.g. Humphrey et al. 2013), which suggest the presence of an HI bubble outside the Ly $\alpha$  nebula, are consistent with a starburst-driven superbubble. However, Yang et al. (2011) and McLinden et al. (2013) report that the velocity offset of Ly $\alpha$  with respect to [OIII] is consistent with zero, suggesting that outflows are not the primary driver of Ly $\alpha$  escape.
- Higher resolution observations haven't particularly clarified the situation. Weijmans et al. (2010) observed LAB1 and showed that Ly $\alpha$  is emitted from five distinct clumps: two are associated with LBGs, one with a heavily obscured submillimeter galaxy, and two don't appear to be associated with a galaxy. The complex morphology is shown in Figure 17. Detailed observations of LABd05 by Prescott et al. (2012) reveal a blob containing 17 small galaxies, none of which are at the peak of the Ly $\alpha$  emission, with a smooth, non-filamentary morphology and a similarly extended UV surface brightness profile. Francis et al. (2013) presented integral field spectroscopy of an LAB at  $z = 2.38$ , noting a chaotic velocity structure, two associated

compact red massive galaxies, evidence of a superwind, an infalling filament of cold gas that resonantly scatters Ly $\alpha$  photons, and bow-shocks and tidally stripped gas in outer subhaloes.

Fainter LABs are similarly complex. Rauch et al. (2011, 2013a,b) report long-slit spectroscopic observations of extended, ultra-faint Ly $\alpha$  emitters at  $z = 2.6 - 3.3$ . The first shows a partly obscured “red core” of emission, accompanied by a more extended ( $\sim 37$  kpc proper) “blue fan” with evidence of substructure. This is interpreted as evidence of an infalling, filamentary cloud of HI that is illuminated by stellar ionizing radiation. The large inferred ionizing escape fraction, together with *HST* evidence of a stellar tidal tail, hint that the filament may be tidal debris from an interaction that has aided the escape of the ionizing continuum. The second system also suggests the influence of galaxy interactions. The system is extended, asymmetric with spatially irregular stellar components, and shows evidence for a very young starburst and possibly a Ly $\alpha$  emitting filamentary structure. The tadpole shape and blue, partly turbulent tails of the filaments seen in the third system is interpreted as evidence of ram-pressure stripping as dwarf galaxies leave behind contrails of gas and stars as they fall into a more massive halo.

Taken together, these systems suggest that galaxy interactions play an important role in the production and escape of Ly $\alpha$  photons in protogalaxies. Such a link has been suggested previously by Cooke et al. (2010), who discovered that all LBG pairs in their sample that are separated by  $\lesssim 15h^{-1}$  kpc (projected) exhibit Ly $\alpha$  in emission, in stark contrast to 50% of the LBG population as a whole. Similarly, Jiang et al. (2013) find a large fraction ( $\sim 50\%$ ) of  $z = 5.7 - 6.5$  LAEs show signs of merging / interaction, as do the handful of  $z = 2.4$  double-peaked Ly $\alpha$  emitters of Chonis et al. (2013). This suggests a scenario in which galaxy interactions, as well as providing fuel for star formation (Tilvi et al. 2011), sufficiently disrupt and ionise the ISM to give Ly $\alpha$  photons an easy escape.

Shimizu & Umemura (2010) presented a model in which galaxies can not only appear as LAEs when a burst of star-formation occurs (i.e. a Ly $\alpha$ -bright phase; see also Dijkstra & Wyithe 2007; Nagamine et al. 2007), but also when a young

satellite galaxy is accreted onto a more massive object. The simulations of Yajima, Li, & Zhu (2012) suggest that a merger can cause a burst in both star-formation and cooling radiation, which can result in an LAB. LABs (and their radio-loud counterparts — see below) are often associated with overdense environments (Keel, Cohen, Windhorst, & Waddington 1999; Steidel et al. 2000; Palunas et al. 2004; Matsuda et al. 2004, 2009), which may suggest a link to galaxy interactions, and/or gas accretion.

Extended Ly $\alpha$  emission is also associated with high-redshift radio galaxies. Selecting sources by their radio emission generally finds the most massive high-redshift objects, either galaxies or AGN. Giant Ly $\alpha$  haloes (or nebulae) have been discovered around many radio galaxies, and their properties have been studied by Reuland et al. (2003); Villar-Martín, Tadhunter, Morganti, & Holt (2005); van Breugel et al. (2006); Villar-Martín et al. (2007); Geach et al. (2007); Villar-Martín et al. (2007); Villar-Martín (2007); Miley & De Breuck (2008); Courbin, North, Eigenbrod, & Chelouche (2008); Zirm, Dey, Dickinson, & Norman (2009). These objects resemble LABs, except that they are radio loud, have a higher surface brightness (by a factor of  $\sim 5$ ) and contain large, multi-component galaxies (van Breugel et al. 2006). Reuland et al. (2003) have suggested the following evolutionary sequence: LABs represent the very first stage in the formation of a large galaxy (or a set of smaller galaxies that later merge), and evolve into radio-loud Ly $\alpha$  haloes when galaxy merging triggers an AGN.

#### 4.6. Ly $\alpha$ Emission in cosmological context

To understand the properties and evolution of the LAE population as a whole, it is essential to investigate Ly $\alpha$  emitting galaxies in their cosmological context. Observations of Ly $\alpha$  emitters are sensitive to the large scale structure of the universe, and in particular to the ionisation state of the IGM.

**LAEs in Semi-Analytic Models:** As large samples of LAEs became available in the early 2000s, semi-analytic models of galaxy formation attempted to model the statistical properties of LAEs. These models incorporate the hierarchi-

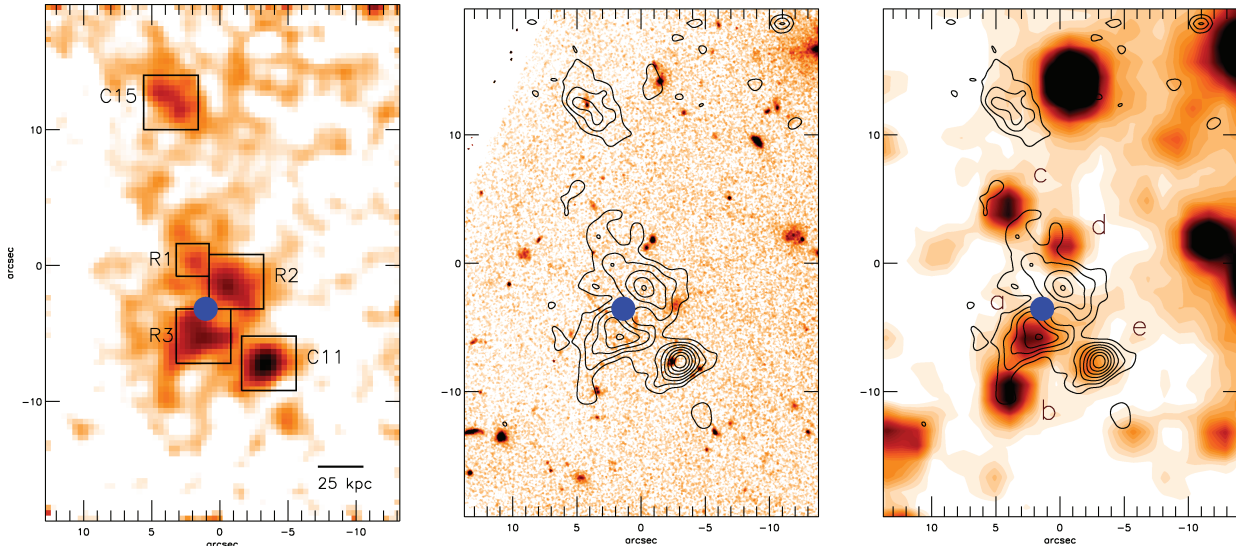


Fig. 17.— Multi-wavelength observations by Weijmans et al. (2010) of a Ly $\alpha$  blob known as LAB1. *Left*: continuum-subtracted Ly $\alpha$  emission, obtained from collapsing the SAURON spectra over a narrow wavelength range centred on the emission line. The boxes mark individual sub-clumps of emission. *Middle*: HST/STIS optical image overlaid with Ly $\alpha$  contours from the left panel. The faintest contour has a surface brightness of  $5.6 \times 10^{-18} \text{ erg s}^{-1} \text{ cm}^{-2} \text{ arcsec}^{-2}$  and contours increase in steps of  $3.7 \times 10^{-18} \text{ erg s}^{-1} \text{ cm}^{-2} \text{ arcsec}^{-2}$ . *Right*: same as middle panel, but now a Spitzer/IRAC  $3.6 \mu\text{m}$  image is displayed. In all plots, the blue dot denotes the position of the radio source (Chapman et al. 2004). All images are plotted on the same scale and are orientated such that north is up and east to the left. The Ly $\alpha$  blob has a complex morphology, with no simple relationship between Ly $\alpha$ , optical and submillimeter emission. Figure from Weijmans et al. (2010, Figure 1); used with permission.

cal evolution of dark matter haloes analytically (Press & Schechter 1974; Sheth & Tormen 2002) or with N-body simulations (e.g. Springel et al. 2005). Galaxies are formed within dark matter haloes according to semi-analytic recipes or SPH simulations. Predictions of observed Ly $\alpha$  emission must incorporate the Ly $\alpha$  escape fraction ( $f_{\text{esc}}$ ). This has been modelled with simple phenomenological prescriptions (e.g. Kobayashi et al. 2007), and more sophisticated calculations based on numerical Ly $\alpha$  radiative transfer (e.g. Garel et al. 2012).

The simplest approach assumes that a constant fraction of Ly $\alpha$  photons escape from each galaxy, with the value of  $f_{\text{esc}}$  is adjusted to fit Ly $\alpha$  LF data (e.g. Le Delliou et al. 2005, 2006; Dayal et al. 2008, 2009; Nagamine et al. 2010). The typical reported value of  $f_{\text{esc}} = 10\%$  is strongly model-dependent because the intrinsic Ly $\alpha$  LF depends on the underlying dark matter simulation and its cosmology,

the baryonic prescriptions used to model galaxy formation, and the IMF. For example, the best-fit  $f_{\text{esc}}$  value varies from 0.02 to 0.20 when changing from a top-heavy IMF to a more standard Kennicutt IMF (Le Delliou et al. 2006).

Alternatively, “duty cycle” models have been investigated (Samui et al. 2009; Nagamine et al. 2010). In these scenarios, only a fraction of galaxies are *turned on* as Ly $\alpha$  emitters at a given time. In the model of Nagamine et al. (2010), based on a cosmological SPH simulation, a duty cycle of 7% (20%) is necessary to reproduce both the UV LFs of LBGs and Ly $\alpha$  LFs of LAEs at  $z = 3$  (6).

These simple models quantify how the intrinsic Ly $\alpha$  LFs from models have to be modified to reproduce the data, either in terms of Ly $\alpha$  luminosity (constant fraction scenario) or LAE density (duty cycle scenario). It remains to be seen whether more physical models support either picture.

An obvious method to deal with the dust extinction of the Ly $\alpha$  line is to treat it the same way as UV continuum, neglecting resonant scattering. Various models have been tried using simple screen- and slab-like distributions of dust (Haiman & Spaans 1999; Mao et al. 2007; Kobayashi et al. 2007; Shimizu et al. 2011). Additional parameters often included to improve the agreement with the UV and Ly $\alpha$  data. In Kobayashi et al. (2007), a phenomenological implementation is developed for the Ly $\alpha$  escape fraction, varying the visibility of an LAE depending on whether the starburst galaxy is in a pre-outflow, outflow, or post-outflow phase. The model reasonably reproduces the UV LFs of LBGs and Ly $\alpha$  LFs of LAEs between  $z \approx 3 - 6$ .

To assess the impact of the Neufeld effect discussed in Section 4.4, clumpy dust distributions have been investigated in the context of cosmological simulations (Dayal et al. 2008; Kobayashi et al. 2010; Shimizu et al. 2011; Dayal et al. 2011). The ISM clumpiness is usually described by the  $q$  (free) parameter, defined in Equation 9. This is equivalent to tuning independently the Ly $\alpha$  and continuum dust extinction. In addition to UV and Ly $\alpha$  LFs, a very clumpy model (e.g. Kobayashi et al. 2010, assume  $q = 0.15$ ) can reproduce other observed quantities, such as the Ly $\alpha$  EW distribution and the anti-correlation between UV magnitudes and Ly $\alpha$  EWs.

Dayal et al. (2011) coupled cosmological SPH simulations and ionizing RT calculations to predict the ionisation state of the intergalactic medium on large scales. They use a phenomenological recipe for ISM dust extinction and an analytic model for Ly $\alpha$  IGM opacity along the line-of-sight.<sup>7</sup> They conclude that the IGM transmission alone cannot explain the Ly $\alpha$  and UV LFs at  $z = 5 - 7$ , and that the ISM extinction, described by a clumpy dust distribution, is required to simultaneously match UV and Ly $\alpha$  data. There is tension between the success of clumpy ISM models, which assume the enhancement of the escape of Ly $\alpha$  radiation over that of UV continuum, and the current interpretation of observations, and

<sup>7</sup>Dayal et al. (2011) computes the IGM attenuation of a Gaussian Ly $\alpha$  spectrum, unprocessed by ISM scattering. Internal radiative transfer effects are expected to alter the line emerging from the galaxy. In particular, outflows are expected redshift the Ly $\alpha$  line, reducing the effect of IGM attenuation (Dijkstra & Wyithe 2010).

with detailed numerical RT simulations, as we have seen in Section 4.4.

The models discussed above all use phenomenological prescriptions to describe  $f_{\text{esc}}$ ; they don't model the resonant scattering of Ly $\alpha$  photons in the ISM. Only recently have simulations have incorporated Ly $\alpha$  RT calculations into galaxy formation models in a cosmological context.

Forero-Romero et al. (2012) computed the Ly $\alpha$  escape fraction of galaxies by post-processing the MareNostrum SPH simulation<sup>8</sup>, approximating the ISM as a dusty slab of gas with the Ly $\alpha$  sources being homogeneously distributed. Following Charlot & Fall (2000), the dust distribution is described using two components: a homogeneous ISM, and dense birth clouds of young stars. Resonant scattering of Ly $\alpha$  photons is taken into account only for the homogeneous phase, using an analytical fit to numerical RT calculations for a slab configuration. The HI opacity of birth clouds is assumed to be low, and so their dust extinction of Ly $\alpha$  photons is taken as for the UV continuum. Their model provides a reasonable match with Ly $\alpha$  and UV LF data at  $z = 5 - 6$ , although the faint-end is strongly overpredicted. They find that  $f_{\text{esc}}$  decreases towards more massive host haloes, echoing the results of Laursen et al. (2009). In an extension of this model, Forero-Romero et al. (2012) argue that the average lower  $f_{\text{esc}}$  of galaxies in massive haloes is an important factor in explaining the small fraction of LAEs found in samples of LBGs.

A similar conclusion is drawn in the work of Garel et al. (2012), though their physical hypotheses are quite different. Noting that galactic winds are ubiquitous in high-redshift galaxies (Steidel et al. 2010), Garel et al. (2012) consider Ly $\alpha$  emission that is powered by star formation and scattered within a neutral outflow represented by a spherical shell. They couple the semi-analytic model of galaxy formation GALICS (Hatton et al. 2003) with a library of numerical Ly $\alpha$  RT experiments (Schaerer et al. 2011), based on the expanding shell model of Verhamme et al. (2006). In their model, higher velocity, denser and more dusty shells are found in more massive, star-forming galaxies. Their Ly $\alpha$  LFs, UV LFs of LAEs and

<sup>8</sup><http://astro.ft.uam.es/marenostrum/>

LBGs are in good agreement with high-redshift observations. In particular, the model predicts a large abundance of faint line emitters ( $10^{41-42}$  erg s $^{-1}$ ): low-SFR galaxies are mostly dust-free and so have a Ly $\alpha$  escape fraction of the order of unity. However,  $f_{\text{esc}}$  is strongly dispersed (from 0 to 1) for massive/star-forming galaxies as a result of a trade-off between larger shell velocities and HI/dust opacities.

Shell models are useful for interpreting Ly $\alpha$  line profiles (Section 4.4) and statistical properties of LAEs (luminosity functions, mean stellar masses, overlap with LBGs, etc.; Garel et al. 2012, see also Orsi et al. 2012). Nonetheless, they assume a physical picture of galactic outflows that is quite idealised, and more realistic models are needed.

**The LAE-LBG connection:** Cosmological models of both LAEs and LBGs can illuminate the apparent tension between their physical properties (as discussed in Section 4.3). Although it is reported that LBGs tend to be more evolved than LAEs, with higher stellar mass and dust content, the simulations of Dayal & Ferrara (2012) suggest that  $z \approx 6$  LAEs and LBGs have similar physical properties. They find that LAEs are a subset of the LBG population; different observed properties result only from different selection criteria.

Using their numerical Ly $\alpha$  radiative transfer models, Verhamme et al. (2008) argue that the link between LBGs and LAEs is mainly governed by RT effects due to variations in HI and dust opacities. They suggest that galaxy mass is the driver of variation of gas and dust content. This would explain the small fraction of LBGs with Ly $\alpha$  in emission (Shapley et al. 2003; Stark et al. 2011): LBGs are highly star-forming, massive galaxies, in which the Ly $\alpha$  emission can be strongly suppressed (see also Garel et al. 2012). Environment must also play a role — using  $\sim 57,000$   $z \sim 3$  LBGs in the CFHTLS Deep Field, Cooke, Omori, & Ryan-Weber (2013) showed from their auto- and cross-correlation functions that LBGs with Ly $\alpha$  in emission vs. absorption live in very different environments, e.g. parent haloes of  $10^{11} M_{\odot}$  vs.  $10^{13} M_{\odot}$ .

While the UV LF of LBGs decreases from  $z = 3$  to  $z = 6$  (Bouwens et al. 2007), the UV LF of LAEs appears to increase over this redshift range

and is a reasonable match for LBGs at  $z = 6$  (Ouchi et al. 2008). This trend can be interpreted as LAEs being a sub-population of LBGs, where the LAE fraction increases towards higher redshift. The dropout technique preferentially detects bright UV-continuum galaxies; hence a significant fraction of low-continuum objects (i.e. LAEs with high equivalent width) are missed by LBG surveys at  $z = 6$  (10-46%, Dow-Hygelund et al. 2007). Therefore, LAEs and LBGs do not necessarily arise from the same population. The apparent overlap of the LAE/LBG UV LF at  $z = 6$  may be accidental (Dijkstra & Wyithe 2007).

**Lyman Alpha and the IGM:** Though this review is focussed on galaxy properties, the interaction of Ly $\alpha$  radiation with the intergalactic medium (IGM) can greatly affect the observed properties of Ly $\alpha$  emitters. Gunn & Peterson (1965) first predicted that the presence of HI in the IGM would absorb radiation blueward of rest-frame Ly $\alpha$  as the expansion of the universe redshifts this light into resonance. Following the recombination of the primordial plasma, the universe was neutral until the formation of sources able to reionise the IGM. In spite of intense research, the nature of these sources is still unknown, and the Epoch of Reionisation (EoR) is only partially constrained. Observations of the cosmic microwave background suggest that the EoR began around  $z = 11$  (Larson et al. 2011). Based on the analysis of the spectra of high-redshift quasars (Fan et al. 2006), the Universe must have been almost completely reionised at  $z \gtrsim 6$ .

The Ly $\alpha$  emission line from high-redshift galaxies is a useful tool for probing the variation in the ionisation state of the IGM. One expects that, as the fog of neutral hydrogen clears during reionisation, a population of hitherto obscured Ly $\alpha$  emitting galaxies will burst into view. An increase in Ly $\alpha$  attenuation could trace a sudden change in the neutral fraction of the IGM ( $x_{\text{HI}}$ ), providing a diagnostic of the epoch of reionisation (Miralda-Escude 1998; Haiman & Spaans 1999; Rhoads & Malhotra 2001). Several authors have suggested that a rapid evolution of the Ly $\alpha$  luminosity function at high redshift would reflect a change in the IGM neutral fraction (Malhotra & Rhoads 2004; Santos 2004; Haiman & Cen 2005; Mao et al. 2007), especially if there were no corresponding

evolution of the UV LF of LAEs. While Hu et al. (2010) find that  $L_{\text{Ly}\alpha}$  remains unchanged between  $z = 5.7$  and  $6.6$ , Ouchi et al. (2010) and Kashikawa et al. (2011) measure a decline of about 30%, along with little evolution of the UV LF (see also Kashikawa et al. 2006). This small increase in the Ly $\alpha$  attenuation translates into a neutral fraction  $x_{\text{HI}} \lesssim 20\%$  according to Ouchi et al. (2010), which would imply that the Universe is still highly ionized at  $z = 6.6$ . On the other hand, Dijkstra et al. (2007b) have shown that the observed drop of the Ly $\alpha$  LF between  $z = 5.7$  and  $6.6$  is expected from the IGM opacity evolution due to cosmic expansion, even if the Universe remains fully ionized (see also Laursen, Sommer-Larsen, & Razoumov 2011).

The spectral line profile can also constrain reionisation. Hu et al. (2010) and Kashikawa et al. (2011) find very similar shapes of Ly $\alpha$  composite spectra at  $z = 5.7$  and  $6.5$ . Nevertheless, they note that the peak of the rest-frame Ly $\alpha$  equivalent width distribution shifts towards lower values from  $z = 5.7$  to  $6.5$ , perhaps due to an increase of the IGM contribution to the damping of the Ly $\alpha$  line. The interpretation of this effect is not straightforward given that infalling and outflowing gas in the vicinity of the galaxy can also strongly affect the Ly $\alpha$  profile. For instance, Dijkstra & Wyithe (2010) demonstrate that radiative transfer through galactic winds can increase the visibility of the Ly $\alpha$  line even for a highly neutral IGM.

Few Ly $\alpha$  surveys at  $z \gtrsim 7$  have been conducted and the number of detections is still small. Nonetheless, small statistics or even non-detections can constrain the change of the LF. Observations tentatively indicate an evolution of the Ly $\alpha$  emitting galaxy population  $z = 6 - 7$  (Shibuya et al. 2012; Clément et al. 2012; Caruana et al. 2013), which can be accounted for using models positing a rapid increase of  $x_{\text{HI}}$  (Mao et al. 2007; Kobayashi et al. 2010; Dijkstra et al. 2011; Jensen et al. 2013). On the other hand, Tilvi et al. (2010), Hibon et al. (2012) and Krug et al. (2012) find no conclusive evidence for a variation of  $L^*$  up to  $z = 7 - 8$ , based on photometric samples. Future spectroscopic follow-up observations will certainly provide more accurate estimates.

The evolution of the fraction of Ly $\alpha$  emitters  $\chi_{\text{Ly}\alpha}$  among samples of Lyman-Break galax-

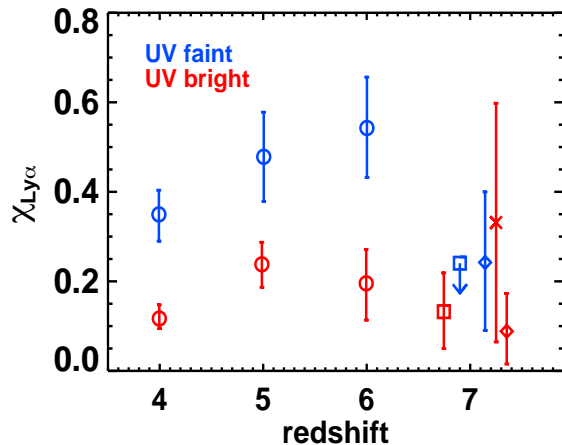


Fig. 18.— Redshift evolution of the fraction  $\chi_{\text{Ly}\alpha}$  of Ly $\alpha$  emitters ( $\text{EW} > 25\text{\AA}$ ) within the Lyman-Break galaxy population. Blue and red symbols correspond to UV-fainter and UV-brighter galaxies respectively. The  $z = 4 - 6$  data from Stark et al. (2010), represented by circles, show an increase of  $\chi_{\text{Ly}\alpha}$  with redshift. The observations at  $z \approx 7$  by Schenker et al. (2012), Pentericci et al. (2011) and Ono et al. (2012) correspond to the diamonds, the squares and the cross respectively. They show that the fraction of Ly $\alpha$  emitters is likely to drop from  $z = 6$  to  $7$ , possibly suggesting an increase of the IGM neutral fraction  $x_{\text{HI}}$ . Also, the decline of  $\chi_{\text{Ly}\alpha}$  at  $z \approx 6$  is stronger for UV faint galaxies than UV bright ones. It may imply that  $x_{\text{HI}}$  is evolving more significantly in low-density regions at this epoch.

ies provides another useful probe of the ionisation state of the IGM. As discussed in Section 4.3, Stark et al. (2010) measure an increase of  $\chi_{\text{Ly}\alpha}$  from  $z = 3$  to  $z = 6$ . Interestingly, the trend starts to reverse at  $z > 6$ . Pentericci et al. (2011), Ono et al. (2012), and Schenker et al. (2012) report that  $\chi_{\text{Ly}\alpha}$  drops from  $z = 6$  to  $z = 7$ , as shown in Figure 18. Furthermore, the drop of the fraction of LAEs is more significant among the fainter UV-selected galaxies. These galaxies are less clustered than brighter ones and located in low density environments (e.g. Giavalisco & Dickinson 2001; Adelberger et al. 2005), which may indicate that reionisation occurred later in low density regions,

privileging an inside-out model. Indeed, galaxies in more clustered regions can blow larger ionized bubbles during the EoR, which should boost the Ly $\alpha$  transmission (McQuinn et al. 2007; Iliev et al. 2008; Mesinger & Furlanetto 2008; Dayal et al. 2009). A strong signal in the two-point correlation of LAEs in the EoR is predicted by McQuinn et al. (2007).

Whether or not reionisation is over by  $z \sim 6$  is not yet clear (e.g. Mesinger 2010; McGreer, Mesinger, & Fan 2011; Raskutti et al. 2012), and there is no conclusive evidence that Ly $\alpha$  observations at  $z = 6-7$  are the signature of a sharp transition of the IGM neutral fraction. Other reasons can explain the Ly attenuation around  $z = 6 - 7$ , such as the intrinsic evolution of the galaxies (Dayal et al. 2008; Dijkstra et al. 2007b; Samui et al. 2009), a change in kinematics and covering factor affecting the escape of Ly photons from galaxies (Dijkstra et al. 2011), observational uncertainties (Pentericci et al. 2011), or the increase of the number density of optically thick absorption systems (Bolton & Haehnelt 2012).

Ly $\alpha$  radiative transfer through the IGM has been studied by a number of authors. Laursen, Sommer-Larsen, & Razoumov (2011) traced Ly $\alpha$  photons from emitters between  $z = 2.5$  and  $6.5$  through a cosmological simulation of the IGM. Figure 19 shows the average transmission of wavelengths around Ly $\alpha$  as a function of the redshift of the emitter. We see that, even at fairly low redshifts, the IGM is able to erase a substantial fraction of the blue side of the intrinsic spectrum. At higher redshifts, even the red side of the line can be affected. Note also that this is the average transmission: individual sightlines can vary substantially. For example, at  $z = 3.5$  the transmission on the blue side ( $\Delta v < -200 \text{ km s}^{-1}$ ) varies between 0.2 and 0.95.

Laursen, Sommer-Larsen, & Razoumov (2011) note that, in some cases, a single, red Ly $\alpha$  peak seen in high-redshift galaxies could be the result of a intrinsic double-peaked spectrum with the blue side erased by the IGM. While this effect is not sufficient to explain the predominance of red-peaks in LAEs, it does demonstrate the importance of the IGM in interpreting Ly $\alpha$  spectra. Conversely, Dijkstra & Wyithe (2010) and Dijkstra et al. (2011) have emphasised that the intrinsic Ly $\alpha$  spectra af-

fects IGM transmission. The presence of a galactic wind in a pre-reionisation galaxy will shift most of the Ly $\alpha$  photons to the red-side before they encounter the IGM. Even a mild wind ( $\sim 25 \text{ km s}^{-1}$ ) increases ISM transmission relative to predictions that assume that Ly $\alpha$  emission peaks at line centre (e.g. Iliev et al. 2008).

Zheng, Cen, Trac, & Miralda-Escudé (2011) have emphasised the importance of large-scale structure for LAE visibility — lower HI densities and larger velocity gradients aid Ly $\alpha$  escape, meaning that, for example, LAEs are more visible for sightlines that look along a filament than across one (see also Wyithe & Dijkstra 2011; Greig, Komatsu, & Wyithe 2012; Behrens & Niemeyer 2013). Such studies are crucial to controlling the systematics of massive observational programs underway to measure cosmological parameters using LAEs as tracers of the cosmic web, such as the Hobby-Eberly Telescope Dark Energy Experiment (HETDEX Hill et al. 2008), whose aim is to measure the spectroscopic redshifts of 800,000 LAEs between  $1.9 < z < 3.5$ .

Ly $\alpha$  may provide a way of directly observing the IGM, and thereby mapping the cosmic web. Hogan & Weymann (1987) predicted that the UV ionizing background falling on clouds of HI in the IGM would produce detectable Ly $\alpha$  fluorescence. This emission would allow us to study the size and morphology of these clouds, as well as the strength of the UV background. The calculations of Hogan & Weymann (1987) were refined by Gould & Weinberg (1996), who correctly predicted that detecting FLEs would be difficult even with a 10m telescopes. The more sophisticated modelling of Cantalupo et al. (2005) have reduced expectations of observing FLEs further still, by showing that simplifications such as a static, plane slab geometry overpredict the visibility of FLEs. Similarly, the cosmological simulations of Kollmeier et al. (2010) predict that, in the absence of a strong ionizing continuum source, the highest fluorescent surface brightnesses at  $z = 3$  are  $\sim 2 \times 10^{-19} \text{ erg s}^{-1} \text{ cm}^{-2} \text{ arcsec}^{-2}$ , which would require  $\gtrsim 1000$  hours to detect. Cantalupo et al. (2007) report that despite the observational efforts of themselves and others in finding a handful of plausible candidates, there is still some doubt about whether UVB-powered FLEs have actually been detected. As noted above, the observations

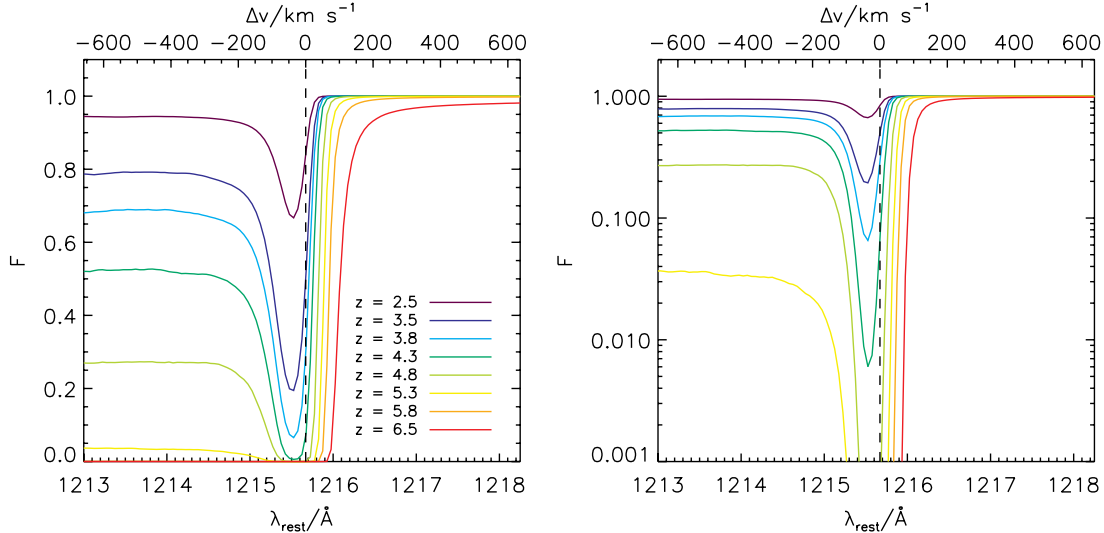


Fig. 19.— The results of Laursen, Sommer-Larsen, & Razoumov (2011), showing the normalized, average IGM transmission  $F(\lambda)$  at wavelengths around  $\text{Ly}\alpha$ , for different redshifts indicated by the colour. In the left panel, the vertical axis is linear, while in the right it is logarithmic, emphasizing the transmission at high redshifts. Even at fairly low redshifts, the IGM is able to erase a substantial fraction of the blue side of the intrinsic spectrum. At higher redshifts, even the red side of the line can be affected. Figure from Laursen, Sommer-Larsen, & Razoumov (2011); reproduced by permission of the AAS.

of Cantalupo et al. (2014) of the  $\text{Ly}\alpha$ -emitting environment of a quasar may represent our best hope of seeing the IGM in emission.

A more comprehensive review of the ability of Lyman alpha emitting galaxies to probe cosmic reionisation can be found in Dijkstra (2014).

## 5. Summary and Future

We have reviewed what observations and theoretical models of  $\text{Ly}\alpha$  emission, and  $\text{Ly}\alpha$  and  $\text{MgII}$  absorption have told us about the interstellar, circumgalactic and intergalactic medium of galaxies. Individually, each tracer provides direct insight into the state and physics of the gas in and around galaxies. Much more can be understood by combining these different spectral probes. We saw in Section 4.5 that modelling of the  $\text{Ly}\alpha$  emission and absorption of DLAs dramatically improves constraints on galaxy properties. The low ion absorption lines of DLAs constrain kinematics, metallicity and, via galaxy formation models, DLA halo mass distribution and even galactic feedback (Section 2). The samples of  $\text{MgII}$  absorbers (and their associated galaxies) in the redshift range that can

be probed by  $\text{Ly}\alpha$  from the ground could shed light on the accretion and feedback physics that shapes star-forming galaxies. Observations of the dust, stellar and star-formation properties of  $\text{Ly}\alpha$  galaxies must continue to inform models of  $\text{Ly}\alpha$  emission.

Our understanding of  $\text{Ly}\alpha$  emission remains largely untouched by 21cm observations. The 21cm transition is an ideal complement to  $\text{Ly}\alpha$ : it is emitted by the same atoms, with a different dependence on temperature, is often optically-thin (at least in the warm-neutral medium), and provides a wealth of kinematic and spatial information. 21cm observations would greatly assist theoretical models of  $\text{Ly}\alpha$  emitters, providing a constraint on the extent, structure and kinematics of HI that is independent of the sources  $\text{Ly}\alpha$  photons. At the moment, resolution and brightness limits have confined 21cm observations to the local universe, while the UV wavelength of  $\text{Ly}\alpha$  keeps ground-based observations to  $z \gtrsim 2$ . Future radio telescopes, space-based  $\text{Ly}\alpha$  observations, and  $\text{MgII}$  observations at intermediate redshifts will continue to close the gap.

The increasing number of detections of LAEs at high redshift in recent times has significantly improved our understanding of the physical nature of these galaxies, and put tighter constraints on theoretical models (see Section 4). Nonetheless, larger samples (especially with spectroscopic confirmation) and multi-wavelength observations will help greatly to refine existing models. Thanks to MUSE, KCWI, HETDEX and more, samples of LAEs will soon become orders of magnitude larger, deeper and more detailed. Space-based observation of local Ly $\alpha$  emitters will also provide important tests of our understanding of the relevant physics. In particular, ISM models and galactic outflows in Ly $\alpha$  radiative transfer calculations could be better informed by local observations, allowing models to replace their current simple approximations. From a theoretical viewpoint, high-resolution hydrodynamic simulations with Ly $\alpha$  radiative transfer and large cosmological volumes are necessary to provide further insights into the complex mechanisms governing Ly $\alpha$  emission in galaxies, and reproduce the wide variety of properties seen in the LAE population.

For DLAs and MgII absorbers, future southern hemisphere surveys, similar to SDSS, will provide a factor of two or so more systems, from which we can learn about the details of gas physics around galaxies. Further advancements in simulations are required to interpret the data. The full range of gas cloud sizes for absorbers — from a few pc to a few kpc — has not yet been resolved in cosmological simulations. Higher resolution simulations and the inclusion of important physical processes such as AGN feedback and self-shielding will shed light on gas within and around galaxies.

### Acknowledgments

We would like to thank the anonymous referee, Mark Dijkstra, Chris Churchill, Stephen Curran and James Allison for their insightful comments.

### REFERENCES

- Adams J. J. et al., 2011, ApJS, 192, 5
- Adams T. F., 1972, ApJ, 174, 439
- Adelberger, K. L., Steidel, C. C., Shapley, A. E., & Pettini, M. 2003, ApJ, 584, 45
- Adelberger K. L., Steidel C. C., Pettini M., Shapley A. E., Reddy N. A., Erb D. K., 2005, ApJ, 619, 697
- Adelberger K. L., Steidel C. C., 2000, ApJ, 544, 218
- Agertz, O., Teyssier, R., & Moore, B. 2009, MNRAS, 397, L64
- Ahn, S.-H., Lee, H.-W., & Lee, H. M. 2000, Journal of Korean Astronomical Society, 33, 29
- Ahn, S.-H., Lee, H.-W., & Lee, H. M. 2001, ApJ, 554, 604
- Ahn, S.-H., Lee, H.-W., & Lee, H. M. 2002, ApJ, 567, 922
- Ahn, S.-H., & Lee, H.-W. 2002, Journal of Korean Astronomical Society, 35, 175
- Ahn, S.-H., Lee, H.-W., & Lee, H. M. 2003, MNRAS, 340, 863
- Ahn, S.-H. 2003, Journal of Korean Astronomical Society, 36, 145
- Ahn, S.-H. 2004, ApJ, 601, L25
- Ajiki M. et al., 2003, AJ, 126, 2091
- Ajiki M., Mobasher B., Taniguchi Y., Shioya Y., Nagao T., Murayama T., Sasaki S. S., 2006, ApJ, 638, 596
- Altay G., Theuns T., Schaye J., Crighton N. H. M., Dalla Vecchia C., 2011, ApJ, 737, L37
- Altay, G., Theuns, T., Schaye, J., Booth, C. M., & Dalla Vecchia, C. 2013, MNRAS, 2469
- Ando M., Ohta K., Iwata I., Akiyama M., Aoki K., Tamura N., 2006, ApJ, 645, L9
- Arons J., 1972, ApJ, 172, 553
- Atek H., Kunth D., Schaerer D., Hayes M., Deharveng J. M., Östlin G., Mas-Hesse J. M., 2009, A&A, 506, L1
- Atek, H., Kunth, D., Schaerer, D., Mas-Hesse, J. M., Hayes, M., Ostlin, G., Kneib, J.-P., & . 2013, arXiv:1308.6577
- Auer L. H., 1968, ApJ, 153, 783
- Bacon R. et al., 2006, The Messenger, 124, 5
- Bahcall, J. N., & Spitzer, L., Jr. 1969, ApJ, 156, L63
- Barai, P., Viel, M., Borgani, S., et al. 2012, arXiv:1210.3582

- Barger, A. J., Cowie, L. L., & Wold, I. G. B. 2012, *ApJ*, 749, 106
- Barnes, L. A. 2009. PhD Thesis. University of Cambridge, UK
- Barnes, L. A., & Haehnelt, M. G. 2009, *MNRAS*, 397, 511
- Barnes, L. A., & Haehnelt, M. G. 2010, *MNRAS*, 403, 870
- Barnes L. A., Haehnelt M. G., Tescari E., Viel M., 2011, *MNRAS*, 416, 1723
- Barnes, L. A., & Haehnelt, M. G. 2014, *MNRAS*, 440, 2313
- Barton, E. J., & Cooke, J. 2009, *AJ*, 138, 1817
- Battisti, A. J., Meiring, J. D., Tripp, T. M., et al. 2012, *ApJ*, 744, 93
- Beers, T. C., & Christlieb, N. 2005, *ARA&A*, 43, 531
- Behrens, C., & Niemeyer, J. 2013, *A&A*, 556, A5
- Bergeron, J., & Boissé, P. 1991, *A&A*, 243, 334
- Bergeron, J. 1988, *Large Scale Structures of the Universe*, 130, 343
- Berry M. et al., 2012, *ApJ*, 749, 4
- Berry, M., Somerville, R. S., Haas, M. R., Gawiser, E., Maller, A., Popping, G., & Trager, S. C. 2013, arXiv:1308.2598
- Bertone, S., Aguirre, A., & Schaye, J. 2013, arXiv:1301.5330
- Binney J., 1977, *ApJ*, 215, 483
- Birboim Y., Dekel A., 2003, *MNRAS*, 345, 349
- Blanc G. A. et al., 2011, *ApJ*, 736, 31
- Bland, J., & Tully, B. 1988, *Nature*, 334, 43
- Bolton J. S., Haehnelt M. G., 2012, *MNRAS*, 412
- Bond N. A., Gawiser E., Koekemoer A. M., 2011, *ApJ*, 729, 48
- Bond N. A., Gawiser E., Guaita L., Padilla N., Gronwall C., Ciardullo R., Lai K., 2012, *ApJ*, 753, 95
- Booth, R. S., de Blok, W. J. G., Jonas, J. L., & Fanaroff, B. 2009, arXiv:0910.2935
- Bordoloi, R., et al. 2011, *ApJ*, 743, 10
- Bordoloi, R., Lilly, S. J., Knobel, C., et al. 2011, *ApJ*, 743, 10
- Bordoloi, R., Lilly, S. J., Kacprzak, G. G., & Churchill, C. W. 2012, arXiv:1211.3774
- Bordoloi, R., Lilly, S. J., Hardmeier, E., et al. 2013, arXiv:1307.6553
- Borthakur, S., Heckman, T., Strickland, D., Wild, V., & Schiminovich, D. 2013, *ApJ*, 768, 18
- Bouché, N., & Lowenthal, J. D. 2004, *ApJ*, 609, 513
- Bouché, N., Murphy, M. T., Péroux, C., Csabai, I. & Wild. V. 2006 *MNRAS*, 371, 495
- Bouché, N., Hohensee, W., Vargas, R., et al. 2012a, *MNRAS*, 426, 801
- Bouché, N., Murphy, M. T., Péroux, C., et al. 2012b, *MNRAS*, 419, 2
- Bouché, N., Murphy, M. T., Kacprzak, G. G., et al. 2013, *Science*, 341, 50
- Bouwens R. J., Illingworth G. D., Blakeslee J. P., Broadhurst T. J., Franx M., 2004, *ApJ*, 611, L1
- Bouwens R. J., Illingworth G. D., Franx M., Ford H., 2007, *ApJ*, 670, 928
- Bouwens R. J. et al., 2011, *ApJ*, 737, 90
- Bouwens, R. J., Illingworth, G. D., Labbe, I., et al. 2011, *Nature*, 469, 504
- Bowen, D. V., Blades, J. C., & Pettini, M. 1995, *ApJ*, 448, 662
- Bowen, D. V., Blades, J. C., & Pettini, M. 1996, *ApJ*, 472, L77
- Bower, R. G., et al. 2004, *MNRAS*, 351, 63
- Braun R., 2012, *ApJ*, 749, 87
- Bridge, C. R., et al. 2012, arXiv:1205.4030
- Brocklehurst, M. 1971, *MNRAS*, 153, 471
- Bromm V., Kudritzki R. P., Loeb A., 2001, *ApJ*, 552, 464
- Brooks A. M., Governato F., Booth C. M., Willman B., Gardner J. P., Wadsley J., Stinson G., Quinn T., 2007, *ApJ*, 655, L17
- Brooks, A. M., Governato, F., Quinn, T., Brook, C. B., & Wadsley, J. 2009, *ApJ*, 694, 396
- Bruzual G., Charlot S., 2003, *MNRAS*, 344, 1000
- Bunker A. J., Warren S. J., Clements D. L., Williger G. M., Hewett P. C., 1999, *MNRAS*, 309, 875
- Burkert, A., & Lin, D. N. C. 2000, *ApJ*, 537, 270

- Cantalupo S., Porciani C., Lilly S. J., Miniati F., 2005, *ApJ*, 628, 61
- Cantalupo S., Lilly S. J., Porciani C., 2007, *ApJ*, 657, 135
- Cantalupo, S., Lilly, S. J., & Haehnelt, M. G. 2012, *MNRAS*, 425, 1992
- Cantalupo, S., Arrigoni-Battaia, F., Prochaska, J. X., Hennawi, J. F., & Madau, P. 2014, *Nature*, 506, 63
- Caruana, J., Bunker, A. J., Wilkins, S. M., Stanway, E. R., Lorenzoni, S., Jarvis, M. J., & Elbert, H. 2013, arXiv:1311.0057
- Cassata P. et al., 2011, *A&A*, 525, A143
- Cen, R., & Zheng, Z. 2012, arXiv:1210.3600
- Cen R., 2012, *ApJ*, 748, 121
- Chapman, S. C., Scott, D., Windhorst, R. A., Frayer, D. T., Borys, C., Lewis, G. F., & Ivison, R. J. 2004, *ApJ*, 606, 85
- Charlot S., Fall S. M., 1991, *ApJ*, 378, 471
- Charlot S., Fall S. M., 1993, *ApJ*, 415, 580
- Charlot S., Fall S. M., 2000, *ApJ*, 539, 718
- Chelouche, D., & Bowen, D. V. 2010, *ApJ*, 722, 1821
- Chen, H.-W., & Tinker, J. L. 2008, *ApJ*, 687, 745
- Chen, H.-W., Kennicutt, R. C., Jr., & Rauch, M. 2005, *ApJ*, 620, 703
- Chen, H.-W., Helsby, J. E., Gauthier, J.-R., Shectman, S. A., Thompson, I. B., & Tinker, J. L. 2010, *ApJ*, 714, 1521
- Chen, H.-W. 2012, *MNRAS*, 427, 1238
- Chevalier R. A., Clegg A. W., 1985, *Nature*, 317, 44
- Chonis, T. S., et al. 2013, *ApJ*, 775, 99
- Christensen L., Wisotzki L., Roth M. M., Sánchez S. F., Kelz A., Jahnke K., 2007, *A&A*, 468, 587
- Christensen L., Noterdaeme P., Petitjean P., Ledoux C., Fynbo J. P. U., 2009, *A&A*, 505, 1007
- Christensen, C., Quinn, T., Governato, F., Stilp, A., Shen, S., & Wadsley, J. 2012, *MNRAS*, 425, 3058
- Christensen, L., et al. 2012, *MNRAS*, 427, 1973
- Chung, A., van Gorkom, J. H., Kenney, J. D. P., Crowl, H., & Vollmer, B. 2009, *AJ*, 138, 1741
- Churchill, C. W., Rigby, J. R., Charlton, J. C., & Vogt, S. S. 1999, *ApJS*, 120, 51
- Churchill, C. W., Mellon, R. R., Charlton, J. C., Jannuzi, B. T., Kirhakos, S., Steidel, C. C., & Schneider, D. P. 2000a, *ApJS*, 130, 91
- Churchill, C. W., Mellon, R. R., Charlton, J. C., Jannuzi, B. T., Kirhakos, S., Steidel, C. C., & Schneider, D. P. 2000b, *ApJ*, 543, 577
- Churchill, C. W., Kacprzak, G. G., Steidel, C. C., et al. 2012b, *ApJ*, 760, 68
- Churchill, C. W., Nielsen, N. M., Kacprzak, G. G., & Trujillo-Gomez, S. 2012b, arXiv:1211.1008
- Churchill, C. W., Nielsen, N. M., Kacprzak, G. G., & Trujillo-Gomez, S. 2013a, *ApJ*, 763, L42
- Churchill, C. W., Trujillo-Gomez, S., Nielsen, N. M., & Kacprzak, G. G. 2013b, arXiv:1308.2618
- Churchill, C. W., Kacprzak, G. G., & Steidel, C. C. 2005, in *Probing Galaxies through Quasar Absorption Lines*, IAU 199 Proceedings, eds. P. R. Williams, C.-G. Shu, & B. Ménard (Cambridge: Cambridge University Press), p. 24
- Churchill, C. W., Steidel, C. C., & Vogt, S. S. 1996, *ApJ*, 471, 164
- Churchill, C. W., Vogt, S. S., & Charlton, J. C. 2003, *AJ*, 125, 98
- Chynoweth, K. M., Langston, G. I., Yun, M. S., Lockman, F. J., Rubin, K. H. R., & Scoles, S. A. 2008, *AJ*, 135, 1983
- Ciardullo R. et al., 2012, *ApJ*, 744, 110
- Clément B. et al., 2012, *A&A*, 538, A66
- Coil, A. L., Weiner, B. J., Holz, D. E., et al. 2011, *ApJ*, 743, 46
- Cooke, J., Wolfe, A. M., Gawiser, E., & Prochaska, J. X. 2006, *ApJ*, 636, L9
- Cooke, J., Wolfe, A. M., Gawiser, E., & Prochaska, J. X. 2006, *ApJ*, 652, 994
- Cooke, J., Berrier, J. C., Barton, E. J., Bullock, J. S., & Wolfe, A. M. 2010, *MNRAS*, 403, 1020
- Cooke, R., Pettini, M., Steidel, C. C., Rudie, G. C., & Jorgenson, R. A. 2011a, *MNRAS*, 412, 1047

- Cooke, R., Pettini, M., Steidel, C. C., Rudie, G. C., & Nissen, P. E. 2011b, *MNRAS*, 417, 1534
- Cooke, J., Omori, Y., & Ryan-Weber, E. V. 2013, *MNRAS*, 433, 2122
- Cooksey, K. L., Prochaska, J. X., Chen, H.-W., Mulchaey, J. S., & Weiner, B. J. 2008, *ApJ*, 676, 262
- Courbin, F., North, P., Eigenbrod, A., & Chelouche, D. 2008, *A&A*, 488, 91
- Cowie L. L., Barger A. J., Hu E. M., 2010, *ApJ*, 711, 928
- Cowie, L. L., Barger, A. J., & Hu, E. M. 2011, *ApJ*, 738, 136
- Cowie L. L., Hu E. M., 1998, *AJ*, 115, 1319
- Crampton D., Lilly S., 1999, in *Astronomical Society of the Pacific Conference Series*, Vol. 191, *Photometric Redshifts and the Detection of High Redshift Galaxies*, Weymann R., Storrie-Lombardi L., Sawicki M., Brunner R., eds., p. 229
- Creasey P., Theuns T., Bower R. G., 2013, *MNRAS*, 437
- Crighton, N. H. M., Hennawi, J. F., & Prochaska, J. X. 2013, *ApJ*, 776, L18
- Crighton, N. H. M., Hennawi, J. F., Simcoe, R. A., et al. 2014, arXiv:1406.4239
- Curtis-Lake E. et al., 2012, *MNRAS*, 422, 1425
- Dalla Vecchia C., Schaye J., 2008, *MNRAS*, 387, 1431
- Dalla Vecchia C., Schaye J., 2012, *MNRAS*, 426, 140
- Dawson S. et al., 2004, *ApJ*, 617, 707
- Dawson S., Rhoads J. E., Malhotra S., Stern D., Wang J., Dey A., Spinrad H., Jannuzi B. T., 2007, *ApJ*, 671, 1227
- Dawson, K. S., et al. 2013, *AJ*, 145, 10
- Dayal P., Ferrara A., Gallerani S., 2008, *MNRAS*, 389, 1683
- Dayal P., Ferrara A., Saro A., Salvaterra R., Borgani S., Tornatore L., 2009, *MNRAS*, 400, 2000
- Dayal P., Maselli A., Ferrara A., 2011, *MNRAS*, 410, 830
- Dayal, P., & Ferrara, A. 2012, *MNRAS*, 421, 2568
- De Cia, A., Ledoux, C., Savaglio, S., Schady, P., & Vreeswijk, P. M. 2013, arXiv:1305.1153
- de Propriis R., Pritchett C. J., Hartwick F. D. A., Hickson P., 1993, *AJ*, 105, 1243
- de Ugarte Postigo, A., et al. 2012, *A&A*, 548, A11
- Deharveng J.-M. et al., 2008, *ApJ*, 680, 1072
- Dekel, A., & Birnboim, Y. 2006, *MNRAS*, 368, 2
- Dekel, A., Birnboim, Y., Engel, G., et al. 2009, *Nature*, 457, 451
- Dekel, A., Sari, R., & Ceverino, D. 2009, *ApJ*, 703, 785
- Dey, A., et al. 2005, *ApJ*, 629, 654
- Dijkstra M., Haiman Z., Spaans M., 2006, *ApJ*, 649, 14
- Dijkstra, M., Haiman, Z., & Spaans, M. 2006, *ApJ*, 649, 37
- Dijkstra M., Kramer R., 2012, *MNRAS*, 424, 1672
- Dijkstra, M., & Jeesson-Daniel, A. 2013, *MNRAS*, 435, 3333
- Dijkstra M., Lidz A., Wyithe J. S. B., 2007a, *MNRAS*, 377, 1175
- Dijkstra, M., & Loeb, A. 2009, *MNRAS*, 400, 1109
- Dijkstra M., Mesinger A., Wyithe J. S. B., 2011, *MNRAS*, 414, 2139
- Dijkstra, M., & Wyithe, J. S. B. 2007, *MNRAS*, 379, 1589
- Dijkstra M., Wyithe J. S. B., 2010, *MNRAS*, 408, 352
- Dijkstra M., Wyithe J. S. B., 2012, *MNRAS*, 419, 3181
- Dijkstra M., Wyithe J. S. B., Haiman Z., 2007b, *MNRAS*, 379, 253
- Dijkstra, M. 2014, arXiv:1406.7292
- Ding, J., Charlton, J. C., & Churchill, C. W. 2005, *ApJ*, 621, 615
- Djorgovski S., Thompson D. J., 1992, in *IAU Symposium*, Vol. 149, *The Stellar Populations of Galaxies*, Barbuy B., Renzini A., eds., p. 337
- Dopita M. A., Sutherland R. S., 2003, *Astrophysics of the diffuse universe*
- Dow-Hygelund, C. C., et al. 2007, *ApJ*, 660, 47

- Dressler A., Hare T., Bigelow B. C., Osip D. J., 2006, in Society of Photo-Optical Instrumentation Engineers (SPIE) Conference Series, Vol. 6269, Society of Photo-Optical Instrumentation Engineers (SPIE) Conference Series
- Dressler A., Martin C. L., Henry A., Sawicki M., McCarthy P., 2011, *ApJ*, 740, 71
- Dubois Y., Teyssier R., 2008, *A&A*, 477, 79
- Duval, F., Schaerer, D., Östlin, G., & Laursen, P. 2013, arXiv:1302.7042
- Eisenstein, D. J., et al. 2011, *AJ*, 142, 72
- Ellison, S. L., Prochaska, J. X., Hennawi, J., Lopez, S., Usher, C., Wolfe, A. M., Russell, D. M., & Benn, C. R. 2010, *MNRAS*, 406, 1435
- Ellison, S. L., Prochaska, J. X., & Mendel, J. T. 2011, *MNRAS*, 412, 448
- Erkal, D., Gnedin, N. Y., & Kravtsov, A. V. 2012, *ApJ*, 761, 54
- Fan X. et al., 2006, *AJ*, 132, 117
- Fardal M. A., Katz N., Gardner J. P., Hernquist L., Weinberg D. H., Davé R., 2001, *ApJ*, 562, 605
- Faucher-Giguère, C.-A., Kereš, D., Dijkstra, M., Hernquist, L., & Zaldarriaga, M. 2010, *ApJ*, 725, 633
- Feldmeier, J. J., et al. 2013, *ApJ*, 776, 75
- Ferrara A., Ricotti M., 2006, *MNRAS*, 373, 571
- Finkelstein S. L., Rhoads J. E., Malhotra S., Pirzkal N., Wang J., 2007, *ApJ*, 660, 1023
- Finkelstein S. L., Rhoads J. E., Malhotra S., Groggin N., 2009, *ApJ*, 691, 465
- Finkelstein S. L. et al., 2011a, *ApJ*, 729, 140
- Finkelstein, S. L., Cohen, S. H., Moustakas, J., Malhotra, S., Rhoads, J. E., & Papovich, C. 2011b, *ApJ*, 733, 117
- Fiore, F. 2001, *New Century of X-ray Astronomy*, 251, 168
- Font-Ribera, A., et al. 2012, *J. Cosmology Astropart. Phys.*, 11, 59
- Ford, A. B., Oppenheimer, B. D., Davé, R., et al. 2013, *MNRAS*, 432, 89
- Forero-Romero J. E., Yepes G., Gottlöber S., Prada F., 2012, *MNRAS*, 419, 952
- Fox, A. J., Ledoux, C., Vreeswijk, P. M., Smette, A., & Jaunsen, A. O. 2008, *A&A*, 491, 189
- Francis, P. J., et al. 2001, *ApJ*, 554, 1001
- Francis, P. J., Dopita, M. A., Colbert, J. W., Palunas, P., Scarlata, C., Teplitz, H., Williger, G. M., & Woodgate, B. E. 2013, *MNRAS*, 428, 28
- Fraternali, F., van Moorsel, G., Sancisi, R., & Oosterloo, T. 2002, *AJ*, 123, 312
- Fruchter, A. S., et al. 2006, *Nature*, 441, 463
- Fukugita, M., Hogan, C. J., & Peebles, P. J. E. 1998, *ApJ*, 503, 518
- Fujita S. S. et al., 2003, *AJ*, 125, 13
- Fujita A., Martin C. L., Mac Low M.-M., New K. C. B., Weaver R., 2009, *ApJ*, 698, 693
- Fumagalli M., O’Meara J. M., Prochaska J. X., Kanekar N., 2010, *MNRAS*, 408, 362
- Fumagalli M., Prochaska J. X., Kasen D., Dekel A., Ceverino D., Primack J. R., 2011, *MNRAS*, 418, 1796
- Fumagalli, M., Hennawi, J. F., Prochaska, J. X., Kasen, D., Dekel, A., Ceverino, D., & Primack, J. 2013, arXiv:1308.1669
- Furlanetto, S. R., Schaye, J., Springel, V., & Hernquist, L. 2005, *ApJ*, 622, 7
- Fynbo J. U., Møller P., Warren S. J., 1999, *MNRAS*, 305, 849
- Fynbo, J. U., et al. 2001, *A&A*, 373, 796
- Fynbo, J. P. U., et al. 2006, *A&A*, 451, L47
- Fynbo, J. P. U., Prochaska, J. X., Sommer-Larsen, J., Dessauges-Zavadsky, M., & Møller, P. 2008, *ApJ*, 683, 321
- Fynbo, J. P. U., et al. 2009, *ApJS*, 185, 526
- Fynbo J. P. U. et al., 2010, *MNRAS*, 408, 2128
- Fynbo J. P. U. et al., 2011, *MNRAS*, 413, 2481
- Gabasch A. et al., 2004, *A&A*, 421, 41
- Gardner J. P., Katz N., Hernquist L., Weinberg D. H., 1997a, *ApJ*, 484, 31
- Gardner J. P., Katz N., Weinberg D. H., Hernquist L., 1997b, *ApJ*, 486, 42
- Gardner J. P., Katz N., Hernquist L., Weinberg D. H., 2001, *ApJ*, 559, 131

- Garel T., Blaizot J., Guiderdoni B., Schaerer D., Verhamme A., Hayes M., 2012, MNRAS, 422, 310
- Gauthier, J.-R., Chen, H.-W., & Tinker, J. L. 2009, ApJ, 702, 50
- Gauthier, J.-R., & Chen, H.-W. 2012, MNRAS, 424, 1952
- Gauthier, J.-R. 2013, MNRAS, 432, 1444
- Gauthier, J.-R., Chen, H.-W., Cooksey, K. L., et al. 2014, MNRAS, 439, 342
- Gawiser, E., Wolfe, A. M., Prochaska, J. X., Lanzetta, K. M., Yahata, N., & Quirrenbach, A. 2001, ApJ, 562, 628
- Gawiser E. et al., 2006, ApJ, 642, L13
- Gawiser E. et al., 2007, ApJ, 671, 278
- Geach, J. E., Smail, I., Chapman, S. C., Alexander, D. M., Blain, A. W., Stott, J. P., & Ivison, R. J. 2007, ApJ, 655, L9
- Geach, J. E., et al. 2009, ApJ, 700, 1
- Giavalisco M., Dickinson M., 2001, ApJ, 550, 177
- Giavalisco M., 2002, ARA&A, 40, 579
- Goerdt, T., Dekel, A., Sternberg, A., Ceverino, D., Teyssier, R., & Primack, J. R. 2010, MNRAS, 407, 613
- Goerdt, T., Dekel, A., Sternberg, A., Gnat, O., & Ceverino, D. 2012, MNRAS, 424, 2292
- Gould A., Weinberg D. H., 1996, ApJ, 468, 462
- Governato F., Willman B., Mayer L., Brooks A., Stinson G., Valenzuela O., Wadsley J., Quinn T., 2007, MNRAS, 374, 1479
- Governato F., Mayer L., Brook C., 2008, in Astronomical Society of the Pacific Conference Series, Vol. 396, Formation and Evolution of Galaxy Disks, Funes J. G., Corsini E. M., eds., p. 453
- Greig, B., Komatsu, E., & Wyithe, J. S. B. 2012, arXiv:1212.0977
- Gronwall C. et al., 2007, ApJ, 667, 79
- Gronwall C., Bond N. A., Ciardullo R., Gawiser E., Altmann M., Blanc G. A., Feldmeier J. J., 2011, ApJ, 743, 9
- Grove L. F., Fynbo J. P. U., Ledoux C., Limousin M., Møller P., Nilsson K. K., Thomsen B., 2009, A&A, 497, 689
- Guaita L. et al., 2010, ApJ, 714, 255
- Guimarães, R., Noterdaeme, P., Petitjean, P., Ledoux, C., Srianand, R., López, S., & Rahmani, H. 2012, AJ, 143, 147
- Gunn, J. E., & Peterson, B. A. 1965, ApJ, 142, 1633
- Haehnelt M. G., Steinmetz M., Rauch M., 1998, ApJ, 495, 647
- Haiman Z., Spaans M., Quataert E., 2000, ApJ, 537, L5
- Haiman Z., Cen R., 2005, ApJ, 623, 627
- Haiman Z., Rees M. J., 2001, ApJ, 556, 87
- Haiman Z., Spaans M., 1999, ApJ, 518, 138
- Hansen M., Oh S. P., 2006, MNRAS, 367, 979
- Harrington J. P., 1973, MNRAS, 162, 43
- Hartmann L. W., Huchra J. P., Geller M. J., O'Brien P., Wilson R., 1988, ApJ, 326, 101
- Hashimoto, T., Ouchi, M., Shimasaku, K., Ono, Y., Nakajima, K., Rauch, M., Lee, J., & Okamura, S. 2013, ApJ, 765, 70
- Hatton S., Devriendt J. E. G., Ninin S., Bouchet F. R., Guiderdoni B., Vibert D., 2003, MNRAS, 343, 75
- Hayashino T. et al., 2004, AJ, 128, 2073
- Hayes M., Östlin G., Mas-Hesse J. M., Kunth D., 2009, AJ, 138, 911
- Hayes M. et al., 2010, Nature, 464, 562
- Hayes M., Schaerer D., Östlin G., Mas-Hesse J. M., Atek H., Kunth D., 2011, ApJ, 730, 8
- Hayes, M., et al. 2013a, ApJ, 765, L27
- Hayes, M., et al. 2013b, arXiv:1308.6578
- Hayes, M., Scarlata, C., & Siana, B. 2011, Nature, 476, 304
- Heckman T. M. et al., 2011, ApJ, 730, 5
- Hennawi, J. F., & Prochaska, J. X. 2013, ApJ, 766, 58
- Herenz, P., Richter, P., Charlton, J. C., & Masiero, J. R. 2013, arXiv:1301.1345
- Hibon, P., et al. 2010, A&A, 515, A97
- Hibon P., Kashikawa N., Willott C., Iye M., Shibuya T., 2012, ApJ, 744, 89
- Hill, G. J., et al. 2008, Panoramic Views of Galaxy Formation and Evolution, 399, 115

- Hill G. J. et al., 2010, in Society of Photo-Optical Instrumentation Engineers (SPIE) Conference Series, Vol. 7735, Society of Photo-Optical Instrumentation Engineers (SPIE) Conference Series
- Hogan, C. J., & Weymann, R. J. 1987, MNRAS, 225, 1P
- Hong, S., Katz, N., Davé, R., Fardal, M., Kereš, D., & Oppenheimer, B. D. 2010, arXiv:1008.4242
- Hopkins, P. F., Quataert, E., & Murray, N. 2011, MNRAS, 417, 950
- Hopkins, P. F., Quataert, E., & Murray, N. 2012, MNRAS, 421, 3522
- Hu E. M., Cowie L. L., McMahon R. G., 1998, ApJ, 502, L99
- Hu E. M., Cowie L. L., Capak P., McMahon R. G., Hayashino T., Komiyama Y., 2004, AJ, 127, 563
- Hu E. M., Cowie L. L., Barger A. J., Capak P., Kakazu Y., Trouille L., 2010, ApJ, 725, 394
- Hu E. M., McMahon R. G., 1996, Nature, 382, 231
- Hummels, C., Bryan, G., Smith, B., & Turk, M. 2012, arXiv:1212.2965
- Hummer D. G., Kunasz P. B., 1980, ApJ, 236, 609
- Hummer D. G., 1962, MNRAS, 125, 21
- Humphrey, A., Binette, L., Villar-Martín, M., Aretxaga, I., & Papaderos, P. 2013, MNRAS, 428, 563
- Hunstead, R. W., Pettini, M., & Fletcher, A. B. 1990, ApJ, 356, 23
- Iliev I. T., Shapiro P. R., McDonald P., Mellema G., Pen U.-L., 2008, MNRAS, 391, 63
- Jakobsson, P., et al. 2004, A&A, 427, 785
- Jakobsson, P., et al. 2006, A&A, 460, L13
- Jarosik N. et al., 2011, ApJS, 192, 14
- Jeeson-Daniel A., Ciardi B., Maio U., Pierleoni M., Dijkstra M., Maselli A., 2012, MNRAS, 424, 2193
- Jensen H., Laursen P., Mellema G., Iliev I. T., Sommer-Larsen J., Shapiro P. R., 2013, MNRAS, 428, 1366
- Jiang, L., et al. 2013, ApJ, 773, 153
- Johansson P. H., Efstathiou G., 2006, MNRAS, 371, 1519
- Johnston, S., et al. 2008, Experimental Astronomy, 22, 151
- Jorgenson, R. A., & Wolfe, A. M. 2014, ApJ, 785, 16
- Kacprzak, G. G., & Churchill, C. W. 2011c, ApJ, 743, L34
- Kacprzak, G. G., Churchill, C. W., Steidel, C. C., Murphy, M. T., & Evans, J. L 2007, ApJ, 662, 909
- Kacprzak, G. G., Churchill, C. W., Steidel, C. C., & Murphy, M. T. 2008, AJ, 135, 922
- Kacprzak, G. G., Churchill, C. W., Ceverino, D., Steidel, C. C., Klypin, A., & Murphy, M. T. 2010a, ApJ, 711, 533
- Kacprzak, G. G., Murphy, M. T., & Churchill, C. W. 2010b, MNRAS, 406, 445
- Kacprzak, G. G., Churchill, C. W., Barton, E. J., & Cooke, J. 2011a, ApJ, 733, 105
- Kacprzak, G. G., Churchill, C. W., Evans, J. L., Murphy, M. T., & Steidel, C. C. 2011b, MNRAS, 416, 3118
- Kacprzak, G. G., Churchill, C. W., & Nielsen, N. M. 2012a, ApJ, 760, L7
- Kacprzak, G. G., Churchill, C. W., Steidel, C. C., Spitler, L. R., & Holtzman, J. A. 2012b, MNRAS, 427, 3029
- Kacprzak, G. G., Cooke, J., Churchill, C. W., Ryan-Weber, E. V., Nielsen, N. M. 2013, ApJ, submitted
- Kacprzak, G. G., Martin, C. L., Bouché, N., et al. 2014, arXiv:1407.4126
- Kashikawa N. et al., 2006, ApJ, 648, 7
- Kashikawa N. et al., 2011, ApJ, 734, 119
- Kashikawa N. et al., 2012, ApJ, 761, 85
- Katz N., Weinberg D. H., Hernquist L., 1996a, ApJS, 105, 19
- Katz N., Weinberg D. H., Hernquist L., Miralda-Escude J., 1996b, ApJ, 457, L57
- Kauffmann G., 1996, MNRAS, 281, 475
- Kaufmann, T., Bullock, J. S., Maller, A., & Fang, T. 2008, ASPCS, 396, 439

- Kay S. T., Pearce F. R., Jenkins A., Frenk C. S., White S. D. M., Thomas P. A., Couchman H. M. P., 2000, *MNRAS*, 316, 374
- Keel, W. C., Cohen, S. H., Windhorst, R. A., & Waddington, I. 1999, *AJ*, 118, 2547
- Keel, W. C., White, R. E., III, Chapman, S., & Windhorst, R. A. 2009, *AJ*, 138, 986
- Kennicutt, R. C., Jr. 1983, *ApJ*, 272, 54
- Kennicutt, Jr. R. C., 1998, *ApJ*, 498, 541
- Kereš D., Katz N., Weinberg D. H., Davé R., 2005, *MNRAS*, 363, 2
- Kereš D., Katz N., Fardal M., Davé R., Weinberg D. H., 2009, *MNRAS*, 395, 160
- Kereš, D., Katz, N., Fardal, M., Davé, R., & Weinberg, D. H. 2009, *MNRAS*, 395, 160
- Khare, P., Kulkarni, V. P., Péroux, C., York, D. G., Lauroesch, J. T., & Meiring, J. D. 2007, *A&A*, 464, 487
- Kobayashi M. A. R., Totani T., Nagashima M., 2007, *ApJ*, 670, 919
- Kobayashi M. A. R., Totani T., Nagashima M., 2010, *ApJ*, 708, 1119
- Kollmeier, J. A., Zheng, Z., Davé, R., Gould, A., Katz, N., Miralda-Escudé, J., & Weinberg, D. H. 2010, *ApJ*, 708, 1048
- Komatsu E. et al., 2009, *ApJS*, 180, 330
- Koo D. C., Kron R. T., 1980, *PASP*, 92, 537
- Kornei K. A., Shapley A. E., Erb D. K., Steidel C. C., Reddy N. A., Pettini M., Bogosavljević M., 2010, *ApJ*, 711, 693
- Kornei, K. A., Shapley, A. E., Martin, C. L., et al. 2012, *ApJ*, 758, 135
- Krogager J.-K., Fynbo J. P. U., Møller P., Ledoux C., Noterdaeme P., Christensen L., Milvang-Jensen B., Sparre M., 2012, *MNRAS*, 424, L1
- Krogager, J.-K., et al. 2013, *MNRAS*, 433, 3091
- Krug H. B. et al., 2012, *ApJ*, 745, 122
- Kudritzki R.-P. et al., 2000, *ApJ*, 536, 19
- Kulas K. R., Shapley A. E., Kollmeier J. A., Zheng Z., Steidel C. C., Hainline K. N., 2012, *ApJ*, 745, 33
- Kulkarni V. P., Hill J. M., Schneider G., Weymann R. J., Storrie-Lombardi L. J., Rieke M. J., Thompson R. I., Jannuzi B. T., 2000, *ApJ*, 536, 36
- Kulkarni V. P., Hill J. M., Schneider G., Weymann R. J., Storrie-Lombardi L. J., Rieke M. J., Thompson R. I., Jannuzi B. T., 2001, *ApJ*, 551, 37
- Kulkarni V. P., Woodgate B. E., York D. G., Thatte D. G., Meiring J., Palunas P., Wassell E., 2006, *ApJ*, 636, 30
- Kulkarni, V. P., Khare, P., Som, D., Meiring, J., York, D. G., Péroux, C., & Lauroesch, J. T. 2010, *New A*, 15, 735
- Kunth D., Lequeux J., Sargent W. L. W., Viallefond F., 1994, *A&A*, 282, 709
- Kunth D., Mas-Hesse J. M., Terlevich E., Terlevich R., Lequeux J., Fall S. M., 1998, *A&A*, 334, 11
- Lai K., Huang J.-S., Fazio G., Cowie L. L., Hu E. M., Kakazu Y., 2007, *ApJ*, 655, 704
- Lai K. et al., 2008, *ApJ*, 674, 70
- Lanzetta, K. M., & Bowen, D. 1990, *ApJ*, 357, 321
- Larson D. et al., 2011, *ApJS*, 192, 16
- Laursen P., Sommer-Larsen J., Andersen A. C., 2009, *ApJ*, 704, 1640
- Laursen, P., Duval, F., Ostlin, G. 2012, *arXiv:1211.2833*
- Laursen, P., Sommer-Larsen, J., & Razoumov, A. O. 2011, *ApJ*, 728, 52
- Laursen P., Sommer-Larsen J., 2007, *ApJ*, 657, L69
- Le Delliou M., Lacey C., Baugh C. M., Guiderdoni B., Bacon R., Courtois H., Sousbie T., Morris S. L., 2005, *MNRAS*, 357, L11
- Le Delliou M., Lacey C. G., Baugh C. M., Morris S. L., 2006, *MNRAS*, 365, 712
- Ledoux, C., Petitjean, P., Fynbo, J. P. U., Møller, P., & Srianand, R. 2006, *A&A*, 457, 71
- Ledoux, C., Vreeswijk, P. M., Smette, A., Fox, A. J., Petitjean, P., Ellison, S. L., Fynbo, J. P. U., & Savaglio, S. 2009, *A&A*, 506, 661
- Lee, T. S., Nagamine, K., Hernquist, L., & Springel, V. 2011, *MNRAS*, 411, 54
- Lehner, N., J.C. Howk, J.C., Tripp, T.M., Tumlinson, J., Prochaska, J.X., O'Meara, J.M., Thom, C., Werk, J.K., Fox, A.J., & Ribaldo, J. 2013, *ApJ*, submitted

- Lidman C., Hayes M., Jones D. H., Schaerer D., Westra E., Tapken C., Meisenheimer K., Verhamme A., 2012, MNRAS, 420, 1946
- Lin, D. N. C., & Murray, S. D. 2000, ApJ, 540, 170
- Lopez, S., et al. 2008, ApJ, 679, 1144
- Lowenthal J. D., Hogan C. J., Green R. F., Woodgate B., Caulet A., Brown L., Bechtold J., 1995, ApJ, 451, 484
- Lu L., Sargent W. L. W., Barlow T. A., Churchill C. W., Vogt S. S., 1996, ApJS, 107, 475
- Lucatello, S., Beers, T. C., Christlieb, N., Barklem, P. S., Rossi, S., Marsteller, B., Sivarani, T., & Lee, Y. S. 2006, ApJ, 652, L37
- Lundgren, B. F., Brunner, R. J., York, D. G., et al. 2009, ApJ, 698, 819
- Lundgren, B. F., Brammer, G., van Dokkum, P., et al. 2012, ApJ, 760, 49
- Lynds, C. R., & Sandage, A. R. 1963, ApJ, 137, 1005
- Ménard, B., & Chelouche, D. 2009, MNRAS, 393, 808
- Ménard, B., & Fukugita, M. 2012, ApJ, 754, 116
- Ménard, B., Wild, V., Nestor, D., Quider, A., & Zibetti, S. 2009, arXiv:0912.3263
- Macchetto F., Lipari S., Giavalisco M., Turnshek D. A., Sparks W. B., 1993, ApJ, 404, 511
- Madau P., 1995, ApJ, 441, 18
- Malhotra, S., Rhoads, J. E., Finkelstein, S. L., Hathi, N., Nilsson, K., McLinden, E., & Pirzkal, N. 2012, ApJ, 750, L36
- Malhotra S., Rhoads J. E., 2002, ApJ, 565, L71
- Malhotra S., Rhoads J. E., 2004, ApJ, 617, L5
- Maller, A. H., & Bullock, J. S. 2004, MNRAS, 355, 694
- Mao J., Lapi A., Granato G. L., de Zotti G., Danese L., 2007, ApJ, 667, 655
- Martin, C. L., & Bouché, N. 2009, ApJ, 703, 1394
- Martin C. L., Sawicki M., Dressler A., McCarthy P., 2008, ApJ, 679, 942
- Martin, C., Moore, A., Morrissey, P., Matuszewski, M., Rahman, S., Adkins, S., & Epps, H. 2010, Proceedings of the SPIE, 7735
- Martin, C. L., Shapley, A. E., Coil, A. L., et al. 2012, ApJ, 760, 127
- Martin C. L., Sawicki M., 2004, ApJ, 603, 414
- Martin C. L., 2005, in Astronomical Society of the Pacific Conference Series, Vol. 331, Extraplanar Gas, Braun R., ed., p. 305
- Mas-Hesse J. M., Kunth D., Tenorio-Tagle G., Leitherer C., Terlevich R. J., Terlevich E., 2003, ApJ, 598, 858
- Mas-Hesse, J. M., Kunth, D., Atek, H., Östlin, G., Leitherer, C., Petrosian, A., & Schaerer, D. 2009, Ap&SS, 320, 35
- Maselli A., Ferrara A., Ciardi B., 2003, MNRAS, 345, 379
- Maselli A., Ciardi B., Kanekar A., 2009, MNRAS, 393, 171
- Matejek, M. S., & Simcoe, R. A. 2012a, ApJ, 761, 112
- Matsuda, Y., et al. 2004, AJ, 128, 569
- Matsuda, Y., Yamada, T., Hayashino, T., Yamauchi, R., & Nakamura, Y. 2006, ApJ, 640, L123
- Matsuda, Y., et al. 2009, MNRAS, 400, L66
- Matsuda, Y., et al. 2012, MNRAS, 425, 878
- McGreer, I. D., Mesinger, A., & Fan, X. 2011, MNRAS, 415, 3237
- McLinden E., Finkelstein S. L., Rhoads J. E., Malhotra S., Hibon P., Richardson M., 2011, in Bulletin of the American Astronomical Society, Vol. 43, American Astronomical Society Meeting Abstracts 217, p. 335.43
- McLinden, E. M., Malhotra, S., Rhoads, J. E., Hibon, P., Weijmans, A.-M., & Tilvi, V. 2013, arXiv:1301.0622
- McLure R. J., Cirasuolo M., Dunlop J. S., Foucaud S., Almaini O., 2009, MNRAS, 395, 2196
- McQuinn M., Hernquist L., Zaldarriaga M., Dutta S., 2007, MNRAS, 381, 75
- Meier D. L., Terlevich R., 1981, ApJ, 246, L109
- Meiring, J. D., Lauroesch, J. T., Haberkzettel, L., et al. 2011, MNRAS, 410, 2516
- Mesinger, A., & Furlanetto, S. R. 2008, MNRAS, 386, 1990
- Mesinger, A. 2010, MNRAS, 407, 1328

- Miley, G., & De Breuck, C. 2008, *A&A Rev.*, 15, 67
- Miralda-Escude J., 1998, *ApJ*, 501, 15
- Mo, H. J., & Miralda-Escude, J. 1996, *ApJ*, 469, 589
- Mo H. J., Mao S., White S. D. M., 1998, *MNRAS*, 295, 319
- Mo H. J., Miralda-Escude J., 1994, *ApJ*, 430, L25
- Møller P., Warren S. J., 1993, *A&A*, 270, 43
- Møller P., Fynbo J. P. U., Fall S. M., 2004, *A&A*, 422, L33
- Møller P., Warren S. J., Fall S. M., Fynbo J. U., Jakobsen P., 2002, *ApJ*, 574, 51
- Møller, P., Fynbo, J. P. U., Ledoux, C., & Nilsson, K. K. 2013, *MNRAS*, 430, 2680
- Mori, M., Umemura, M., & Ferrara, A. 2004, *ApJ*, 613, L97
- Mosleh M. et al., 2012, *ApJ*, 756, L12
- Murayama T. et al., 2007, *ApJS*, 172, 523
- Nagamine K., Springel V., Hernquist L., 2004, *MNRAS*, 348, 421
- Nagamine K., Wolfe A. M., Hernquist L., Springel V., 2007, *ApJ*, 660, 945
- Nagamine K., Ouchi M., Springel V., Hernquist L., 2010, *PASJ*, 62, 1455
- Narayanan, A., Misawa, T., Charlton, J. C., & Kim, T.-S. 2007, *ApJ*, 660, 1093
- Nath B. B., Silk J., 2009, *MNRAS*, 396, L90
- Navarro J. F., Frenk C. S., White S. D. M., 1996, *ApJ*, 462, 563
- Neeleman, M., Wolfe, A. M., Prochaska, J. X., & Rafelski, M. 2013, *ApJ*, 769, 54
- Nelson, D., Vogelsberger, M., Genel, S., Sijacki, D., Kereš, D., Springel, V., & Hernquist, L. 2013, *MNRAS*, 429, 3353
- Nestor, D. B., Turnshek, D. A., & Rao, S. M. 2005, *ApJ*, 628, 637
- Nestor, D. B., Johnson, B. D., Wild, V., et al. 2011, *MNRAS*, 412, 1559
- Neufeld D. A., 1990, *ApJ*, 350, 216
- Neufeld D. A., 1991, *ApJ*, 370, L85
- Nielsen, N. M., Churchill, C. W., & Kacprzak, G. G. 2012, *arXiv:1211.1380*
- Nilsson, K. K., Fynbo, J. P. U., Møller, P., Sommer-Larsen, J., & Ledoux, C. 2006, *A&A*, 452, L23
- Nilsson K. K., Tapken C., Møller P., Freudling W., Fynbo J. P. U., Meisenheimer K., Laursen P., Östlin G., 2009, *A&A*, 498, 13
- North, P. L., Courbin, F., Eigenbrod, A., & Che-louche, D. 2012, *A&A*, 542, A91
- Noterdaeme P., Petitjean P., Ledoux C., Srianand R., 2009, *A&A*, 505, 1087
- Noterdaeme, P., Srianand, R., & Mohan, V. 2010, *MNRAS*, 403, 906
- Noterdaeme P. et al., 2012a, *A&A*, 540, A63
- Noterdaeme P. et al., 2012b, *A&A*, 547, L1
- Ocvirk, P., Pichon, C., & Teyssier, R. 2008, *MNRAS*, 390, 1326
- Oesch P. A. et al., 2010, *ApJ*, 709, L21
- Ohyama, Y., et al. 2002, *PASJ*, 54, 891
- Ohyama, Y., et al. 2003, *ApJ*, 591, L9
- Ono Y. et al., 2010a, *MNRAS*, 402, 1580
- Ono Y., Ouchi M., Shimasaku K., Dunlop J., Farrah D., McLure R., Okamura S., 2010b, *ApJ*, 724, 1524
- Ono Y. et al., 2012, *ApJ*, 744, 83
- Oppenheimer, B. D., & Davé, R. 2006, *MNRAS*, 373, 1265
- Oppenheimer, B. D., & Davé, R. 2008, *MNRAS*, 387, 577
- Oppenheimer, B. D., Davé, R., Kereš, D., Fardal, M., Katz, N., Kollmeier, J. A., & Weinberg, D. H. 2010, *MNRAS*, 406, 2325
- Orsi A., Lacey C. G., Baugh C. M., 2012, *MNRAS*, 425, 87
- Osterbrock D. E., Ferland G. J., 2006, *Astrophysics of gaseous nebulae and active galactic nuclei*
- Osterbrock D. E., 1962, *ApJ*, 135, 195
- Osterbrock D. E., 1989, *Astrophysics of gaseous nebulae and active galactic nuclei*
- Östlin G., Hayes M., Kunth D., Mas-Hesse J. M., Leitherer C., Petrosian A., Atek H., 2009, *AJ*, 138, 923
- Oteo, I., et al. 2012, *ApJ*, 751, 139

- Ouchi M. et al., 2003, *ApJ*, 582, 60
- Ouchi M. et al., 2008, *ApJS*, 176, 301
- Ouchi M. et al., 2010, *ApJ*, 723, 869
- Overzier, R. A., Nesvadba, N. P. H., Dijkstra, M., Hatch, N. A., Lehnert, M. D., Villar-Martín, M., Wilman, R. J., & Zirm, A. W. 2013, *ApJ*, 771, 89
- Padilla, N., Lacerna, I., Lopez, S., Barrientos, L. F., Lira, P., Andrews, H., & Tejos, N. 2009, *MNRAS*, 395, 1135
- Palunas, P., Teplitz, H. I., Francis, P. J., Williger, G. M., & Woodgate, B. E. 2004, *ApJ*, 602, 545
- Papovich C., Dickinson M., Ferguson H. C., 2001, *ApJ*, 559, 620
- Partridge R. B., Peebles P. J. E., 1967, *ApJ*, 147, 868
- Pentericci L., Grazian A., Fontana A., Salimbeni S., Santini P., de Santis C., Gallozzi S., Giallongo E., 2007, *A&A*, 471, 433
- Pentericci L., Grazian A., Fontana A., Castellano M., Giallongo E., Salimbeni S., Santini P., 2009, *A&A*, 494, 553
- Pentericci L. et al., 2011, *ApJ*, 743, 132
- Péroux, C., Bouché, N., Kulkarni, V. P., & York, D. G. 2013, *MNRAS*, 436, 2650
- Pérez-Ràfols, I., Miralda-Escudé, J., Lundgren, B., et al. 2014, *arXiv:1402.1342*
- Péroux C., Bouché N., Kulkarni V. P., York D. G., Vladilo G., 2011a, *MNRAS*, 410, 2237
- Péroux C., Bouché N., Kulkarni V. P., York D. G., Vladilo G., 2011b, *MNRAS*, 410, 2251
- Péroux C., Bouché N., Kulkarni V. P., York D. G., Vladilo G., 2012, *MNRAS*, 419, 3060
- Péroux, C., Bouché, N., Kulkarni, V. P., & York, D. G. 2013, *MNRAS*, 436, 2650
- Persic, M., & Salucci, P. 1992, *MNRAS*, 258, 14P
- Pettini M., Shapley A. E., Steidel C. C., Cuby J.-G., Dickinson M., Moorwood A. F. M., Adelberger K. L., Giavalisco M., 2001, *ApJ*, 554, 981
- Pettini, M., Smith, L. J., King, D. L., & Hunstead, R. W. 1997, *ApJ*, 486, 665
- Pettini M., 2004, in *Cosmochemistry. The melting pot of the elements*, Esteban C., García López R., Herrero A., Sánchez F., eds., pp. 257–298
- Pettini M., 2006, in *The Fabulous Destiny of Galaxies: Bridging Past and Present*, Le Brun V., Mazure A., Arnouts S., Burgarella D., eds., p. 319
- Pirzkal N., Malhotra S., Rhoads J. E., Xu C., 2007, *ApJ*, 667, 49
- Pontzen A. et al., 2008, *MNRAS*, 390, 1349
- Pontzen, A., et al. 2010, *MNRAS*, 402, 1523
- Prescott, M. K. M., et al. 2012, *ApJ*, 752, 86
- Prescott, M. K. M., Dey, A., & Jannuzi, B. T. 2009, *ApJ*, 702, 554
- Prescott, M. K. M., Dey, A., & Jannuzi, B. T. 2013, *ApJ*, 762, 38
- Press W. H., Schechter P., 1974, *ApJ*, 187, 425
- Pritchett C. J., 1994, *PASP*, 106, 1052
- Prochaska, J. X., Gawiser, E., Wolfe, A. M., Castro, S., & Djorgovski, S. G. 2003, *ApJ*, 595, L9
- Prochaska, J. X., & Herbert-Fort, S. 2004, *PASP*, 116, 622
- Prochaska, J. X., et al. 2004, *ApJ*, 611, 200
- Prochaska J. X., Herbert-Fort S., Wolfe A. M., 2005, *ApJ*, 635, 123
- Prochaska, J. X., Chen, H.-W., Dessauges-Zavadsky, M., & Bloom, J. S. 2007, *ApJ*, 666, 267
- Prochaska, J. X., Chen, H.-W., Wolfe, A. M., Dessauges-Zavadsky, M., & Bloom, J. S. 2008, *ApJ*, 672, 59
- Prochaska, J. X., et al. 2013b, *ApJ*, 776, 136
- Prochaska, J. X., Chen, H.-W., & Bloom, J. S. 2006, *ApJ*, 648, 95
- Prochaska, J. X., Hennawi, J. F., & Simcoe, R. A. 2013a, *ApJ*, 762, L19
- Prochaska J. X., Wolfe A. M., 1997, *ApJ*, 487, 73
- Prochaska J. X., Wolfe A. M., 2009, *ApJ*, 696, 1543
- Quider, A. M., Nestor, D. B., Turnshek, D. A., et al. 2011, *AJ*, 141, 137
- Quinn T., Katz N., Efstathiou G., 1996, *MNRAS*, 278, L49
- Rafelski, M., Wolfe, A. M., Prochaska, J. X., Neeleman, M., & Mendez, A. J. 2012, *ApJ*, 755, 89

- Rafelski, M., Neeleman, M., Fumagalli, M., Wolfe, A. M., & Prochaska, J. X. 2013, arXiv:1310.6042
- Rahmani H., Srianand R., Noterdaeme P., Petitjean P., 2010, MNRAS, 409, L59
- Rahmati, A., & Schaye, J. 2013b, arXiv:1310.3317
- Rahmati, A., Pawlik, A. H., Raičević, M., & Schaye, J. 2012, arXiv:1210.7808
- Rahmati, A., Schaye, J., Pawlik, A. H., & Raičević, M. 2013a, MNRAS, 431, 2261
- Rahmati, A., & Schaye, J. 2014, MNRAS, 438, 529
- Raiter, A., Schaerer, D., & Fosbury, R. A. E. 2010, A&A, 523, A64
- Rao S. M., Turnshek D. A., Nestor D. B., 2006, ApJ, 636, 610
- Rao S. M., Belfort-Mihalyi M., Turnshek D. A., Monier E. M., Nestor D. B., Quider A., 2011, MNRAS, 416, 1215
- Raskutti S., Bolton J. S., Wyithe J. S. B., Becker G. D., 2012, MNRAS, 421, 1969
- Rau, A., et al. 2010, ApJ, 720, 862
- Rauch M. et al., 2008, ApJ, 681, 856
- Rauch, M., Becker, G. D., Haehnelt, M. G., Gauthier, J.-R., Ravindranath, S., & Sargent, W. L. W. 2011, MNRAS, 418, 1115
- Rauch, M., Becker, G. D., Haehnelt, M. G., Gauthier, J.-R., & Sargent, W. L. W. 2013a, MNRAS, 429, 429
- Rauch, M., Becker, G. D., Haehnelt, M. G., & Gauthier, J.-R. 2013b, arXiv:1305.5849
- Rauch M., Haehnelt M. G., 2011, MNRAS, 412, L55
- Rauch M., 1998, ARA&A, 36, 267
- Razoumov A. O., Norman M. L., Prochaska J. X., Wolfe A. M., 2006, ApJ, 645, 55
- Razoumov A. O., Norman M. L., Prochaska J. X., Sommer-Larsen J., Wolfe A. M., Yang Y.-J., 2008, ApJ, 683, 149
- Reuland, M., et al. 2003, ApJ, 592, 755
- Rhoads J. E., Malhotra S., Dey A., Stern D., Spinrad H., Jannuzi B. T., 2000, ApJ, 545, L85
- Rhoads J. E., Malhotra S., 2001, ApJ, 563, L5
- Ribaudo, J., Lehner, N., Howk, J. C., et al. 2011, ApJ, 743, 207
- Richter, P. 2012, ApJ, 750, 165
- Rigby, J. R., Charlton, J. C., & Churchill, C. W. 2002, ApJ, 565, 743
- Rosdahl, J., & Blaizot, J. 2012, MNRAS, 423, 344
- Rubin, K. H. R., Prochaska, J. X., Koo, D. C., Phillips, A. C., & Weiner, B. J. 2010, ApJ, 712, 574
- Rubin, K. H. R., Prochaska, J. X., Koo, D. C., & Phillips, A. C. 2012, ApJ, 747, L26
- Rubin, K. H. R., Prochaska, J. X., Koo, D. C., et al. 2013, arXiv:1307.1476
- Rudie, G. C., et al. 2012, ApJ, 750, 67
- Ryan-Weber, E. V., Webster, R. L., & Staveley-Smith, L. 2003, MNRAS, 343, 1195
- Rybicki G. B., Lightman A. P., 1979, Radiative processes in astrophysics
- Saito, T., Shimasaku, K., Okamura, S., Ouchi, M., Akiyama, M., Yoshida, M., & Ueda, Y. 2008, ApJ, 675, 1076
- Samui S., Srianand R., Subramanian K., 2009, MNRAS, 398, 2061
- Sancisi, R., Fraternali, F., Oosterloo, T., & van der Hulst, T. 2008, A&A Rev., 15, 189
- Santos M. R., 2004, MNRAS, 349, 1137
- Sargent, W. L. W., Boksenberg, A., & Steidel, C. C. 1988, ApJS, 68, 539
- Savage, B. D., Wakker, B., Jannuzi, B. T., et al. 2000, ApJS, 129, 563
- Savaglio, S., et al. 2012, MNRAS, 420, 627
- Savaglio, S., Fall, S. M., & Fiore, F. 2003, ApJ, 585, 638
- Savaglio, S. 2006, New Journal of Physics, 8, 195
- Savaglio, S. 2013, EAS Publications Series, 61, 381
- Scarlata, C., et al. 2009, ApJ, 704, L98
- Schaerer D., Hayes M., Verhamme A., Teyssier R., 2011, A&A, 531, A12
- Schaerer D., de Barros S., 2009, A&A, 502, 423
- Schaerer D., Verhamme A., 2008, A&A, 480, 369
- Schaerer D., 2003, A&A, 397, 527

- Schenker M. A., Stark D. P., Ellis R. S., Robertson B. E., Dunlop J. S., McLure R. J., Kneib J.-P., Richard J., 2012, *ApJ*, 744, 179
- Schiano A. V. R., Wolfe A. M., Chang C. A., 1990, *ApJ*, 365, 439
- Schaerer Seyffert, E. N., Cooksey, K. L., Simcoe, R. A., et al. 2013, arXiv:1308.5971
- Shapley A. E., Steidel C. C., Adelberger K. L., Dickinson M., Giavalisco M., Pettini M., 2001, *ApJ*, 562, 95
- Shapley A. E., Steidel C. C., Pettini M., Adelberger K. L., 2003, *ApJ*, 588, 65
- Shen, S., Madau, P., Guedes, J., et al. 2012, arXiv:1205.0270
- Sheth R. K., Tormen G., 2002, *MNRAS*, 329, 61
- Shibuya T., Kashikawa N., Ota K., Iye M., Ouchi M., Furusawa H., Shimasaku K., Hattori T., 2012, *ApJ*, 752, 114
- Shimasaku K. et al., 2006, *PASJ*, 58, 313
- Shimizu, I., & Umemura, M. 2010, *MNRAS*, 406, 913
- Shimizu I., Yoshida N., Okamoto T., 2011, *MNRAS*, 418, 2273
- Shioya Y. et al., 2009, *ApJ*, 696, 546
- Silk, J., & Mamon, G. A. 2012, *Research in Astronomy and Astrophysics*, 12, 917
- Silk J., 1977, *ApJ*, 211, 638
- Smith, D. J. B., & Jarvis, M. J. 2007, *MNRAS*, 378, L49
- Smith, D. J. B., Jarvis, M. J., Lacy, M., & Martínez-Sansigre, A. 2008, *MNRAS*, 389, 799
- Smith, D. J. B., Jarvis, M. J., Simpson, C., & Martínez-Sansigre, A. 2009, *MNRAS*, 393, 309
- Sommer-Larsen J., Götz M., Portinari L., 2003, *ApJ*, 596, 47
- Spergel D. N. et al., 2003, *ApJS*, 148, 175
- Spergel D. N. et al., 2007, *ApJS*, 170, 377
- Springel, V., & Hernquist, L. 2003, *MNRAS*, 339, 289
- Springel V. et al., 2005, *Nature*, 435, 629
- Springel V., 2005, *MNRAS*, 364, 1105
- Stark D. P., Ellis R. S., Chiu K., Ouchi M., Bunker A., 2010, *MNRAS*, 408, 1628
- Stark D. P., Ellis R. S., Ouchi M., 2011, *ApJ*, 728, L2
- Steidel, C. C., & Sargent, W. L. W. 1992, *ApJS*, 80, 1
- Steidel C. C., Adelberger K. L., Giavalisco M., Dickinson M., Pettini M., 1999, *ApJ*, 519, 1
- Steidel, C. C., Adelberger, K. L., Shapley, A. E., Pettini, M., Dickinson, M., & Giavalisco, M. 2000, *ApJ*, 532, 170
- Steidel, C. C., Kollmeier, J. A., Shapely, A. E., Churchill, C. W., Dickinson, M., & Pettini, M. 2002, *ApJ*, 570, 526
- Steidel C. C., Adelberger K. L., Shapley A. E., Pettini M., Dickinson M., Giavalisco M., 2003, *ApJ*, 592, 728
- Steidel C. C., Erb D. K., Shapley A. E., Pettini M., Reddy N., Bogosavljević M., Rudie G. C., Rakic O., 2010, *ApJ*, 717, 289
- Steidel C. C., Bogosavljević M., Shapley A. E., Kollmeier J. A., Reddy N. A., Erb D. K., Pettini M., 2011, *ApJ*, 736, 160
- Steidel C. C., Hamilton D., 1993, *AJ*, 105, 2017
- Steidel, C. C. 1995, in *QSO Absorption Lines*, ed. G. Meylan, (Springer-verlag: Berlin Heidelberg), p. 139
- Stewart, K. R., Kaufmann, T., Bullock, J. S., et al. 2011, *ApJ*, 738, 39
- Stewart, K. R., Brooks, A. M., Bullock, J. S., et al. 2013, arXiv:1301.3143
- Stocke, J. T., Keeney, B. A., Danforth, C. W., et al. 2012, arXiv:1212.5658
- Strickland, D. K., Heckman, T. M., Colbert, E. J. M., Hoopes, C. G., & Weaver, K. A. 2004, *ApJS*, 151, 193
- Tamura, Y., et al. 2013, arXiv:1301.2596
- Taniguchi, Y., & Shioya, Y. 2000, *ApJ*, 532, L13
- Taniguchi Y. et al., 2005, *PASJ*, 57, 165
- Tapken C., Appenzeller I., Mehlert D., Noll S., Richling S., 2004, *A&A*, 416, L1
- Tapken C., Appenzeller I., Noll S., Richling S., Heidt J., Meinköhn E., Mehlert D., 2007, *A&A*, 467, 63
- Tasitsiomi A., 2006, *ApJ*, 645, 792

- Tenorio-Tagle G., Silich S. A., Kunth D., Terlevich E., Terlevich R., 1999, MNRAS, 309, 332
- Terlevich E., Diaz A. I., Terlevich R., Vargas M. L. G., 1993, MNRAS, 260, 3
- Tescari E., Viel M., Tornatore L., Borgani S., 2009, MNRAS, 397, 411
- Teyssier R., 2002, A&A, 385, 337
- Thom, C., Werk, J. K., Tumlinson, J., et al. 2011, ApJ, 736, 1
- Thompson D., Djorgovski S., Trauger J., 1995, AJ, 110, 963
- Thoul, A. A., & Weinberg, D. H. 1995, ApJ, 442, 480
- Tilvi V. et al., 2010, ApJ, 721, 1853
- Tilvi, V., Scannapieco, E., Malhotra, S., & Rhoads, J. E. 2011, MNRAS, 418, 2196
- Tinker, J. L., & Chen, H.-W. 2008, ApJ, 679, 1218
- Tremonti, C. A., Moustakas, J., & Diamond-Stanic, A. M. 2007, ApJ, 663, L77
- Tripp, T. M., & Bowen, D. V. 2005, in *Probing Galaxies through Quasar Absorption Lines*, IAU 199 Proceedings, eds. P. R. Williams, C.-G. Shu, & B. Ménard (Cambridge: Cambridge University Press), p. 5
- Tripp, T. M., Jenkins, E. B., Bowen, D. V., et al. 2005, ApJ, 619, 714
- Trujillo-Gomez, S., Klypin, A., Primack, J., & Romanowsky, A. J. 2011, ApJ, 742, 16
- Tumlinson, J., Thom, C., Werk, J. K., et al. 2011, Science, 334, 948
- Vallini L., Dayal P., Ferrara A., 2012, MNRAS, 421, 3266
- Valls-Gabaud D., 1993, ApJ, 419, 7
- van Breugel, W., de Vries, W., Croft, S., De Breuck, C., Dopita, M., Miley, G., Reuland, M., Röttgering, H. 2006, Astronomische Nachrichten, 327, 175
- van Breukelen C., Jarvis M. J., Venemans B. P., 2005, MNRAS, 359, 895
- van de Voort, F., Schaye, J., Booth, C. M., Haas, M. R., & Dalla Vecchia, C. 2011, MNRAS, 414, 2458
- van de Voort F., Schaye J., Altay G., Theuns T., 2012, MNRAS, 421, 2809
- Vargas, C. J., et al. 2013, arXiv:1309.6341
- Veilleux, S., Cecil, G., & Bland-Hawthorn, J. 2005, ARA&A, 43, 769
- Verhamme A., Schaerer D., Maselli A., 2006, A&A, 460, 397
- Verhamme A., Schaerer D., Atek H., Tapken C., 2008, A&A, 491, 89
- Verhamme A., Dubois Y., Blaizot J., Garel T., Bacon R., Devriendt J., Guiderdoni B., Slyz A., 2012, A&A, 546, A111
- Verheijen, M. A. W., Oosterloo, T. A., van Cappellen, W. A., Bakker, L., Ivashina, M. V., & van der Hulst, J. M. 2008, The Evolution of Galaxies Through the Neutral Hydrogen Window, 1035, 265
- Viegas S. M., 1995, MNRAS, 276, 268
- Villar-Martín, M., Humphrey, A., De Breuck, C., Fosbury, R., Binette, L., & Vernet, J. 2007, MNRAS, 375, 1299
- Villar-Martín, M., Sánchez, S. F., Humphrey, A., Dijkstra, M., di Serego Alighieri, S., De Breuck, C., & González Delgado, R. 2007, MNRAS, 378, 416
- Villar-Martín, M., Tadhunter, C., Morganti, R., & Holt, J. 2005, MNRAS, 359, L5
- Villar-Martín, M. 2007, New Astronomy Reviews, 51, 194
- Vreeswijk, P. M., et al. 2004, A&A, 419, 927
- Warren S. J., Møller P., Fall S. M., Jakobsen P., 2001, MNRAS, 326, 759
- Watson, D., et al. 2006, ApJ, 652, 1011
- Weaver R., McCray R., Castor J., Shapiro P., Moore R., 1977, ApJ, 218, 377
- Weijmans, A.-M., Bower, R. G., Geach, J. E., Swinbank, A. M., Wilman, R. J., de Zeeuw, P. T., & Morris, S. L. 2010, MNRAS, 402, 2245
- Weiner B. J. et al., 2009, ApJ, 692, 187
- Weiner, B. J., et al. 2009, ApJ, 692, 187
- Werk, J. K., Prochaska, J. X., Thom, C., et al. 2012, ApJS, 198, 3
- White S. D. M., Rees M. J., 1978, MNRAS, 183, 341
- Wold, I. G. B., Barger, A. J., & Cowie, L. L. 2014, ApJ, 783, 119

- Wolfe, A. M., & Chen, H.-W. 2006, *ApJ*, 652, 981
- Wolfe A. M., Lanzetta K. M., Turnshek D. A., Oke J. B., 1992, *ApJ*, 385, 151
- Wolfe A. M., Gawiser E., Prochaska J. X., 2005, *ARA&A*, 43, 861
- Wolfe A. M., 1986, *Royal Society of London Philosophical Transactions Series A*, 320, 503
- Wyithe, J. S. B., & Dijkstra, M. 2011, *MNRAS*, 415, 3929
- Yajima, H., & Li, Y. 2012, arXiv:1211.0088
- Yajima, H., Li, Y., Zhu, Q., Abel, T., Gronwall, C., & Ciardullo, R. 2012, arXiv:1209.5842
- Yajima H., Li Y., Zhu Q., Abel T., 2012a, *MNRAS*, 424, 884
- Yajima, H., Choi, J.-H., & Nagamine, K. 2012, *MNRAS*, 427, 2889
- Yajima, H., Li, Y., & Zhu, Q. 2012, arXiv:1210.6440
- Yamada S. F. et al., 2005, *PASJ*, 57, 881
- Yang, Y., Zabludoff, A., Jahnke, K., Eisenstein, D., Davé, R., Shectman, S. A., & Kelson, D. D. 2011, *ApJ*, 735, 87
- Yoon, J. H., & Putman, M. E. 2013, *ApJ*, 772, L29
- York, D. G., Dopita, M., Green, R., & Bechtold, J. 1986, *ApJ*, 311, 610
- Yuma S., Ohta K., Yabe K., Shimasaku K., Yoshida M., Ouchi M., Iwata I., Sawicki M., 2010, *ApJ*, 720, 1016
- Zheng, Z., & Wallace, J. 2013, arXiv:1308.1405
- Zheng Z., Cen R., Trac H., Miralda-Escudé J., 2010, *ApJ*, 716, 574
- Zheng, Z., Cen, R., Weinberg, D., Trac, H., & Miralda-Escudé, J. 2011, *ApJ*, 739, 62
- Zheng, Z., Cen, R., Trac, H., & Miralda-Escudé, J. 2011, *ApJ*, 726, 38
- Zheng Z., Miralda-Escudé J., 2002, *ApJ*, 578, 33
- Zhu, G., & Ménard, B. 2013, *ApJ*, 770, 130
- Zhu, G., Ménard, B., Bizyaev, D., et al. 2014, *MNRAS*, 439, 3139
- Zibetti, S., Ménard, B., Nestor, D. B., Quider, A. M., Rao, S. M., & Turnshek, D. A. 2007, *ApJ*, 658, 161
- Zirm, A. W., Dey, A., Dickinson, M., & Norman, C. J. 2009, *ApJ*, 694, L31
- Zonak, S. G., Charlton, J. C., Ding, J., & Churchill, C. W. 2004, *ApJ*, 606, 196
- Zwaan M. A., van der Hulst J. M., Briggs F. H., Verheijen M. A. W., Ryan-Weber E. V., 2005, *MNRAS*, 364, 1467
- Zwaan, M. A., Meyer, M. J., Staveley-Smith, L., & Webster, R. L. 2005, *MNRAS*, 359, L30
- Zwaan M., Walter F., Ryan-Weber E., Brinks E., de Blok W. J. G., Kennicutt, Jr. R. C., 2008, *AJ*, 136, 2886